Université du Québec
Institut National de la Recherche Scientifique
Centre Énergie, Matériaux et Télécommunications

UPCONVERTING NANOPARTICLES FOR INTEGRATION IN BIOIMAGING AND THERAPEUTIC APPLICATIONS

Par

Yue Huang

Thèse présentée pour l'obtention du grade de
Philosophiæ doctor (Ph.D.)
en sciences de l'énergie et des matériaux

Jury d'évaluation

Président du jury et examinateur interne	Shuhui Sun INRS-EMT
Examinateur externe	Tomislav Friscic McGill University
Examinateur externe	Pat Forgione Concordia University
Directeur de recherche	Fiorenzo Vetrone INRS-EMT
Codirecteur de recherche	Federico Rosei INRS-EMT

ABSTRACT

In recent years, lanthanide (Ln^{3+})-doped upconverting nanoparticles (UCNPs) have emerged as efficient and versatile bioimaging as well as therapeutic tools. In general, these nanoparticles can be excited with near-infrared (NIR) light and emit higher-energy photons spanning the ultraviolet (UV), visible and NIR ranges *via* a multiphoton process known as upconversion. The multiphoton excitation occurs through a plethora of 4*f* excited electronic energy states, which have long lifetimes (micro- to millisecond). Compared with conventional fluorophores, UCNPs possess several advantages including reduced autofluorescence background, remarkable tissue penetration, and low cytotoxicity. Driven by these factors, Ln^{3+}-doped UCNPs could serve as excellent candidates for numerous biological applications. In this thesis, our work is mainly focused on the development of novel nanostructures combining UCNPs with other modalities for bioimaging and therapeutic applications.

In the first part, we develop novel hybrid nanomaterials that exploit the interesting optical properties of both UCNPs and gold nanorods (GNRs), and bring them together onto a single nanoplatform. It is well known that GNRs are good candidates for photothermal therapy (PTT) where cancer cells are destroyed by optical heating. In order to generate a temperature increase in diseased cells, GNRs absorb light causing electrons to undergo transitions from the ground state to the excited state. The electronic excitation energy subsequently results in an increase in the kinetic energy, which leads to overheating of the local environment around the light absorbing species. Therefore, local cells or tissues

could be destroyed by the heat produced. In addition, UCNPs can be applied as nanothermometers based on the temperature dependent luminescence where their luminescence intensity ratios (LIR) vary as a function of temperature. Thermal sensing with UCNPs could therefore be used for controlling the photothermal treatment, which would minimize collateral damage in healthy tissues surrounding the hyperthermia target.

In detail, Part I is divided into two sections based on two different nanostructures (Section I and Section II). In Section I, we developed a novel core/shell nanostructure using a multistep strategy consisting of a GNR core with an upconverting shell of $NaYF_4$:Er^{3+}, Yb^{3+} (GNR@UCNPs). The absorption of GNR was tuned to ~660 nm, which was resonant with the upconverted red Er^{3+} emission emanating from the $^4F_{9/2}$ excited state. Upon laser irradiation, UCNPs converted NIR light to UV/visible photons *via* energy transfer, which could then be absorbed by GNRs and converted into heat. Meanwhile, the intensity ratio of the upconverted green emission showed remarkable thermal sensitivity, which was used to calculate the temperature change due to rapid heat conversion from the GNR core. Doxorubicin (DOX), a model anticancer drug, was selected to load into the GNR@UCNPs. In terms of the drug release profile, it was shown that the release of DOX was significantly enhanced at lower pH and higher temperature caused by photothermal effect. This multifunctional nanocomposite, which is well suited for bioimaging and local heating, shows strong potential for use in cancer therapy.

In section II, we developed another novel multifunctional nanocomposite consisting of GNRs, silicon dioxide (SiO_2), and $NaGdF_4$:Er^{3+}, Yb^{3+} UCNPs (GNR@SiO_2@UCNPs), with highly integrated functionalities including luminescence imaging, PTT and

photodynamic therapy (PDT) capabilities. PDT is a light-activated clinical treatment, which causes the controlled death of diseased cells, such as tumor cells. It is based on a process in which a light sensitive drug called a photosensitizer is introduced in the cells, and is subsequently excited with light at an appropriate wavelength. The absorbed energy is transferred to the molecular oxygen present in the surroundings, generating reactive oxygen species (ROS) whose presence can trigger the death of the cells. Regarding this novel nanostructure, the surface plasmon resonance (SPR) of GNRs was tuned to 980 nm, which overlapped with the Yb^{3+} absorption. Under exposure of laser irradiation, UCNPs and GNRs could be excited simultaneously resulting in the generation of heat by the GNR with the ability to detect the temperature increment from the $NaGdF_4$:Er^{3+}, Yb^{3+} UCNPs as above. In addition, it is worth noting that luminescence enhancement was observed when compared with bare UCNPs due to the localized field created by the GNRs. Finally, a photosensitizer, zinc phthalocyanine (ZnPc), was loaded into the mesoporous silica. Under laser irradiation, UCNPs absorbed NIR light and converted it to visible light, subsequently activating the photosensitizer to release singlet oxygen for future applications in PDT. Therefore, such multifunctional nanocomposites, which are well suited for bioimaging, photothermal and photodynamic effects and show strong potential in cancer therapy.

Part II is focused on the hybrid nanocarrier consisting $NaGdF_4$:Er^{3+}, Yb^{3+} UCNPs that were encapsulated in the aqueous core of liposomes and the potential of the obtained nanocarriers for drug delivery was shown by co-loading DOX. Liposomes, which composed of a lamellar phase lipid bilayer, are considered as good candidates for drug delivery, since their structure is similar to that of cell membranes. They can be selectively

trapped by tumor tissues due to the high permeability of tumor vasculature toward liposomes in combination with the lack of proper lymphatic drainage. Therefore, liposomes have been introduced as suitable nanocarriers for UCNPs. Under 980 nm excitation, a decrease of the green upconversion emission of the UCNPs was observed when DOX was co-loaded with the UCNPs in the liposome nanocarrier. This quenching effect was assigned to the energy transfer between the donor UCNP and the acceptor DOX, and most importantly, it allowed for the spectral monitoring of the DOX loading and release from the liposome nanocarriers. Thus, the drug loading, release, and spectral monitoring properties of the obtained liposome nanocarriers were thoroughly characterized allowing us to assess their potential as bioimaging and therapeutic nanocarriers.

ACKNOWLEDGEMENTS

Foremost I would like to thank my advisors, Prof. Fiorenzo Vetrone and Prof. Federico Rosei, for continual guidance and assistance throughout the duration of my Ph.D. I thank them for their enthusiasm, advice and effort, which make this thesis a reality. Their invaluable suggestions and inspirations make me find the right direction, which allow me explore a fascinating scientific field. Being able to study under their supervision is one of the most important achievements in my life. Their attitude towards academic research has greatly motivated me to be a good researcher. I learned lots from them.

I would be also grateful to all the group members from my lab for their help throughout the work. Thanks to have been part of such a supportive, hardworking, and inspiring group of graduate students and postdoctoral fellows. These people include: Rafik Naccache, Marta Quintanilla Morales, Antonio Benayas Hernandez, Eva Hemmer, Wagner Ferreira, Joe Gerald, Artiom Skripka, Riccardo Marin, Miao Wang as well as other collaborators including Jianming Zhang at Université du Québec à Montréal, Patricia Haro González, Lucía Labrador Páez at Universidad Autónoma de Madrid.

I would like to extend my gratitude to our various collaborators. I would like to acknowledge Prof. Jerome P. Claverie at Université du Québec à Montréal and Prof. Daniel Jaque at Universidad Autónoma de Madrid for their kind help and important comments on my project research.

A massive thanks to all my friends who have made the last four years so enjoyable: Guozhu Chen, Shun Li, and Jalani Ghulam, *etc*., without you I cannot have such wonderful memories these years.

I also thank the departmental and technical staffs at INRS-EMT. They are very helpful.

I am eternally grateful to my dearest parents, who have been a constant source of love, encouragement for me. You have taught me everything I know about life and have not only been my parents but also my friends and my biggest supporters. I wish to thank to my wife, Nan Su, for your patience and love throughout this time. I thank my family and my friends for their continuing love and heartily support.

Finally, I wish to acknowledge the following organizations for their financial support to my research: the Natural Sciences and Engineering Research Council of Canada and Canada Foundation for Innovation. I also highly appreciate the Fonds de recherche du Québec-Nature et technologies (FRQNT) and the merit scholarship program for foreign students from the Ministere de l'Éducation , du Loisir et du Sport du Québec for my fellowship.

CONTENTS

Chapter 1 Introduction 1

1.1 Basics 1

1.1.1 Lanthanide ion-based luminescent nanomaterials 1

1.1.2 Upconversion luminescence 4

1.1.2.1 Excited state absorption 4

1.1.2.2 Cross-relaxation upconversion and energy transfer upconversion 5

1.1.3 Composition of upconverting nanoparticles (UCNPs) 6

1.1.3.1 Host for UCNPs 6

1.1.3.2 Sensitizers for UCNPs 7

1.1.3.3 Activators for UCNPs 7

1.2 Synthesis of UCNPs 9

1.3 UCNPs for bioapplications 10

1.3.1 UCNPs for *in vitro* and *in vivo* bioimaging 12

1.3.2 UCNPs for photodynamic therapy 14

1.3.3 UCNPs for photothermal therapy 16

1.3.4 UCNPs for drug delivery 19

1.4 UCNPs for other applications 22

1.4.1 UCNPs for thermal sensing 22

1.4.2 UCNPs for photocatalysis 24

Chapter 2 Research Objectives 28

2.1 Our objectives 28

Part I: Multifunctional nanocomposites combining UCNPs and gold nanorods (GNRs) 28

Part II: Multifunctional liposomes encapsulated UCNPs and doxorubicin 30
2.2 Thesis organization 31
Chapter 3 Experiments and Characterizations 33
3.1 Materials 33
3.2 Methods 34
3.2.1 Experimental details relevant to GNRs and GNR@SiO_2 34
3.2.1.1 Synthesis of GNRs 34
3.2.1.2 Synthesis of porous silica coated GNRs (GNR@SiO_2) 35
3.2.2 Experimental details relevant to UCNPs 35
3.2.2.1 Synthesis of UCNPs *via* hydrothermal method 35
3.2.2.1.1 Synthesis of $Y(OH)CO_3$:Er^{3+}, Yb^{3+} precursors 35
3.2.2.1.2 Synthesis of $NaYF_4$:Er^{3+}, Yb^{3+} UCNPs hollow nanoshells 36
3.2.2.2 Synthesis of UCNPs *via* the thermal decomposition method 36
3.2.2.2.1 Synthesis of $(CF_3COO)_3Ln$ (Ln = Gd, Yb, Er) precursors 36
3.2.2.2.2 Synthesis of $NaGdF_4$:Er^{3+}, Yb^{3+} UCNPs 36
3.2.2.2.3 Oleate-citrate ligand exchange 37
3.2.3 Preparation of liposome encapsulated UCNPs and doxorubicin 38
3.2.3.1 Preparation of liposome encapsulated UCNPs 38
3.2.3.2 Loading of the doxorubicin into the liposome 38
3.3 Characterization 39
3.3.1 Transmission electron microscopy (TEM), energy dispersive X-ray spectroscopy (EDX). 39
3.3.2 X-ray diffraction (XRD) 39
3.3.3 UV-Visible spectroscopy 40
3.3.4 Luminescence spectroscopy 40

Chapter 4 41
Chapter 5 51
Chapter 6 82
Chapter 7 Conclusion and Perspectives 102
7.1 Conclusions 102
7.2 Perspectives 105
7.2.1 Optimization of UCNPs properties and materials 105
7.2.2 Investigation of distance dependence of upconversion luminescence 106
7.2.3 Surface modification of UCNPs-based nanostructures 108
7.2.4 Biological experiments with a collaborator 108
References 110
Appendice B 119

LIST OF TABLES

Table 1.1 Ground state electronic configurations of the lanthanide elements [9, 10].

LIST OF FIGURES

Figure 1.1 Schematic representation of the excited state absorption process.

Figure 1.2 Schematic representation of the cross-relaxation upconversion process.

Figure 1.3 Schematic representation of the energy transfer upconversion process.

Figure 1.4 Energy level diagram for UCNPs in Yb^{3+}/Er^{3+} and Yb^{3+}/Tm^{3+} [19].

Figure 1.5 UCNPs-based multimode bioimaging [64].

Figure 1.6 Schematic diagram showing UCNPs-based targeted PDT in a mouse model of melanoma intravenously injected with UCNPs [44].

Figure 1.7 Two main strategies to bring upconversion to photothermal therapy: an upconverting nanoparticle is decorated with metal nanoparticles (left side of the particle) or a metal shell is grown around it (right side of the particle). When the UCNP is excited in the NIR, the subsequent emitted light can be absorbed by the metal and thus, be transformed into heat. On the right side of the figure a scheme of the effect of different temperatures in cells is added [62].

Figure 1.8 Schematic representations of the UCNPs-based drug delivery systems: (A) mesoporous shells, (B) hollow spheres, and (C) PEG grafted amphiphilic polymer.

Figure 1.9 (A) Intracellular temperature as a function of the applied voltage, (B) luminescence emission spectra under laser excitation as obtained at two different temperatures [90].

Figure 1.10 Energy transfer mechanism accounting for enhanced photocatalytic processes in semiconductor catalysts modified with UCNPs [98].

LIST OF CHEMICAL COMPOUNDS, ABBREVIATIONS AND SYMBOLS

Chemical compounds

ABDA	9,10-Anthracenediyl-bis(methylene)dimalonic acid
$AgNO_3$	silver nitrate
APTES	3-aminopropyltriethoxysilane
$BiFeO_3$ (BFO)	bismuth ferrite
$C_6H_8O_6$	ascorbic acid
$C_{60}MA$	monomalonic fullerene
$CO(NH_2)_2$	urea
CTAB	cetyltrimethylammonium bromide
DOPC	1,2-Dioleoyl-*sn*-glycero-3-phosphocholine
HCl	hydrochloride acid
HNO_3	nitric acid
$HAuCl_4 \bullet 3H_2O$	hydrogen tetrachloroaurate (III) hydrate
$LnCl_3$ (Ln= Y, Yb, Er)	lanthanide chlorides
Ln_2O_3 (Ln=Gd, Yb, Er)	lanthanide oxides
OA	oleic acid
ODE	octadecene
OLA	oleylamine
PEI	polyethylenimine
SiO_2	silicon dioxide
$NaBF_4$	sodium tetrafluoroborate
$NaBH_4$	sodium borohydride
ZnPc	zinc phthalocyanine

Abbreviations

CR	cross-relaxation
CT	computed tomography
DOT	diffuse optical tomography
DOX	doxorubicin hydrochloride
EDX	energy dispersive X-ray spectroscopy
EG	ethylene glycol
ESA	excited state absorption
ETU	energy transfer upconversion
EPR	enhanced permeability and retention effect
FBS	fetal bovine serum
FCC	face centered cubic
FRET	Förster resonance energy transfer
GNR(s)	gold nanorod(s)
GSA	ground state absorption
LIR	luminescence intensity ratios
LRET	luminescence resonance energy transfer
LSPR	localized surface plasmon resonance
MRI	magnetic resonance imaging
NIR	near-infrared
PBS	phosphate buffered saline
PEG	polyethylene glycol
PET	positron emission tomography
PL	photoluminescence
QD(s)	quantum dot(s)

ROS	reactive oxygen species
SP(s)	surface plasmon(s)
SPR	surface plasmon resonance
TEM	transmission electron microscopy
TPL	two-photo luminescence
UCNP(s)	upconverting nanoparticle(s)
UV	ultraviolet
XRD	X-ray diffraction

Chapter 1 Introduction

1.1 Basics

1.1.1 Lanthanide ion-based luminescent nanomaterials

Lanthanides refer to the series of metallic chemical elements with atomic numbers 57 through 71 located at the sixth period and IIIB group in the periodic table, ranging from lanthanum to lutetium. These lanthanide elements, along with the other chemical similar elements scandium and yttrium, are also known as the rare earth elements. Historically, the term “rare earth” was first named by the chemist Johan Gadolin in 1794 [1]. The rare earths were so named because of their low concentration in minerals, which were rare. However, some of the elements are neither “rare” nor “earths” [2, 3]. The lanthanides were first discovered in 1787 when a mineral was found in a town called Ytterby in Sweden [4]. The mineral was later separated into the various lanthanide elements. After that, Professor Gadolin obtained yttria (an impure form of yttrium oxide) in 1794 from the mineral [1]. Subsequently, with the development of lanthanide chemistry over two centuries, these elements have been applied in different fields including chemical industry, agriculture, and biomedicine [5-8].

The lanthanides have similarities in their electronic configuration, which presents most of their physical similarities. A summary of the electronic configurations of the lanthanides is shown in Table 1.1. These elements have electrons in the *f* orbital, which are different from the main group elements. After Lanthanum, the electron starts to fill the 4*f* sub-shell before the 5*d* sub-shell, due to the energy of the 4*f* sub-shell falls below that of the 5*d*

sub-shell. Some of the lanthanides, such as Yb^{2+}, Tb^{4+} and Ce^{4+}, may exist in the 2+, 4+ oxidation states, owing to the fact that the *f* orbital is fully, half occupied or empty, while the most common and stable lanthanide ions (Ln^{3+}) are the 3+ oxidation state. This is because the 3+ oxidation state leaves the ions in the 4*f* sub-shell and the ionization energy of the *f* electrons is large, which could be considered core-like. This stability also indicates that modification through chemical methods is highly difficult. Since the 6*s* and 5*d* electrons are drawn closer towards the nucleus resulting in the well-known lanthanide contraction effect, the *f* electrons exhibit poor nuclear charge shielding behavior. The *f* electrons are the poorest for shielding, while the *s* electrons are the best. The $5s^2$ and $5p^6$ electrons penetrate the *f* sub-shell and as the nuclear charge increases, an increase in the contraction is also observed. The shielding of the *f* electrons by their *s* and *p* counterparts has a direct impact on the magnetic and spectroscopic properties especially in the fact that they are highly uninfluenced by the ligands coordinating the lanthanide atoms. In addition, the crystal field splitting is significantly less in comparison to that of the *d* block elements. As a result, the bands in the electronic spectra of the lanthanides are very sharp showing narrow emission profiles.

Z	**Name**	**Symbol**	**Electronic outside the Ln**	**Configuration [Xe] core Ln^{3+}**	**Metallic radius pm**	**Ionic radius M^{3+} pm**	**Colour of Ln^{3+}**
57	Lanthanum	La	$5d^16s^2$	-	187	106	Colourless
58	Cerium	Ce	$4f^15d^16s^2$	$4f^1$	183	103	Colourless
59	Praseodymium	Pr	$4f^36s^2$	$4f^2$	182	101	Green
60	Neodymium	Nd	$4f^46s^2$	$4f^3$	181	100	Lilac
61	Promethium	Pm	$4f^56s^2$	$4f^4$	-	98	Yellow
62	Samarium	Sm	$4f^66s^2$	$4f^5$	179	96	Yellow
63	Europium	Eu	$4f^76s^2$	$4f^6$	204	95	Pale pink
64	Gadolinium	Gd	$4f^75d^16s^2$	$4f^7$	180	94	Colourless
65	Terbium	Tb	$4f^96s^2$	$4f^8$	178	92	Pale pink
66	Dysprosium	Dy	$4f^{10}6s^2$	$4f^9$	177	91	Yellow
67	Holmium	Ho	$4f^{11}6s^2$	$4f^{10}$	176	89	Yellow
68	Erbium	Er	$4f^{12}6s^2$	$4f^{11}$	175	88	Rose pink
69	Thulium	Tm	$4f^{13}6s^2$	$4f^{12}$	174	87	Pale green
70	Ytterbium	Yb	$4f^{14}6s^2$	$4f^{13}$	194	86	Colourless
71	Lutetium	Lu	$4f^{14}5d^16s^2$	$4f^{14}$	174	85	Colourless

Table 1.1 Ground state electronic configurations of the lanthanide elements [9, 10]

Lanthanides possess intrinsic luminescence that originates from *f*–*f* electron transitions in the 4*f* sub-shell and offer unique properties for optical imaging. Recently, much attention has been given to lanthanide luminescence when doped in inorganic hosts, in particular when the host has particle sizes in the nanometer regime. Typically, this occurs upon direct excitation into an excited state followed by emission and return to the ground state again. A suitable excitation source, which wavelength is resonant with the energy gap separating the ground and excited states, is required.

A promising method to achieve lanthanide emission is through a process known as upconversion. In brief, upconversion is a process where low energy near-infrared (NIR) excitation light is converted to higher energies covering a broad wavelength region from the ultraviolet (UV) to the visible to the NIR (with wavelengths shorter than the excitation source). In this process, upconversion is achieved by absorbing energy through two or more excitation photons to generate one emission photon, and it is characterized by the emission of light at shorter wavelengths than the excitation wavelength [11]. In particular, unlike two-photon luminescence (TPL), absorption of the photons is sequential and not simultaneous [12]. In the latter case, it requires excitation with costly ultrafast (femtosecond) pulsed lasers. The upconversion process benefits from real intermediate excited states possessing long lifetimes typically in the μs to ms range [13]. This allows for the sequential and step-wise absorption of NIR photons to achieve excitation of the final energy state followed by the generation of a higher energy photon.

Upconversion is well known to occur *via* three major mechanisms namely excited state absorption (ESA), cross-relaxation (CR) upconversion, and energy transfer upconversion (ETU). They are highlighted briefly below.

1.1.2 Upconversion luminescence

1.1.2.1 Excited state absorption (ESA)

ESA is an upconversion process, which involves only a single ion and is the successive absorption of two photons by a single Ln^{3+} ion. As shown in the Figure 1.1, if an incoming photon of a wavelength resonant with the energy gap separating ground state G and excited state E1, it will bring the ion to an intermediate excited level (E1) from the ground state (G). This phenomenon is referred to as ground state absorption (GSA). After that, due to the long lifetime of E1, a second photon promotes it to the upper emitting level (E2). The transition of electrons from E2 back to G results in the emission of a photon having higher energy than either of the photons absorbed. This is the least efficient upconversion mechanism, and this phenomenon occurs in materials having low lanthanide dopant concentrations since the distance separating them is too large for any effective interaction.

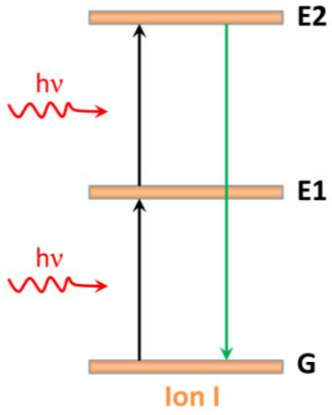

Figure 1.1 Schematic representation of the excited state absorption process.

1.1.2.2 Cross-relaxation (CR) upconversion and energy transfer upconversion (ETU)

There exist two upconversion mechanisms, which involve energy transfer between two neighbouring ions in close proximity where one ion acts as a donor of energy, while the second acts as an acceptor of energy. The first, CR upconversion, two identical ions in close proximity are both excited from the ground state (G) to intermediate excited state (E1) by GSA, then energy transfer occurs through a non-radiative process in which one ion returns to the ground state while another is promoted to the upper emitting level (E2) (Figure 1.2).

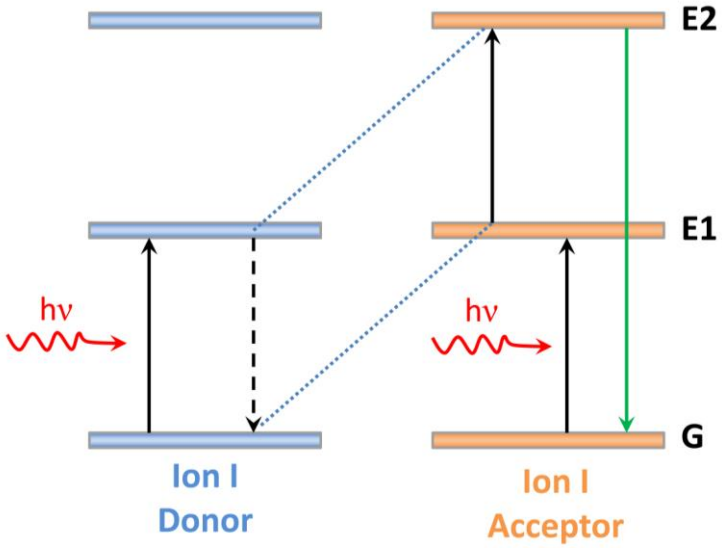

Figure 1.2 Schematic representation of the cross-relaxation upconversion process.

The second, ETU, occurs in co-doped materials, which involves the successive energy transfer from a donor ion to an acceptor ion. In this upconversion process, donor ions are excited to their intermediate states *via* GSA. Then, a non-radiative energy transfer from donor ions to the acceptor ions results in the promotion of the latter to its intermediate state. A second transfer subsequently occurs and promotes the acceptor ions to the emitting state (Figure 1.3).

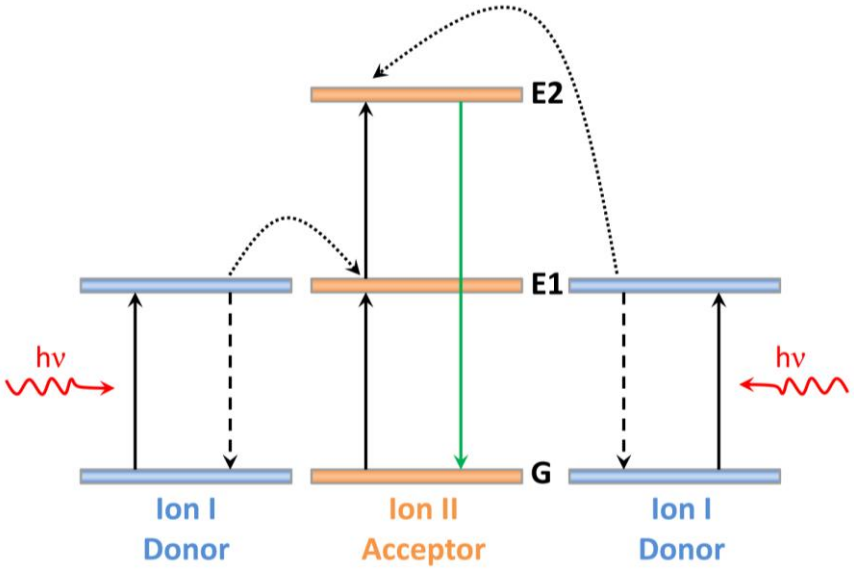

Figure 1.3 Schematic representation of the energy transfer upconversion process.

1.1.3 Composition of UCNPs

UCNPs generally consist of an inorganic host doped with Ln^{3+} ions, in which the distance between Ln^{3+} ions should be below ~10 Å to allow energy transfer, which constitutes the most efficient mechanism of upconversion. The amount and type of dopants, size and phase of nanoparticles can be tuned to achieve multiple emissions over a wide spectral range [14].

1.1.3.1 Host for UCNPs

Host materials should optimally be highly transparent in the visible and NIR regions, as well as be characterized by low energy phonons to minimize host absorption losses and maximize the luminescence output. In that regard, the best materials known to date belong to the "fluorides family", because fluorides usually exhibit low phonon energies (<500 cm^{-1}), high chemical stability and thus are often used as host materials for upconversion processes [15]. Based on this, $NaREF_4$ such as $NaYF_4$ [16-19], $NaGdF_4$ [20,

21], $NaLuF_4$ [22] has been the most popular host for lanthanide-doped UCNPs due to their relative low phonon energy and excellent chemical stability [23]. To date, there are two phase structures of $NaREF_4$ UCNPs, namely (α-) cubic phase and (β-) hexagonal phase. Generally, it is accepted that (β-) hexagonal phase is the most efficient phase due to their unique crystal structure [24].

1.1.3.2 Sensitizers for UCNPs

Regarding the ETU process, the sensitizer should possess a high absorption cross-section for the excitation wavelength and energy levels matching those of activator. In this case, Yb^{3+} is the best choice. This is because the energy level of Yb^{3+} is quite simple, with only one excited state ($^2F_{5/2}$) that is in resonance with 980 nm wavelength light. Hence, a 980 nm laser is applied as the excitation source to match the $^2F_{7/2} \rightarrow {}^2F_{5/2}$ transition of Yb^{3+}. From Figure 1.4, we can find this energy gap between $^2F_{7/2}$ and $^2F_{5/2}$ is resonant with the energy gaps between several excited states of commonly used activator ions, such as Er^{3+} *etc*. Therefore, Yb^{3+} can be considered as an excellent sensitizer to donate energy to other ions.

1.1.3.3 Activators for UCNPs

According to the ETU process, the acceptors should be characterized by energy levels homogeneously distributed, with an energy separation between them equivalent to the sensitizer emission. Once sensitizers are excited, activators are likely to extract energy from nearby excited sensitizers to promote transitions to higher energy levels. Based on these considerations, Er^{3+}, Tm^{3+} and Ho^{3+} (especially Er^{3+} and Tm^{3+}) are ideal ETU activators owing to the unique ladder-like arrangement of their energy levels [25].

Among the commonly used activators, Er^{3+} shows the highest upconversion efficiency, due to similar energy gaps from $^4I_{15/2}$ to $^4I_{11/2}$ (first transition) and $^4I_{11/2}$ to $^4F_{7/2}$ (second transition) (Figure 1.4). In Yb^{3+}-Er^{3+} co-doped UCNPs, the green and red emissions are most commonly observed under 980 nm laser irradiation. This mechanism is shown in Figure 1.4, where the green and red emissions emanate from the $^2H_{11/2}$, $^4S_{3/2}\rightarrow{}^4I_{15/2}$ and $^4F_{9/2}\rightarrow{}^4I_{15/2}$ transitions, respectively. Upon the laser irradiation, Yb^{3+} absorbs NIR photons with the generation of the $^2F_{7/2}\rightarrow{}^2F_{5/2}$ transition. Subsequently, the $^4I_{11/2}$ energy level of Er^{3+} is resonant with the $^2F_{5/2}$ level of Yb^{3+}resulting in a very efficient energy transfer process, while Yb^{3+} drops back to its $^2F_{7/2}$ ground state. Due to the energy level match, the Er^{3+} can be populated to the higher excited state ($^4F_{7/2}$, $^4F_{9/2}$ state) through similar resonant energy transfer from the sensitizer. After multiphonon relaxation to the $^2H_{11/2}$ and $^4S_{3/2}$, green emissions corresponding to 525 and 545 nm are observed to radiative decay from the $^2H_{11/2}$ and $^4S_{3/2}$ excited states to the $^4I_{15/2}$ ground state. Alternatively, the red emission at 655 nm arises from the $^4F_{9/2}$ state, which is attributed to either multiphonon relaxation from the higher $^4S_{3/2}$ state or exciting Er^{3+} ions from the $^4I_{13/2}$ state to the $^4F_{9/2}$ state *via* energy transferring from the $^2F_{5/2}$ of Yb^{3+}.

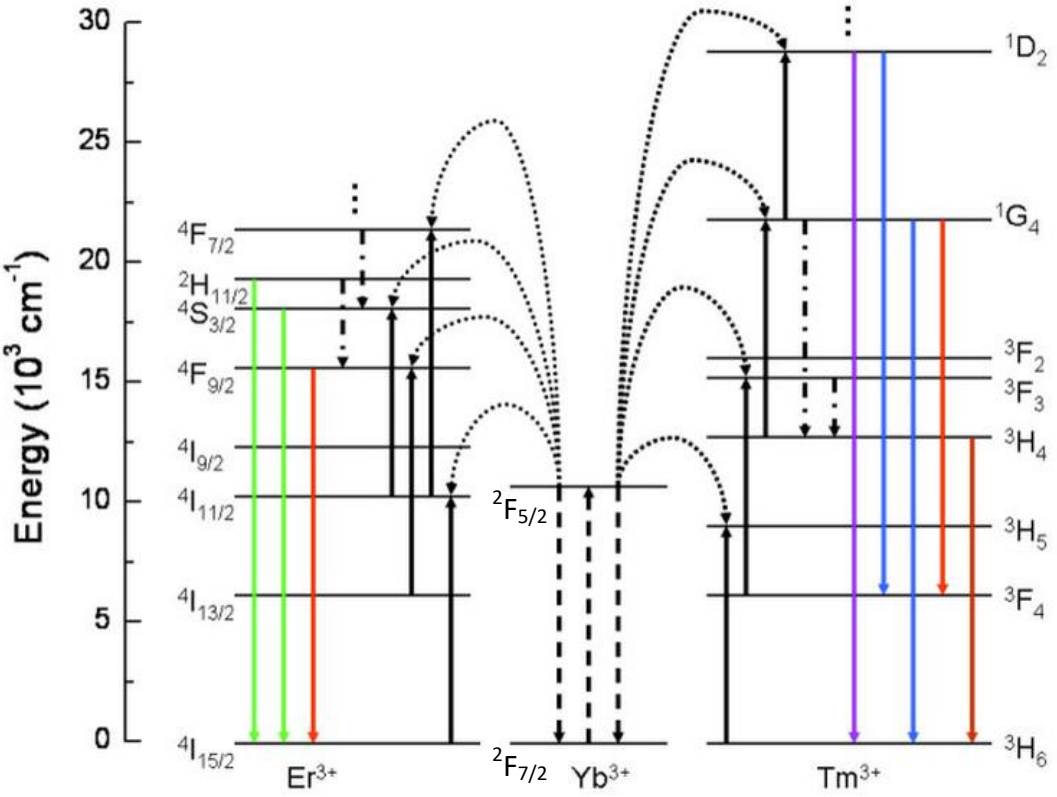

Figure 1.4 Energy level diagram for UCNPs in Yb^{3+}/Er^{3+} and Yb^{3+}/Tm^{3+} [26].

1.2 Synthesis of UCNPs

The controlled synthesis of monodispersed UCNPs is necessary for extended bioimaging and therapeutic applications. To date, several methods including thermal decomposition (thermolysis) [27, 28], hydrothermal/sovothermal [29, 30], microwave [31, 32], *etc*., have been developed. Among all these methods, thermal decomposition with metal trifluoroacetate precursors has been recognized as a common route to synthesize high quality monodisperse UCNPs with small size and narrow size distribution. Thermal decomposition refers to a chemical decomposition caused by heat. This method was first used for synthesis of highly monodisperse LaF_3 in 2005 [33]. LaF_3 triangular nanoplates

(2.0 × 16.0 nm) were synthesized by trifluoroacetate precursors $(CF_3COO)_3La$ in octadecene/oleic acid solvent. The approach was later modified and first extended to the synthesis of $NaYF_4$ nanoparticles in 2006 [27]. The $NaYF_4$ nanoparticles vary in size from 10 to 50 nm in this work. Metal trifluoroacetates were used as precursors, octadecene used as high-boiling-point organic solvent and oleylamine was used as both solvent and surfactant to prevent the aggregation of nanoparticles. In this thesis, thermal decomposition method is adapted for the synthesis of UCNPs based on our group's previous work [34].

In recent years, the synthesis of hollow UCNPs has also been developed. Based on the hollow structure, the interior cavities of UCNPs can be applied as effective tools for storage and delivery of therapeutic agents. The synthesis route of hollow UCNPs is generally divided into three categories, including hard templating synthesis, soft templating synthesis and self-templating synthesis [35]. In our group, we mainly focus on the formation of hollow structure of UCNPs through the self-templating method. Xu *et al*. utilized this method to synthesize $GdPO_4:Eu^{3+}$ hollow spheres [36], and the Gd element was also replaced by Yb in the following research [37]. This method was further optimized, and α-$NaYF_4$ hollow spheres were fabricated [38, 39].

1.3 UCNPs for bioapplications

Optical imaging techniques have been developed for biological applications. However, conventional fluorophores such as organic dyes or semiconductor quantum dots (QDs) require excitation with high energy radiation in the UV or visible region and emission at longer wavelengths [40, 41]. Excitation at these wavelengths incurs a set of

drawbacks including low penetration depth into biological tissues due to diverse absorption and scattering processes, the risk of photon induced tissue damage due to the phototoxicity of UV light, photobleaching restricting their temporal use (in organic dyes) and autofluorescence of the background resulting in low contrast. Consequently, there is specific need to develop novel optical bioprobes that overcome these limitations and eventually allow for reliable and efficient optical deep tissue *in vivo* bioimaging. Thus, UCNPs are very promising as a luminescent probe for biological applications [42-44]. The main advantage of UCNPs is the ability to be excited by NIR photons and emit range from the UV to the visible to the NIR. Compared with normal UV excited bio-probes, for example QDs, conventional organic dyes, the development of UCNPs that can be both excited as well as emit in the NIR "biological window" (700-1000 nm) could potentially overcome the limitations of traditional fluorophores. In fact these nanoparticles possess several advantages, which include (1) significantly reduced background autofluorescence from the biological structures; (2) remarkable penetration depths *in vivo*; and (3) low cyto- and phototoxicity to the biological specimen under study. For these reasons, Ln^{3+}-doped UCNPs could serve as excellent candidates for numerous biological applications.

UCNPs have demonstrated significant potential in bio-imaging and cancer therapy applications. In bio-imaging, UCNPs have been used for *in vitro* imaging [45], *in vivo* imaging [46, 47] and more recently, combination with some other bio-imaging techniques such as positron emission tomography (PET) [48] and diffuse optical tomography (DOT) [49]. UCNPs have also been studied for cancer therapy where their luminescence has been harnessed for applications such as photodynamic therapy [50, 51], photothermal therapy [52, 53] and drug delivery [54-56].

1.3.1 UCNPs for *in vitro* and *in vivo* bioimaging

Since the first successful synthesis of UCNPs around 2001 by Dang and co-workers [57], UCNPs have been widely applied to cell and small-animal imaging. Regarding *in vitro* imaging, water dispersibility and cytotoxicity is a big issue for the effective use of UCNPs. Shan *et al.* attempted to prepare hydrophobically ligated $NaYF_4$ UCNPs with amino and carboxyl groups, and their cellular cytotoxicity, cellular imaging were investigated [58]. Also, Vetrone *et al.* studied intracellular imaging of HeLa cells by using polyethylenimine (PEI) capped $NaYF_4$:Er^{3+}, Yb^{3+} UCNPs. The results showed redistribution of UCNPs inside the cell as the incubation time increased, which could have promising applications for real time imaging of cellular dynamics [59].

With regards to *in vivo* imaging, it was first reported that Caenorhabditis elegans were injected with UCNPs by Lim *et al.* [60]. In their studies, it was observed that there was strong luminescence in the intestines of the worms, and no cytotoxicity was detected over a 24 h period. However, the UCNPs used in this study were relatively large and the upconversion emission was weak. These drawbacks hinder the further applications of UCNPs for bioimaging. In 2008, Zhang *et al*. [61] selected rats as models and injected UCNPs subcutaneously. Upon laser irradiation, stronger upconversion luminescence was observed, when comparing with the control group with conventional inorganic QDs, which was also injected subcutaneously. It was further confirmed that NIR excitation provided a higher penetration depth and a higher signal-to-noise ratio than UV excitation because the excitation wavelength is located in the “biological window” of the biological tissues. In addition, it is also worth noting that these subcutaneously injected UCNPs

would be only trapped underneath the skin and did not participate in blood circulation. In fact, UCNPs intravenously injected would be more significant and clinically valuable.

Besides the bioimaging utilizing the upconversion emission, multimodal bioimaging is also studied through the combination of UCNPs and other optical image probes. For example, the computed tomography (CT), ultrasound imaging, magnetic resonance imaging (MRI) and PET could be integrated with UCNPs into one single nanoparticle for multimodal imaging [62-64] (Figure 1.5). These studies demonstrated that UCNPs could be potential candidate for multimodal bioimaging.

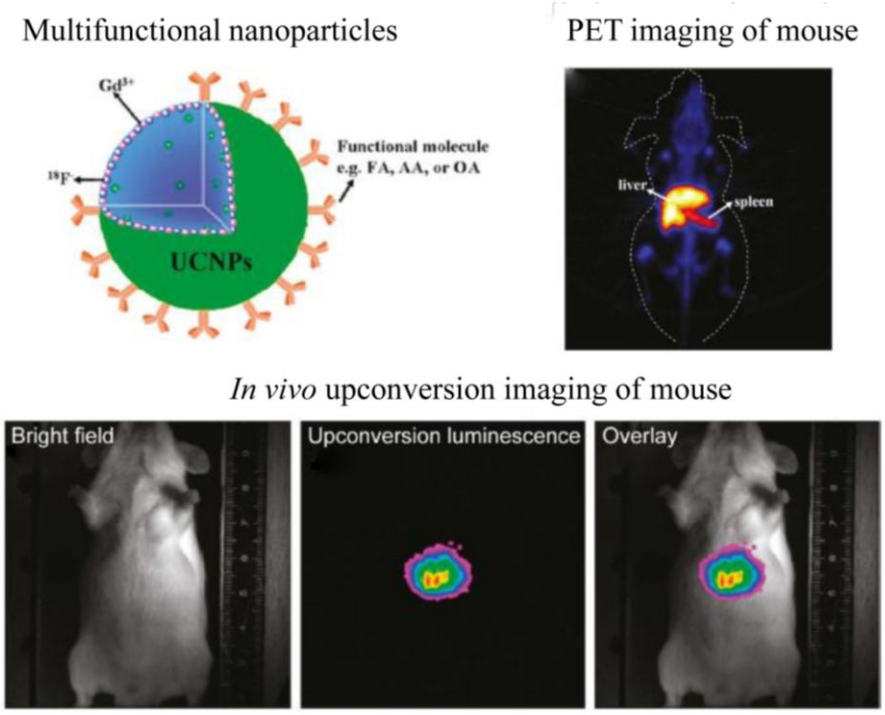

Figure 1.5 UCNPs-based multimode bioimaging [64].

1.3.2 UCNPs for photodynamic therapy

Photodynamic therapy (PDT) is a type of light-activated clinical treatment in which a light sensitive drug, called a photosensitizer, is used to cause the controlled death of viruses or diseased cells, such as cancer cells. In this process, the photosensitizer is first introduced in the cells, and then excited with light at the appropriate wavelength (depending on the specific photosensitizer but will generally be in the visible range). The absorbed energy is transferred to the molecular oxygen present in the surroundings, generating reactive oxygen species (ROS) whose presence can trigger the death of the cells [65, 66]. Although PDT is a promising therapeutic modality, already being used for numerous clinical cancer treatments, some limitations still persist, such as the need of UV or visible light to excite the photosensitizers. UV and visible light exhibit a limited penetration depth into and subsequently propagation out of biological samples not allowing for deep-tissue imaging. Recently, however, the combination of PDT drugs with UCNPs has attracted increased attention. NIR-excited UCNPs can emit UV/visible photons that can be used to activate the photosensitizers in close proximity and subsequently generate ROS to kill the surrounding cancer cells. Thus, the application of UCNPs will allow the use of NIR excitation wavelengths, increasing the penetration depth in biological tissue from ~2 mm (in the case of standard PDT) to a few centimeters. This would, for instance, allow the treatment of deeper carcinoma and extend the versatility of this therapeutic modality [67, 68]. Moreover, the possibility of specific targeting cancer cells of PDT compounds could be monitored by UCNPs localizing the diseases though fluorescence imaging**.**

Up to now, several studies have successfully combined UCNPs and PDT molecules, most of them using $NaYF_4:Er^{3+}$, Yb^{3+} as the upconverting material and different surface modifications to create a PDT system, with either one photosensitizer [69], or more, in which case their absorption bands match different upconverted emissions of the UCNPs [51]. The first work combing UCNPs and PDT was published by Zhang *et al.* [65]. In their study, UCNPs were coated by a silica layer where PDT molecules were incorporated and their results demonstrated the concept works. However, depending on the photodynamic drug selected, other dopant ions could also be considered as good alternatives. Indeed, it has been demonstrated that an improvement of energy transfer between the UCNP and the PDT compound can be achieved using additional lanthanide ions as dopants. Following this idea, X.M. Liu *et al*. prepared core-shell $NaYF_4$ nanoparticles with Tm^{3+}/Yb^{3+} in the core (mainly emitting blue light) and Er^{3+}/Yb^{3+} in the shell (mainly emitting green light). They used the emitted light to activate monomalonic fullerene ($C_{60}MA$), a novel PDT drug that stands out because of its high quantum yield to form reactive species, and that has a broad absorption band. $C_{60}MA$ was covalently conjugated to the UCNPs by a crosslinking reaction between the amino group of the UCNPs and the carboxyl group of $C_{60}MA$. In this work, the efficiency of the resulting structure *in vitro* as well as the increased effect obtained thanks to the addition of Tm^{3+}/Yb^{3+} dopants to the UCNPs was demonstrated [70]. To date, the fast progress of UCNPs-based PDT and *in vitro* successful results also motivated the start of *in vivo* treatments and long-term toxicity experiments using these nanostructures [51] (Figure 1.6).

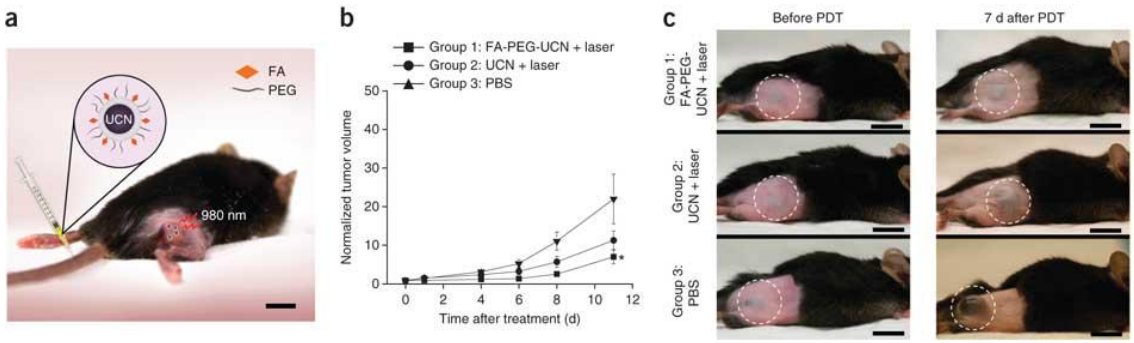

Figure 1.6 Schematic diagram showing UCNPs-based targeted PDT in a mouse model of melanoma intravenously injected with UCNPs [51].

1.3.3 UCNPs for photothermal therapy

Photothermal therapy (PTT) is a treatment strategy based on the damage that high temperatures can produce in cells (Figure 1.7), *i.e.* it uses heat to kill cancer cells [71]. Like PDT, PTT also has the advantage of allowing for the selectivity of cancer cells, so that surrounding healthy cells and tissue would not be subjected to harmful effects [72]. In order to generate a temperature increase in the cells, a highly efficient mechanism is to transfer it from a light source, more conveniently a laser (due to its high power, monochromaticity and easy position control), through optical absorption. Therefore, nanoparticles with a high optical absorption coefficient and thermal dissipation rate would increase the PTT efficiency.

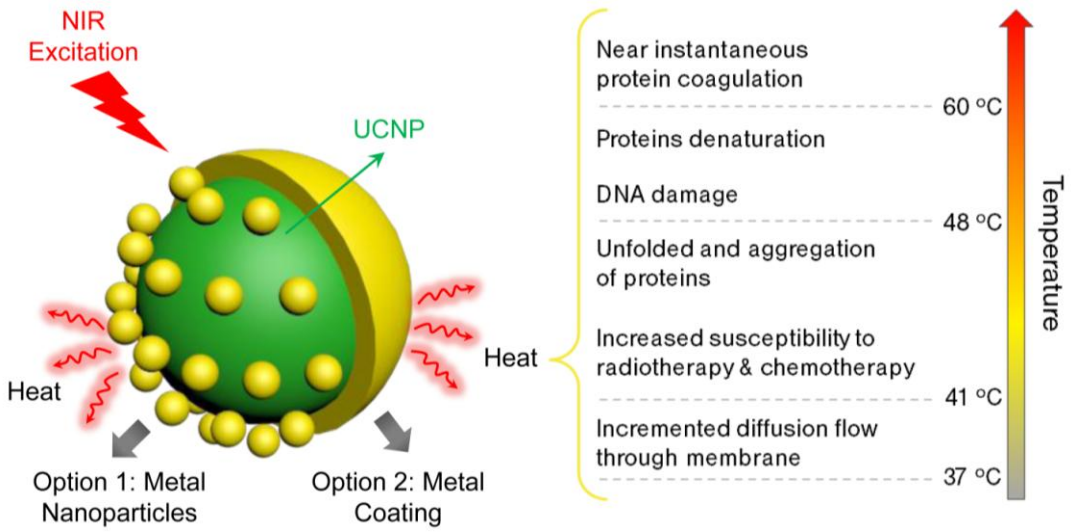

Figure 1.7 Two main strategies to bring upconversion to photothermal therapy: an UCNP is decorated with metal nanoparticles (left side of the particle) or a metal shell is grown around it (right side of the particle). When the UCNP is excited in the NIR, the subsequent emitted light can be absorbed by the metal and thus, be transformed into heat. On the right side of the figure, a scheme of the effect of different temperatures in cells is added [73].

Noble metals, such as gold or silver, are considered as excellent candidates for PTT due to their strong surface plasmon resonance (SPR) absorption that can be followed by light emission and, more importantly here, heat release. SPR is the resonant oscillation of conduction electrons at the metal interface stimulated by incident light. These nanoparticles often have the SPR in the visible range, although for certain morphologies it can get down to the NIR. Particularly, gold nanospheres, that are especially convenient due to ease of synthesis, have the SPR absorption band located in the green/yellow spectral range, though the exact wavelength can be tuned by changing the particle size. Consequently, Er^{3+} doped UCNPs that emit green light after NIR excitation, can be used to excite gold nanoparticles and thus to bring the advantages of NIR excitation (higher

penetration depth and minimized heat transfer along the laser path) to PTT. Also, the PTT nanoparticle-based approach could be further improved with the addition of UCNPs allowing for imaging the location of the cancer cells or monitoring cellular events, which is not possible using only the metal nanostructures.

This option has been explored by several groups [74]. A particularly nice example was given by Qian *et al*. that prepared gold decorated UCNPs ($NaYF_4$:Er^{3+}, Yb^{3+}/$NaYF_4$/silica (core/shell/shell)) applying a reverse microemulsion method [75]. They observed that the total emission intensity of gold decorated UCNPs decreased compared with that of simple UCNPs. Absorption of the luminescence from gold nanoparticles, which triggered a temperature increase, was indeed one of the reasons for this emission decrease. However, a second effect was also pointed out to explain the intensity decrease: NIR light penetration into the particles could be smaller due to the presence of gold, so the excitation light reaching UCNPs would be weaker. Nevertheless, *in vitro* data illustrated that BE(2)-C cancer cells were effectively killed after irradiation with the laser at 980 nm, proving that UCNPs can be used as antennas for the radiation. The decrease of emission intensity can be avoided through, as when a gold nanostructure is excited to its plasmon resonance, it generates an electromagnetic field in its surroundings that can actually enhance the emission intensity of the particles in this area. However, the emission enhancement strongly depends on the design of the nanostructure [76]. Na Niu *et al.*, for instance, developed mesoporous upconversion nanocomposites with 5 nm diameter gold nanoparticles integrated onto the surface. Meanwhile, an anticancer drug, doxorubicin (DOX) was selected and loaded in the mesoporous structure. In their case, upon laser irradiation, enhancement of upconversion intensity was observed

owing to the effect of the plasmonic field created by the gold nanoparticles. In addition, the green emission generated by the upconversion nanocomposite could be used to trigger photothermal effect through energy transfer to the gold nanoparticles, as well as rapid drug release [77].

1.3.4 UCNPs for drug delivery

Another area of recent application of upconversion in therapy is targeted drug delivery. Current drug delivery systems are based on different nanostructures (nanoparticles, liposomes, micelles, dendrimers, nanoemulsions, *etc.*) [78] with a size distribution in the range between 10 and 100 nm to prevent the clearance by the reticulo-endothelial system [79] and thus, keeping them in the bloodstream for a longer time [80]. The properties of these nanostructures can be improved, though, through optical tagging, to visualize their distribution *in vivo*, and thus, monitor the efficacy of the treatment. For this reason, UCNPs have emerged as an interesting element in drug delivery nanosystems, participating in monitoring drug location and studying the interaction with other cellular components.

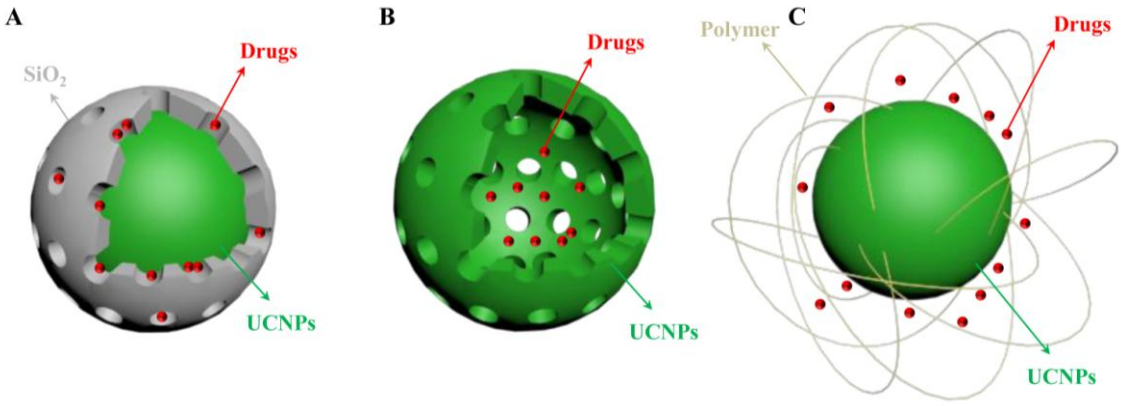

Figure 1.8 Schematic representations of the UCNPs-based drug delivery systems: (A) mesoporous shells, (B) hollow spheres, and (C) PEG grafted amphiphilic polymer.

Generally, drug delivery systems consist of a porous shell to load the drug and slowly release it in a rate normally regulated by diffusion or, alternatively, by the erosion of the shell. Because of the biocompatibility of silica materials, silanization is to date one of the most popular techniques for surface modification. In the case of UCNPs, a common strategy is to encapsulate them in a mesoporous silica shell, where the drug can be loaded through capillarity (Figure 1.8A). With the help of this shell, the potential application of UCNPs would be extended. The UCNP core can act as a luminescence imaging probe, and the porous shell can load drugs for localized therapy. An example is the work by Yang *et al*. using LaF_3:Er^{3+}/Yb^{3+} UCNPs with a silica shell and Ibuprofen as the model drug, which was observed to be totally released after 72h [81]. It is stated that this type of shell exhibits a high surface area, and the loading and drug diffusion capabilities are controlled by the size of the pores, which are advantageous properties to design a drug carrier. Moreover, it has been shown through intracellular analysis that this nanomaterial is non-toxic, which motivates further research following this path [82]. Parallel nanoplatforms have been developed using the $NaYF_4$ host material instead. Also in this case, drug storage and *in vitro* release was demonstrated [83, 84].

An alternative strategy to the use of mesoporous silica shells is the use of hollow spheres made out of UCNPs encapsulating the drug (Figure 1.8B). The first challenge to follow such structures is the preparation of the hollow spheres, and thus, several techniques have been proposed. For example, the group of J. Lin followed a self-sacrificing method to prepare upconversion hollow spheres [37]. They synthesized core-shell structured $Yb(OH)CO_3$@$YbPO_4$:Er^{3+} hollow spheres ($\sim$380 nm size), and showed that DOX loaded spheres, that release the drug in 24 h, maintain the Er^{3+} luminescence and have

more cytotoxicity than free DOX on HeLa cells [37]. Applying a surface-protected "etching" and hydrothermal ion-exchange process, $Yb(OH)CO_3:Yb^{3+}/Er^{3+}$ spheres can be used as templates to form hollow mesoporous $NaYF_4:Yb^{3+}/Er^{3+}$ nanospheres, a more efficient upconversion material whose surface can be later modified with folic acid for targeted delivery [39]. A similar evolution of the structure was observed in a study by Ruichan *et al*., where GdF_3 hollow shells were successfully prepared without any surfactant and catalyst [85].

In addition to UCNPs coated with mesoporous silica and to the use of upconverting hollow spheres, a third strategy has been applied for drug delivery with upconversion. This is, to coat the UCNPs with an amphiphilic polymer (Figure 1.8C), which allows to transfer hydrophobic UCNPs into the biological environment. The group of Z. Liu prepared polyethylene glycol (PEG) grafted amphiphilic polymer encapsulating UCNPs, modified the surface with folic acid to improve cancer targeting, and loaded DOX *via* physical adsorption [54]. In agreement with the results found working with hollow spheres, they found that drug release is affected by environmental pH, it being larger in acidic media. Following this path and aiming for controlled drug delivery, pH-sensitive polymers attracted the attention of the community and some nanoplatforms using them have been recently developed. Good examples are the use of TWEEN 80 [86] or poly(acrylicacid)-modified UCNPs [87], both showing optimal properties as carriers and pH dependent drug release. An alternative for controlled drug release is the use of a light-responsive copolymer. After excitation at 980 nm, the UCNP emitted UV light that triggered the light-responsive amphiphilic copolymer shell uncaging the upconversion nanocomposites, resulting in the release of anticancer drugs [88]. Recently, liposome,

which used to deliver cytotoxic drugs or genes, provides a multitude of innovative approaches for pharmaceutical and biomedical applications based on the encapsulation of nanostructures, such as QDs, metallic nanoparticles, or iron oxide [89-92]. In our group, we also developed the liposomes co-encapsulated $NaGdF_4$:Er^{3+}, Yb^{3+} UCNPs and the anticancer drug DOX for simultaneous bioimaging and therapeutic applications [93].

1.4 UCNPs for other applications

1.4.1 UCNPs for thermal sensing

In recent years, luminescence nanothermometry has emerged as a novel technique which is used to detect the local temperature of a living cell with sub-micrometric spatial resolution. Luminescence is the emission of light from a given substance, which depends on the properties of electronic states. These, in turn, depend on the local temperature and thus the relationship between temperature and luminescence properties can be exploited to achieve thermal sensing from the spatial and spectral analysis of the luminescence. Luminescence nanothermometry can be obtained based on the particular parameter of luminescence which is analyzed, the examples encompass temperature-dependent emission intensity and/or lifetime of organic dyes [94, 95], semiconducting QDs [96-101] and UCNPs [102-107], *etc*.

To date, there are several examples demonstrating that the intensity of the intra-4*f* transitions and of the lifetime of a particular 4*f* excited state are temperature dependent. Therefore, UCNPs can be considered as promising candidates used for nanothermometry. The upconversion luminescence mostly depends on the energy separation between the energy levels of the lanthanide ions. If this energy separation is small, then the electrons

will thermally populate and re-distribute among energy levels with similar energy, according to the Boltzmann distribution:

$$R = C \times \exp(\frac{-\Delta E}{kT})$$

where R represents the luminescence intensity ratios between the emissions with proximity of energy levels, C is a constant, ΔE is the energy gap between the two excited states, k is the Boltzmann constant and T is the temperature. Based on the Boltzmann distribution, if the two energy states are very close to each other, small temperature changes can induce large population re-distributions. The most studied UCNP-based thermometer uses the Yb^{3+}/Er^{3+} ion pair [108-112]. The Yb^{3+} ions were excited under laser irradiation at 980 nm, followed by energy transfer to nearby Er^{3+} ions [25]. Finally, green emission occurring from the $^2H_{11/2}$ and $^4S_{3/2}$ excited states to the $^4I_{15/2}$ ground state as well as red emission from the $^4F_{9/2}$ excited state to the $^4I_{15/2}$ ground state is observed. Since the states of two green emissions are very close in energy (typically separated by only several hundred cm^{-1}), the lower energy $^4S_{3/2}$ state will thermally populate the higher $^2H_{11/2}$ state. As the temperature of the surroundings increase, the probability of the lower ($^4S_{3/2}$) state thermally populating the higher ($^2H_{11/2}$) state increases causing a change in the relative intensities of the two emission bands ($^2H_{11/2} \rightarrow {}^4I_{15/2}$ and $^4S_{3/2} \rightarrow {}^4I_{15/2}$). Thus, by exploiting the intensity ratio of these two emissions, it is possible to use Er^{3+}-doped materials as ratiometric thermal sensors. Single-cell thermal sensing based on $NaYF_4:Er^{3+}$, Yb^{3+} UCNPs was demonstrated by Vetrone *et al*. [59]. It was reported that UCNPs could homogeneously distribute in living cells without causing any remarkable toxicity [113]. Intracellular thermal sensing was achieved by incubating UCNPs in living

HeLa cells, which were exposed to laser irradiation. The optical transmission image of a single HeLa cell is shown in Figure 1.9A when different voltages were applied to a metallic plate in physical contact with the cell. Cell temperature was obtained from the changes of the relative intensities of luminescence bands (see Figure 1.9B). Based on the proper analysis of these changes, intracellular temperature in the 25–45 ℃ range with a sub-degree resolution as a function of the applied voltage could be monitored.

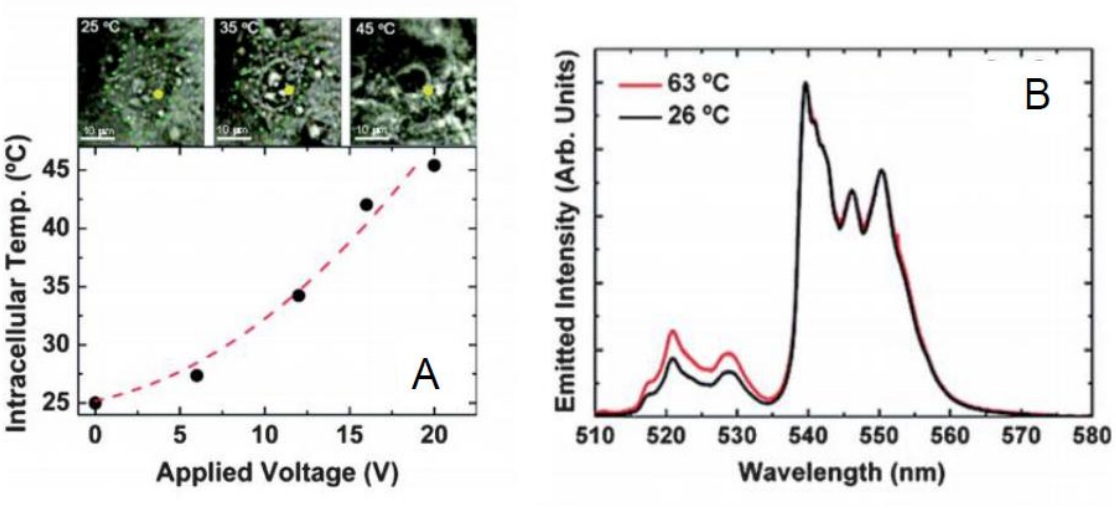

Figure 1.9 (A) Intracellular temperature as a function of the applied voltage, (B) luminescence emission spectra under laser excitation as obtained at two different temperatures [106].

1.4.2 UCNPs for photocatalysis in emerging energy applications

Aside from the application of UCNPs in biology and nanomedicine mentioned above, they have also recently been studied for implementation for use in alternative energy applications such as photovoltaics [114, 115] or photocatalysis [116-118]. The latter is a chemical reaction between organic species and free radicals generated from photocatalysts under light irradiation from the UV to NIR. It is a significant technology which can meet goals of sustainable energy development *via* unlimited access to clean

solar energy. The basic mechanism of photocatalysis is shown in Figure 1.10 based on a semiconductor to generate free radicals (*e.g.* •OH and $•O^{2-}$). To date, the energy conversion efficiency which is an ongoing research process is far from satisfactory since they only respond to a relatively small fraction of the solar photons with energy higher than the threshold bandgap (E_g) of the system. To boost the conversion efficiency, the outstanding optical properties of UCNPs have generated increasing interest for photocatalyst application. UCNPs have the ability to convert lower energy NIR excitation light to higher energy photons, covering a broad wavelength region from the UV to the visible to the NIR *via* the previously discussed upconversion process. The converted UV or visible emission can be recaptured and reused by photon acceptors, such as oxide semiconductors. In addition, they can transform two (or more) sub-bandgap NIR photons into one usable above-bandgap photon, hence minimizing non-absorption energy losses [115, 119].

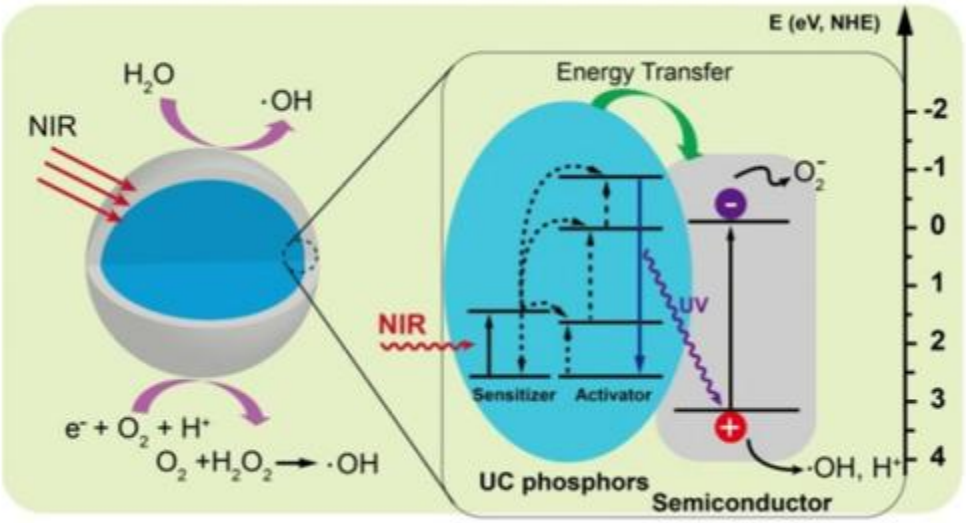

Figure 1.10 Energy transfer mechanism accounting for enhanced photocatalytic processes in semiconductor catalysts modified with UCNPs [119].

The first report for upconversion materials used for photocatalysis can be dated back to 2005, when Wang *et al.* developed the first visible photocatalyst, based on a combination of Er_2O_3 upconversion materials with TiO_2 [120]. From then on, significant progress has been made. To date, several studies have been demonstrated that by hybridizing with UCNPs (*e.g.*, $NaYF_4$:Tm^{3+}, Yb^{3+}), conventional oxides, *e.g.*, TiO_2, becomes NIR light active in photocatalysis, as the NIR illumination was converted into UV photons by UCNPs [121-123]. During this process, excellent photocatalytic activity was achieved *via* energy transfer between the UCNPs and TiO_2, and thus allowing the efficient realization of upconversion effects in photocatalysis. Recently, bismuth ferrite ($BiFeO_3$), which is one of the most important multiferroic materials, has been considered as a good candidate for photocatalysis [124-128]. With a bandgap of ~2.0-2.6 eV (*vs* 3.0-3.2 eV for TiO_2), $BiFeO_3$ (BFO) exhibits excellent response both to UV and visible light [129, 130]. Therefore, an appropriate combination of UCNPs with BFO is expected to yield efficient photon harvesting from the visible to NIR spectral ranges for application. In our group, we prepared UCNP@BFO core@shell hybrid nanostructures for visible-NIR photocatalysis and demonstrate that they are active for the photodegradation of organic compounds under visible and NIR irradiation [131]. The good response of the BFO shell is highly beneficial to capture visible light in a wide spectral range, and the intimate contact between the UCNP core and BFO shell results in the UCNPs and BFO acting as energy donors and energy acceptors, respectively, where the upconverted green emission is partially absorbed by the BFO. The efficient non-radiative energy transfer occurs between UCNP and BFO, thus opening the door to broad-spectrum highly active photocatalysis. While this work is not included in the thesis, this material can also have

applications in biomedicine as UCNPs@TiO_2 hybrid nanomaterials have been used for applications in PDT [132, 133].

Chapter 2 Research Objectives

2.1 Our objectives

This thesis is divided into two parts with two corresponding objectives:

Part I: Multifunctional nanocomposites combining UCNPs and GNRs

So far, UCNPs have been shown to be efficient and versatile tools for bioapplications. One of the most interesting applications is the use of UCNPs as optical nanothermometers. The majority of UCNP nanothermometers are based on the temperature dependent luminescence where their luminescence intensity ratios vary as a function of temperature. These types of nanothermometers open the door for therapeutic possibilities for many diseases, where a local temperature increases to thermally induced death. Based on this, these nanothermometers are envisioned to combine with local nanoheaters whose principle role is to cause contained temperature increases in order to induce cell death. During this process, GNRs are considered as excellent candidates for nanoheaters, owing to their strong, tunable SPR absorption between 650 and 1200 nm, especially when the plasmon is located in the NIR, making it compatible for *in vivo* applications. The GNRs absorb light causing electrons to undergo transitions from the ground state to the excited state. The electronic excitation energy subsequently results in an increase in the kinetic energy, which leads to the overheating of the local environment around the light absorbing species. Therefore, local cells or tissue could be destroyed by the heat produced. Recently, PTT using the localized SPR bands of gold nanoparticles and the UCNPs has been reported. However, there are still some considerable challenges and issues that need to be addressed. For example, the surrounding healthy cells could be

damaged due to the temperature increase along with the diseased cells. Therefore, care must be taken to obtain accurate control over the local temperature increment so as to not expose the surrounding healthy cells to this localized heating. To accomplish this, the nanoheaters could be coupled with a nanothermometer but must be located in the same cellular space. Hence, they should be transported together in the same vehicle. Thus, thermal sensing with UCNPs could be used for controlling the PTT treatment, which would minimize collateral damage in healthy tissues surrounding the hyperthermia target. Therefore, the nanocomposite could not only be well suited for bioimaging, but also can potentially be used for applications where a thermal gradient must be generated and monitored by a thermometer. In particular, a molecular drug could be also loaded in these nanocomposites, and the drug release behavior could be enhanced by the heat generated from the GNRs. This would result in a multi-pronged or multi-modal nanocomposite capable of delivering two therapeutic modalities.

Therefore, the objectives for this part are as follow:

1. Preparing and characterizing novel multifunctional nanocomposites combining UCNPs and GNRs.
2. Investigating the luminescence intensity ratio of UCNPs as a function of temperature and using it to detect temperature changes of nanocomposites under laser irradiation.
3. Comparing the UCNPs luminescence before and after combining GNRs and analyzing the GNRs influence on luminescence changing.
4. Model drugs were selected and loaded into the nanocomposites, drug release profiles were evaluated.

Part II: Multifunctional liposomes encapsulated UCNPs and doxorubicin (DOX)

Liposomes are artificially prepared nanocarriers composed of a lamellar phase lipid bilayer. They are considered as good candidates for drug administration due to the fact that their structure is similar to that of cell membranes. Great potential for dramatically enhanced biocompatibility, reduced toxicity and improved therapeutic efficacy has been reported for liposome-based drug delivery. Recently, in the context of liposome-based nanocarriers, research reports have shown that the encapsulation of nanostructures, such as QDs, metallic, or iron oxide nanoparticles within liposomes provides a multitude of innovative approaches for pharmaceutical and biomedical applications. However, their use as delivery systems for various types of nanoparticles is still in the research stage. In particular for liposome encapsulated UCNPs, the data are still scarce, and further studies on the design, characterization, and application of liposome encapsulated UCNPs are required to develop their application in biomedicine. Therefore, we constructed a liposome co-encapsulated UCNPs and DOX, which combined optical imaging and therapeutic modalities. Both UCNPs and DOX were distributed in the internal aqueous phase of the liposomes because of their hydrophilic nature. Meanwhile, because there is a partial spectra overlap between the absorption spectrum of DOX and the upconverted green emission of the UCNPs in the wavelength region from 510 to 570 nm, the UCNPs and DOX molecules act as energy donors and energy acceptors, respectively. Luminescence resonance energy transfer (LRET) would occur based on the close distance between UCNPs and DOX, which could further used for highly sensitive, real-time drug release monitoring system. Therefore, this liposome nanocarrier encapsulated

with UCNPs and DOX could be used for multimodal biomedicine, involving the simultaneous detection and therapy of disease.

Therefore, the objectives for Part II are:

1. Preparing and characterizing liposome encapsulated UCNPs and DOX.
2. Investigating the UCNPs luminescence and analyzing the influence of UCNPs luminescence by DOX loading.
3. Using the luminescence intensity of UCNPs to monitor drug release by quantitatively investigating LRET from UCNPs to DOX.

2.2 Thesis organization

This thesis is divided into seven chapters and organized as follows:

Chapter 1 Introduction: briefly introducing the basic concepts of the background;

Chapter 2 Research objectives: presenting the motivation and main goals of this thesis;

Chapter 3 Experiments and characterization: describing experimental details of synthesis processes of GNRs, UCNPs and liposomes. The main characterization techniques are also described in this chapter;

Chapter 4 GNR@UCNPs multifunctional nanocomposites used for photothermal therapy and drug delivery, and the publication related to this chapter is

Y. Huang, F. Rosei, F. Vetrone. A single multifunctional nanoplatform based on upconversion luminescence and gold nanorods. *Nanoscale*, 2015; 7(12): 5178-85 [53].

Chapter 5 GNR@SiO_2@UCNPs multifunctional nanocomposites used for photothermal and photodynamic therapy, and the publication related to this chapter is

Y. Huang, L. L. Páez, P. H. González, D. Jaque, F. Rosei, F. Vetrone. Upconverting nanoparticles used as multifunctional nanocomposites combining with photothermal and photodynamic effects. *In preparation*.

Chapter 6 Liposome encapsulated UCNPs and DOX used for bioimaging and drug delivery, and the publication related to this chapter is

Y. Huang, E. Hemmer, F. Rosei, F. Vetrone. Multifunctional liposome nanocarriers combining upconverting nanoparticles and anticancer drugs. *J. Phys. Chem. B.* 2016; 120(22): 4992-5001 [93].

Chapter 7 Conclusions and perspectives: concluding the main results and discussing some prospective potential investigations in future work.

Most of work in this thesis was done by Yue Huang, however, some parts were conducted through collaboration. More specifically, cellular assays were performed by Lucía Labrador Páez, Dr. Patricia Haro González working with our collaborator Prof. Daniel Jaque's group at Universidad Autónoma de Madrid. UCNPs used in chapter 6 were provided by Dr. Eva Hemmer in our group, who also assisted with the PL measurements.

Following the main body of this thesis is an appendix containing a summary of this thesis in French according to INRS policy.

Chapter 3 Experiments and Characterizations

In this chapter, experimental details for the synthesis, characterization of GNRs, UCNPs and liposomes are described. The first section mainly introduces the synthesis of GNRs at different SPR absorption (660 nm and 980 nm), and then GNRs were coated with a layer of silica. The second section focuses on the synthesis of UCNPs using different methods. In order to obtain the UCNPs nanoshell, we first used the hydrothermal method to prepare UCNPs and further coated the GNRs in the core to form the GNR@UCNPs core@shell structure nanocomposites (chapter 4). We also synthesized the UCNPs *via* the thermal decomposition method. Moreover, the oleate-capped UCNPs were further transferred to water through ligand exchange, and the oleate ligand was replaced by the sodium citrate molecule. The last section focuses on the liposome preparation. We prepare the liposomes using the thin-film hydration method and encapsulate the water dispersible UCNPs in the aqueous core of the liposomes, DOX was further loaded into the liposomes *via* an ammonium sulfate gradient method.

3.1 Materials

The lanthanide chlorides ($LnCl_3$ (99.99%), Ln = Y, Yb, Er), lanthanide oxides (Ln_2O_3 (99.99%), Ln = Gd, Yb, Er), trifluoroacetic acid (99%), sodium trifluoroacetate (98%), oleic acid (90%), 1-octadecene (90%), hydrogen tetrachloroaurate (III) hydrate ($HAuCl_4 \cdot 3H_2O$), silver nitrate ($AgNO_3$, >99%), L-ascorbic acid ($C_6H_8O_6$, >99%), 5-bromosalicylic acid (>98.0%), zinc phthalocyanine (ZnPc, 95%), doxorubicin hydrochloride (DOX) were purchased from Alfa Aesar. Cetyltrimethylammonium bromide (CTAB), sodium tetrafluoroborate ($NaBF_4$), sodium salicylate (99%),

polyethylenimine (PEI), urea [$CO(NH_2)_2$], sodium borohydride ($NaBH_4$, 99.99%), oleylamine (70%), cholesterol (≥99%), fetal bovine serum (FBS), phosphate buffered saline (PBS, pH=7.4), 3-aminopropyltriethoxysilane (APTES, 99%), 9,10-anthracenediyl-bis(methylene)dimalonic acid (ABDA), Triton^{TM} X-100 were purchased from Sigma Aldrich. 1,2-Dioleoyl-*sn*-glycero-3-phosphocholine (DOPC, >99%) was acquired from Avanti Polar Lipids. Ultrapure deionized water (Millipore system) was used throughout the experiments. All the starting chemicals in this work were used without further purification.

3.2 Methods

3.2.1 Experimental details relevant to GNRs and GNRs@SiO_2

3.2.1.1 Synthesis of GNRs

The seed solution for GNRs was prepared as reported previously [134]. A 5 mL of 0.5 mM $HAuCl_4 \cdot 3H_2O$ was mixed with 5 mL of 0.2 M CTAB solution. After that, 0.60 mL of ice-cold 0.010 M $NaBH_4$ was added under vigorous stirring, which resulted in a color change from yellow to brownish-yellow. The seed solution was kept at room temperature before use.

For the growth solution preparation, 0.36 g of CTAB together with defined amounts of additives was dissolved in 10 mL of deionized water. When this solution was kept at 30 ℃, 4 mM $AgNO_3$ was added and kept undisturbed for 15 min. Subsequently, 10 mL of 1 mM $HAuCl_4$ was added. After 15 min of slow stirring, 0.064 M ascorbic acid was slowly added to the mixture. The final step was the addition of 32 μL of the seed solution

to the growth solution causing a gradual color change of the solution. The temperature of the growth solution was kept constant at 30 ℃ during the entire procedure.

3.2.1.2 Synthesis of porous silica coated GNRs (GNR@SiO_2)

To remove excess CTAB surfactant, the synthesized GNRs were washed by centrifugation to remove excess CTAB. The sample was dispersed in 10 mL of deionized water. After that, 100 μL of 0.1 M NaOH was added. Following this step, three 30 μL injections of 20% TEOS in methanol were added under gentle stirring at 30 min intervals. The mixture was reacted for 2 days.

3.2.2 Experimental details relevant to UCNPs

3.2.2.1 Synthesis of UCNPs *via* hydrothermal method

3.2.2.1.1 Synthesis of $Y(OH)CO_3:Er^{3+}$, Yb^{3+} precursors

The monodisperse $Y(OH)CO_3:Er^{3+}$, Yb^{3+} colloidal nanospheres were prepared *via* a urea-based homogenous precipitation process. In total, 1 mmol of $LnCl_3$ (Y : Yb : Er = 78 : 20 : 2) and 2 g of urea were dissolved in 100 mL of deionized water. The above solution was homogenized under magnetic stirring for 10 min. Subsequently, the mixture was heated to 90 ℃ for 2 h with vigorous stirring. Finally, the obtained $Y(OH)CO_3:Er^{3+}$, Yb^{3+} nanospheres were collected and washed with deionized water and ethanol several times. The preparation of GNR@SiO_2@$Y(OH)CO_3:Er^{3+}$, Yb^{3+} was similar to the above procedure except for the addition of 0.05 g of GNR@SiO_2 (synthesized previously) to the starting lanthanide chloride/urea solution.

3.2.2.1.2 Synthesis of $NaYF_4:Er^{3+}$, Yb^{3+} UCNPs hollow nanoshells

The obtained $Y(OH)CO_3:Er^{3+}$, Yb^{3+} nanospheres were dispersed in 20 mL of deionized water using an ultrasonic bath. Then, 0.25 g PEI was added into the above solution followed by ultrasonication and stirring. After that, 1 mmol of $NaBF_4$ was added into the above mixture with continuous stirring for 10 min and the obtained solution was transferred to a 25 mL Teflon autoclave (VWR) and kept at 110 ℃ for 3.5 h. The resulting dispersions were separated by centrifugation, washed with water, and then dried at 80 ℃ for 12 h. A similar procedure was performed to prepare GNR@UCNPs nanocomposites by replacing $Y(OH)CO_3:Er^{3+}$, Yb^{3+} samples with $GNR@SiO_2@Y(OH)CO_3:Er^{3+}$, Yb^{3+}.

3.2.2.2 Synthesis of UCNPs *via* the thermal decomposition method

3.2.2.2.1 Synthesis of $(CF_3COO)_3Ln$ (Ln = Gd, Yb, Er) precursors

In a typical synthesis of the lanthanide trifluoroacetate precursors, 0.975 mmol (353.4 mg) Gd_2O_3, 0.25 mmol (98.5 mg, 20 mol% doping rate) Yb_2O_3 and 0.025 mmol (9.6 mg, 2 mol% doping rate) Er_2O_3 were mixed in a 100 mL three-neck round-bottom flask with 5 mL distilled water and 5 mL trifluoroacetic acid, followed by refluxing under magnetic stirring at 80 ℃ until a clear solution was obtained. Subsequently, the temperature was reduced to 60 ℃ in order to evaporate the residual trifluoroacetic acid and water. The dried precursor was isolated in form of a colorless powder.

3.2.2.2.2 Synthesis of $NaGdF_4:Er^{3+}$, Yb^{3+} UCNPs

For the synthesis of $NaGdF_4:Er^{3+}$, Yb^{3+} UCNPs, 2.5 mmol (340 mg) sodium trifluoroacetate as well as 20 mL 1-octadecene, 10 mL oleic acid and 10 mL oleylamine

were added to the obtained $(CF_3COO)_3Ln$ precursor. Subsequently, the mixture was degased for 30 min at 100 ℃ under vacuum and under magnetic stirring. The reaction mixture was then heated to 240 ℃ under stirring and gentle argon flow and maintained at this temperature for 2 h. Subsequently, the solution was allowed to cool to room temperature and the resultant oleate-capped UCNPs were precipitated with ethanol and collected by centrifugation. The obtained product was washed three times with hexane/ethanol (4:1) and dispersed in 5 mL hexane as stock solution.

3.2.2.2.3 Oleate-citrate ligand exchange

In order to obtain water dispersible UCNPs, ligand exchange was carried out as previously described in the literature [135]. 60 mg of oleate-capped $NaGdF_4:Er^{3+}$, Yb^{3+} UCNPs obtained from the previous step were dispersed in 5 mL of hexane, and mixed with 5 mL of a 0.2 M trisodium citrate buffer (adjusted to pH 4). The mixture was kept on a shaker for 3 h, and subsequently transferred into a separation funnel, from which the aqueous phase containing the UCNPs was collected. The UCNPs were precipitated with acetone (1:5 aqueous:organic ratio), collected by centrifugation and re-dispersed in 5 mL of trisodium citrate buffer (adjusted to pH 7). The dispersion was placed on the shaker for an additional 2 h. Finally, the UCNPs were precipitated with acetone, washed three times with acetone and water, collected by centrifugation and dispersed in 2 mL water for further experiments.

3.2.3 Preparation of liposome encapsulated UCNPs and DOX

3.2.3.1 Preparation of liposome encapsulated UCNPs

Liposomes were prepared by a thin-film hydration method according to the literature [136]. For the blank liposomes, a mixture of 0.025 mmol of DOPC and 0.0125 mmol of cholesterol was dissolved in a 5 mL solution of chloroform and methanol (4:1 v/v). In the subsequent drying step (30 min at 40 ℃), which was carried out in a rotary evaporator (Büchi, Switzerland), the lipid film was formed. The obtained lipid film was flushed with argon and maintained overnight in a desiccator to remove any residual traces of chloroform. In the following step, the lipid film was hydrated by use of 2 mL of PBS, followed by vortexing and sonication at 30 ℃ for 10 min, resulting in a homogeneous suspension of blank liposomes.

To encapsulate $NaGdF_4:Er^{3+}$, Yb^{3+} UCNPs in liposomes, the lipid film was hydrated with 60 mg of UCNPs in 2 mL of PBS, followed by vortexing and sonication as described earlier. The final suspension (UCNPs encapsulated in liposomes) was further purified by centrifuging at 4,000 rpm for 10 min to remove non-entrapped UCNPs followed by filtering through a 0.22 μm pore size membrane to discard any larger residues.

3.2.3.2 Loading of the DOX into the liposome

DOX was loaded into the liposome nanocarrier *via* an ammonium sulfate gradient method [137]. Briefly, the previously prepared lipid film was hydrated by adding 250 mM ammonium sulfate with or without 60 mg of UCNPs, sonicated with a bath type sonicator at 30 ℃, followed by passing it through a Sephadex G-50 column for desalting. The sample was then mixed with 0.005 mmol of DOX (5:1 lipid:DOX molar ratio) and

incubated at 30 ℃ for 30 min. Non-entrapped DOX was removed by a Sephadex G-50 column, while non-entrapped UCNPs was removed by slow centrifugation. Finally, the loading efficiency of DOX was determined by using absorption spectroscopy at a wavelength of 480 nm after lysis of the liposome using 1% Triton^{TM} X-100.

3.3 Characterization

3.3.1 Transmission electron microscopy (TEM), energy dispersive X-ray spectroscopy (EDX).

TEM is used to directly observe the morphology and size of the nanostructures. The chemical composition of the nanomaterials can be easily identified using EDX, inside a TEM apparatus. In order to perform these measurements, a small drop of solution containing the nanomaterials was deposited onto a Cu grid coated with a thin (5-50 nm in thickness) carbon film, and excess solution was wicked away by a filter paper. The grid was subsequently dried in air and observed with a JEOL-2100F TEM (Université de Montréal, Montréal, Canada). Meanwhile, the EDX spectra was measured at different locations on the sample. Particle size was determined by measuring more than 50 individually dispersed particles identified in TEM images.

3.3.2 X-ray diffraction (XRD)

XRD is a method used for determining the atomic and molecular structure of a crystal, in which the crystalline atoms cause a beam of X-rays to diffract into many specific directions. Incident X-rays are scattered by a crystalline sample according to Bragg's law:

(Eq. 3.1) $$n\lambda = 2d\sin\theta$$

where λ is the wavelength of the X-ray beam, θ is the incident angle, and d is the distance between crystal planes. The value for d is dependent on the Miller indices h, k and l. In this thesis, the measurements of powdered samples were analyzed by XRD (Bruker D8 Advanced Diffractometer, Cu Kα radiation).

3.3.3 UV-Visible spectroscopy

A UV-Visible spectrophotometer (Varian 5000) was used to measure the absorption spectra of GNRs to identify their SPR peak features at room temperature in 10 mm PMMA semi-microcuvettes. The scan speed was set to 600nm/min. For the measurement of GNRs samples, all spectra were collected over the range of 400-1200 nm. All experimental data was corrected for background absorption by water.

3.3.4 Luminescence spectroscopy

Luminescence spectroscopy is used to measure the luminescence properties of UCNPs under 980 nm laser excitation which using a Thorlabs fiber-coupled laser diode (maximum power 330 mW). The laser beam was focused on the sample using a lens to obtain a spot with a Gaussian intensity distribution with a 0.4 mm diameter. The emitted light was collected by a lens in a 90 ° configuration, and then transferred to a spectrophotometer (Avaspec - 2048L - USB2) using an optical fiber.

DOI : 10.1039/c4nr07369j

Chapter 4

A single multifunctional nanoplatform based on upconversion luminescence and gold nanorods

Yue Huang, Federico Rosei, Fiorenzo Vetrone

Nanoscale, 2015, 7, 5178-5185.

As introduced in Chapter 1, UCNPs have emerged as efficient and versatile optical nanoprobes with potential in biological applications. This stems primarily from their ability to convert NIR excitation light to higher energy photons spanning the UV-visible-NIR regions. Over the last few years, there has been intense research for their applications as luminescent nanothermometers, spawned by our initial manuscript on $NaYF_4:Er^{3+}$, Yb^{3+} as non-invasive and non-contact optical nanothermometers for living cancer cells. This came about as several of the luminescent transitions of the lanthanides are sensitive to temperature. Similarly, GNRs with their LSPR have been actively studied for applications in photothermal treatment of various cancers due to their great ability to convert optical light to heat. Yet, one of the major drawbacks of this technique is the propensity to destroy healthy cells in the surroundings due to the lack of control over the temperature, *i.e.* real-time temperature monitoring. In this paper, we combine the positive attributes of both nanomaterials, the GNRs for optical heating and the UCNPs for temperature monitoring, a novel multifunctional core/shell nanocomposite based on gold nanorods (GNRs) in the core and a nanoshell of upconverting $NaYF_4:Er^{3+}$, Yb^{3+} material.

The GNRs in the core were prepared using the seeded growth method possessing an LSPR at *ca.* 660 nm, which overlaps well with the red upconversion luminescence from the $^4F_{9/2}$ excite state of the Er^{3+} ion. A temperature gradient can be created *via* the absorption of the upconverted red light from the GNR core. Given the remarkable thermal sensitivity of the upconverted green luminescence of the Er^{3+} ion, the temperature change owing to rapid heat conversion from the GNR could be determined using the luminescence intensity ratios (LIR) of the two green emission bands of the Er^{3+} ion.

Finally, to further illustrate the notion of multimodality, a model anticancer drug was loaded in this nanocomposite and the drug release efficiency was evaluated. It is worth noting that the release efficiency could be enhanced by the photothermal effect (when the laser was on), especially at low pH values, which is favorable in a tumor microenvironment.

Chapter 5

Multifunctional nanocomposites based on upconverting nanoparticles with combined photothermal and photodynamic effects

Yue Huang, Luc á Labrador P áez, Patricia Haro Gonz ález, Daniel Jaque, Federico Rosei, Fiorenzo Vetrone

In preparation.

As introduced in Chapter 1, UCNPs are well known for their ability to emit photons of shorter wavelength than the excitation light, which covering a broad wavelength region from the UV to the visible to the NIR *via* a process commonly referred to as upconversion. These outstanding optical properties of UCNPs have resulted in increasing interest for their bioimaging and therapeutic applications. Recently, it was reported that UCNPs have the ability to form the luminophores for sensing temperature, which temperature exerts an individual effect on the intensity of each emission peaks of UCNPs (depending on dopant ions). Thus, the use of UCNPs as nanothermometry has been highlighted. In addition, GNRs have been intense studied as ideal nanostructures for cancer thermotherapy because of their highly photothermal conversion efficiency. In this paper, we tried to construct a novel multifunctional nanocomposite combining both nanomaterials together. GNRs were used for temperature heating, and UCNPs were applied for real-time temperature monitoring.

The GNRs were prepared and coated with mesoporous silica shell, the SPR was tuned to *ca.* 980 nm which overlaps well with the Yb^{3+} absorption. Under laser irradiation, both

UCNPs and GNRs could be simultaneously excited. GNRs create a localized electromagnetic field that enhanced the emission intensity from UCNPs. In addition, the temperature could be measured *via* thermally sensitive luminescence from the LIR of the two green emission bands of Er^{3+}.

Then, Zinc phthalocyanine (ZnPc), a photodynamic molecule, was further loaded into the porous silica layer. Upon excitation by the laser, luminescence quenching occurred after ZnPc loading, especially the red emission dropped by 54%. It might attribute to the overlap of red emission of UCNPs at 660 nm and the absorption of ZnPc at 665 nm, the energy transfer from the UCNPs to ZnPc molecule, which further activate the ZnPc to release reactive oxygen species (ROS) to kill cancer cells.

Finally, cellular experiments were performed, the results of the absence of cytotoxicity and cellular imaging in the incubated cell make it excellent biocompatible nanocomposites.

Multifunctional Nanocomposites Based on Upconverting Nanoparticles with Combined Photothermal and Photodynamic Effects

Yue Huang[a], Luc á Labrador P áez[b], Patricia Haro Gonz ález[b], Daniel Jaque[b], Federico Rosei[a,c,d], Fiorenzo Vetrone[a,c,d]*

[a]*Institut National de la Recherche Scientifique - Énergie, Mat ériaux et T él écommunications, Universit é du Qu ébec, Varennes J3X 1S2 Qu ébec, Canada*

[b]*Fluorescence Imaging Group, Departamento de F ísica de Materiales, Facultad de Ciencias, Universidad Aut ónoma de Madrid, Madrid, Spain*

[c]*Centre for Self-Assembled Chemical Structures, McGill University, Montr éal, Canada*

[d] *Institute for Fundamental and Frontier Science, University of Electronic Science and Technology of China, Chengdu, PR China*

Abstract

Lanthanide-doped upconverting nanoparticles (UCNPs) are well known in biological applications due to their unique optical properties by converting near-infrared (NIR) light to visible light. Combining with a variety of therapeutic models based on the UCNPs has become a new concept to get diagnostics and therapies in the field of cancer treatment. Herein, we develop a novel multifunctional nanocomposite consisting of UCNPs, gold nanorods (GNRs) and photosensitizers, with highly integrated functionalities including luminescence image, photothermal effect and photodynamic effect. Under exposure of laser irradiation, UCNPs and GNRs could be excited simultaneously, owing to the surface plasmon resonance (SPR) of the GNRs was overlap with the Yb^{3+} absorption at 980 nm. The ratio of intensity of green emission of UCNPs is sensitive to temperature, which can be used to calculate the temperature change due to heat production from the GNRs. Furthermore, the luminescence enhancement is observed when compared with bare UCNPs, this is because localized field created by the GNRs influence the luminescence intensity of UCNPs. Finally, a photosensitizer, zinc phthalocyanine, was loaded into the mesoporous silica. Upon the laser irradiation, UCNPs absorbed NIR light to convert to visible light, subsequently activate the photosensitizer to release singlet oxygen for killing cancer. Therefore, such multifunctional nanocomposite, which not only well suited for bioimaging, but also providing photothermal and photodynamic effects, shows strong potential in cancer therapy.

1. Introduction

In recent years, lanthanide (Ln^{3+})-doped upconverting nanoparticles (UCNPs) have been investigated for a plethora of applications in biomedicine. In particular, significant research has focused on their use as multifunctional nanoplatforms with combined therapeutic and diagnostic (theranostic) modalities [1-3]. The rising interest in UCNPs stems from their unorthodox excitation schemes where these nanoparticles can be excited with near-infrared (NIR) light and ultimately emit higher energy photons spanning the ultraviolet (UV), visible and NIR regions *via* a multiphoton excitation process, known as upconversion [4, 5]. The upconverted (or anti-Stokes) luminescence of UCNPs is advantageous when compared with conventional fluorescence (Stokes) from other nanomaterials for several reasons. The NIR excitation light causes minimal photodamage, induces practically no autofluorescence background, and can penetrate tissues to a much greater extent [6, 7]. As an added benefit, some of the upconverted Ln^{3+} emission bands are sensitive to the surrounding temperatures allowing them to be effectively used thermal nanoprobes (nanothermometer). One of the most well-known examples of an optical nanothermometer exploits the temperature sensitive green emissions of the Er^{3+} ion. The two emission bands emanating from the $^{2}H_{11/2}$ and $^{4}S_{3/2}$ excited states of Er^{3+} are sensitive to temperature and the relative intensity of these bands change as a function of temperature. Consequently, Er^{3+}-doped UCNPs have been used as non-contact, non-invasive optical nanothermometers for living cells [8, 9].

In parallel to research on UCNPs, a significant body of work has focused on applying the heat generation capabilities of certain nanostructures, such as noble metal nanoparticles, for the photothermal therapy of cancer (also known as hyperthermia). Metal nanoparticles

possess a high optical absorption coefficient and thermal dissipation rate, which is desired for high efficiency photothermal therapy (PTT) since they could efficiently convert photon energy into heat following laser irradiation of their surface plasmon resonance (SPR), the resonant oscillation of conduction electrons at the metal interface, subsequently resulting in the controlled death of surrounding cells [10, 11]. Among metal nanostructures for PTT, gold nanorods (GNRs) are considered to be one of the most promising and versatile platforms [12-14]. GNRs with fine-tuned optical properties show excellent photothermal conversion effects and generate localized hyperthermia, since GNRs have higher surface-to-volume ratio which more efficiently involved in heating process [15]. However, the use of excess cetyltrimethylammonium bromide (CTAB) as bilayer stabilizer around the surface of the GNRs during the preparation of GNRs would restrict their clinical application, because of the cytotoxicity caused by CTAB [16]. Therefore, surface functionalization of GNRs has been investigated for a wide variety of nanomedicine-based diagnostic and therapeutic approaches [17]. Mesoporous silica is one of the excellent options and has been successfully used to encapsulate GNRs. This mesoporous coating not only reduces the cytotoxicity and aggregation of GNRs, but also imparts drug (or cargo) loading ability and also provides an excellent scaffold for subsequent surface functionalization [18, 19].

The marriage of these two optically excited nanostructures onto a single nanoplatform could lead to additional functionalities. For instance, controlling temperature in hyperthermia applications is a critical factor preventing healthy cells from also being destroyed (and consequently inducing severe side effects) [20]. Thus, coupling the nanoheaters with a “built-in” nanothermometer would minimize the possibly of

destroying healthy tissue surrounding the hyperthermia target and accordingly, the patient's side effects. In addition, when UCNPs and GNRs are in close proximity, it was demonstrated that their interaction could influence the luminescence intensity of UCNPs. For example, if the SPR of GNRs was tuned to the excitation frequency of UCNPs, the local field would become much larger and the luminescence intensity will be enhanced [21]. For this enhancement to occur, the distance between plasmonic metal nanoparticles and UCNPs is critical and using SiO_2 as spacer, for example, would influence the luminescence intensity [22, 23].

We developed a novel class of multifunctional nanocomposite based on the combination of UCNPs with GNRs, prepared through layer by layer. The GNR core is decorated with $NaGdF_4$:Er^{3+}, Yb^{3+} UCNPs and the two species are separated by as silica (SiO_2) shell. This multifunctional nanocomposite is ideal for controlled photothermal heating since both the nanoheaters (GNRs at the core) and the nanothermometers (UCNPs decorated on the surface) can be excited at 980 nm. To add additional functionality, zinc phthalocyanine (ZnPc), a model photodynamic therapy (PDT) drug, was loaded into the mesoporous layer, which has been shown to have high cytotoxic efficiency in cancer cells due to singlet oxygen generation following light excitation [24, 25]. ZnPc and its analogues are usually excited with visible light, which limits its deployment in clinical cancer treatment due to the limited penetration depth of the excitation light. UCNPs can overcome this inherent drawback since they can convert NIR light to visible light, which can then be absorbed by the photosensitizer (ZnPc), to release singlet oxygen for killing cancer cells. Here, we investigate the luminescence properties of these new GNR@SiO_2@UCNPs nanoplatforms and study their ability for controlled

photoheating/nanothermometry and photodynamic effects. Finally, the cytotoxicity and cellular uptake of this nanocomposite were further investigated. The multifunctional nanocomposite developed here could not only be well suited for bioimaging, but also multi-pronged cancer therapeutics through the combination of PTT and PDT effects.

2. Experimental Section

2.1 Materials

The lanthanide oxides (Ln_2O_3 (99.99%), Ln = Gd, Yb, Er), trifluoroacetic acid (99%), sodium trifluoroacetate (98%), oleic acid (90%), 1-octadecene (90%), hydrogen tetrachloroaurate (III) hydrate ($HAuCl_4 \cdot 3H_2O$), cetyltrimethylammonium bromide (CTAB, 98%), silver nitrate ($AgNO_3$, >99%), L-ascorbic acid ($C_6H_8O_6$, >99%), 5-bromosalicylic acid (>98.0%), zinc phthalocyanine (ZnPc, 95%) were purchased from Alfa Aesar. Sodium borohydride ($NaBH_4$, 99.99%), 3-aminopropyltriethoxysilane (APTES, 99%), 9,10-anthracenediyl-bis(methylene)dimalonic acid (ABDA), Triton^{TM} X-100 were purchased from Sigma Aldrich. Ultrapure deionized water (Millipore system) was used throughout the experiments. All the initial chemicals in this work were used without further purification.

2.2 Synthesis of $(CF_3COO)_3Ln$ (Ln = Gd, Yb, Er) precursors

In a typical synthesis of the lanthanide trifluoroacetate precursors, 0.975 mmol (353.4 mg) Gd_2O_3, 0.025 mmol (9.6 mg, 2 mol% doping rate) Er_2O_3, and 0.25 mmol (98.5 mg, 20 mol% doping rate) Yb_2O_3 were mixed in a 100 mL three-neck round-bottom flask with 5 mL distilled water and 5 mL trifluoroacetic acid, followed by refluxing under magnetic stirring at 80 ℃ until a clear solution was obtained. Subsequently, the temperature was reduced to 60 ℃ in order to evaporate the residual trifluoroacetic acid and water. The dried precursor was isolated in form of a colorless powder.

2.3 Synthesis of $NaGdF_4:Er^{3+}, Yb^{3+}$ UCNPs

For the synthesis of $NaGdF_4:Er^{3+}$, Yb^{3+} UCNPs, 2.5 mmol (340 mg) sodium trifluoroacetate as well as 20 mL 1-octadecene, 10 mL oleic acid and 10 mL oleylamine were added to the obtained $(CF_3COO)_3Ln$ precursor. Subsequently, the mixture was degassed for 30 min at 100 ℃ under vacuum and under magnetic stirring. The reaction mixture was then heated to 240 ℃ under stirring and gentle argon flow and maintained at this temperature for 2 h. Subsequently, the solution was allowed to cool to room temperature and the resultant oleate-capped UCNPs were precipitated with ethanol and collected by centrifugation. The obtained product was washed three times with hexane/ethanol (4:1) and dispersed in 5 mL hexane as stock solution.

2.4 Oleate-citrate ligand exchange

In order to obtain water dispersible UCNPs, ligand exchange was carried out as previously described in literature [26]. 60 mg of oleate-capped $NaGdF_4:Er^{3+}$, Yb^{3+} UCNPs obtained from the previous step were dispersed in 5 mL of hexane, and mixed with 5 mL of a 0.2 M trisodium citrate buffer (adjusted to pH 4). The mixture was kept on a shaker for 3 h, and subsequently transferred into a separation funnel, from which the aqueous phase containing the $NaGdF_4:Er^{3+}$, Yb^{3+} was collected. The UCNPs were precipitated with acetone (1:5 aqueous:organic ratio), collected by centrifugation and re-dispersed in 5 mL of trisodium citrate buffer (adjusted to pH 7). The dispersion was placed on the shaker for an additional 2 h. Finally, the UCNPs were precipitated with acetone, washed three times with acetone and water, collected by centrifugation and dispersed in 2 mL water for further experiments.

2.5 Preparation of gold nanorods (GNRs)

The seed solution for GNRs was prepared as reported previously [27]. A 5 mL of 0.5 mM $HAuCl_4$ was mixed with 5 mL of 0.2 M CTAB solution. After that, 0.60 mL of ice-cold 0.010 M $NaBH_4$ was added under vigorous stirring, which resulted in color changed from yellow to brownish-yellow. The seed solution was kept at room temperature before use.

For the growth solution preparation, 0.36 g of CTAB together with 0.044 g of 5-bromosalicylic acid was dissolved in 10 mL of deionized water. When this solution was kept at 30 ℃, 0.60 mL of 4 mM $AgNO_3$ was added and kept undisturbed for 15 min. Subsequently, 10 mL of 1 mM $HAuCl_4$ was added, and 0.084 mL HCl (37 wt.%) was added. After 15 min of slow stirring, 80 μL of 0.064 M ascorbic acid was slowly added to the mixture. The final step was the addition of 32 μL of the seed solution to the growth solution causing a gradual color change of the solution. The temperature of the growth solution was kept constant at 30 ℃ during the entire procedure.

2.6 Preparation of silica coated GNRs (GNRs@SiO_2)

To remove excess CTAB surfactant, the synthesized GNRs were washed by centrifugation and the sample was dispersed in 10 mL of deionized water. After that, 100 μL of 0.1 M NaOH was added. Following this step, three 30 μL injections of 20% TEOS in methanol were added under gentle stirring at 30 min intervals. The mixture was reacted for 2 days.

2.7 APTES functionalized GNR@SiO_2

The solution of GNR@$SiO_2$was centrifuged and suspended in ethanol, and then 20 μL of APTES was added and mixed by gentle shaking for another 6 h to accomplish the aminolization. Finally, this sample was centrifuged and washed with ethanol.

2.8 UCNPs attachment to GNR@SiO_2

The APTES functionalized GNR@SiO_2 was added dropwise to the solution of UCNPs under vigorous stirring. After 2 h, the final products (GNR@SiO_2@UCNPs) were centrifuged out, and then redispersed either in ethanol or water for further characterization.

2.9 Measurement of singlet oxygen ($^1O_2$)

The $^1O_2$ production is detected by singlet oxygen sensors such as 9,10-anthracenediyl-bis(methylene) dimalonic acid (ABDA) [28], different samples in phosphate buffer (0.1 M, pH 7-7.4) was mixed with ABDA (1 mM) and placed in a cuvette. The solution was irradiated by a 980 nm laser for different periods of time, and the generation of $^1O_2$ results in the bleaching of ABDA absorption at 380 nm.

2.10 Cellular viability

The cell viability was investigated in HeLa cells. The cells were seeded onto 96-well plates with a density of 1×10^4 cells per well and incubated for 24 h. After cell attachment, different samples were added to the wells and subsequently incubated at 37 ℃ for an additional 48 h. Cell viability was measured using the 3-(4,5-dimethylthiazol-2-yl)-2,5-diphenyltetrazolium bromide (MTT) assay [29].

2.11 Cellular imaging

Following incubation of cancer cells on glass-bottomed dishes containing culture medium at 37 ℃ for 24 h, different samples were added to each dish and incubated for another 2 h at 37 ℃. The medium was then removed and cells were washed with ice cold PBS

followed by fixing with 4% paraformaldehyde in PBS. After fixing, the fluorescent images of the cells were analyzed with a 980 nm diode laser.

2.12 Characterization

The crystalline phase of all nanostructures under investigation was analyzed by X-ray diffraction (XRD, Bruker D8 Advanced Diffractometer, Cu Kα radiation). The morphology and size distribution of the GNRs and UCNPs were determined with a Philips CM200 high resolution transmission electron microscope (HR-TEM), equipped with an energy-dispersive X-ray (EDX) unit. The UV-Visible (UV-VIS) spectra were obtained using a UV-VIS spectrometer (Varian 5000). Luminescent measurements were carried out under 980 nm excitation using a laser diode. The laser beam was focused on the sample using a lens to obtain a spot with a Gaussian intensity distribution with a 0.4 mm diameter. The emitted light was collected by a lens in a 90° configuration, and then transferred to a spectrophotometer (Avaspec-2048L-USB2) using an optical fiber. Cellular imaging was investigated by using a home-made confocal microscope under diode laser excitation at 980 nm. The collected luminescence at 660 nm was collimated and after passing several filters was spectrally analyzed by a monocromator (iH320, Horiba) attached to a high sensitivity Si CCD camera (Synapse, Horiba).

3. Results and discussion

3.1 Preparation and characterization of GNR@SiO_2@UCNPs

To prepare a novel multifunctional nanocomposite based on UCNPs and GNRs with combined optical, photodynamic and photothermal properties useful in theranostics, the nanocomposite was prepared through layer-by-layer. Moreover, the mesoporous silica (SiO_2) layer separating the UCNPs decorated on the surface and the GNR core has a dual role. First, it acts as a spacer between the plasmonic nanostructure (GNR) and the fluorescent species (UCNPs) leading to minimal luminescence quenching and potentially, plasmonic enhancement. Second, the pores could be loaded with photosensitizer molecules capable of converting the upconverted visible radiation to reactive oxygen species (*i.e.* $^1O_2$) adding another modality to the nanoplatform. To accomplish this, a multistep synthetic method was proposed and summarized in Scheme 1, and described in detail in the Experimental section. Firstly, $NaGdF_4:Er^{3+}$, Yb^{3+} UCNPs were synthesized by the previously described thermal decomposition method [30]. As seen in the Fig.1A, the synthesized UCNPs were monodisperse and uniform with an average diameter of approximately 6.5 nm. The HR-TEM image of the UCNPs is shown in the Fig. 1B and the lattice fringes can be clearly observed with a spacing of ~0.275 nm, ~0.317 nm assigned to the {200}, {111} plane of cubic (α-) phase $NaGdF_4:Er^{3+}$, Yb^{3+} UCNPs, respectively. This result is consistent with XRD studies (Fig. 2B) which confirmed that the UCNPs crystallized in the α-phase, and no impurity crystalline phase was found in the diffraction pattern. Separately, GNRs were prepared according to previously published protocol [31] and their morphology as well as size were shown by means of TEM (Fig. 1C). It is clearly observed that GNRs with an average of 72 nm in length and 12 nm in

diameter were synthesized successfully, yielding an aspect ratio of approximately 6:1. To characterize their absorption properties, a key parameter in the photogeneration of heat, their SPR was investigated using UV-VIS absorption. We observed that there are two SPR absorptions around 525 and 972 nm, owing to the transverse absorption and longitudinal absorption, respectively (Fig. 2A). Subsequently, the SiO_2 layer was grown on the surface of the GNRs according to the previous protocol [32]. In this process, the CTAB served as the organic template for the formation of the mesoporous SiO_2 layer with a thickness of *ca.* 15 nm (see Fig. 1D), offering the opportunity for the loading of the therapeutic photosensitizer molecules. Following the growth of SiO_2 layer, the longitudinal SPR of the GNR@SiO_2 nanostructures exhibits a small red-shift (~11 nm), and is now located at 983 nm (Fig. 2A). The electric fields distribution surrounding the surface of the GNR and the GNR@SiO_2 was simulated and summarized in Fig. S1 in the supporting information.

Scheme 1 Schematic illustration of the synthetic procedure for the GNR@SiO_2@UCNPs nanocomposite

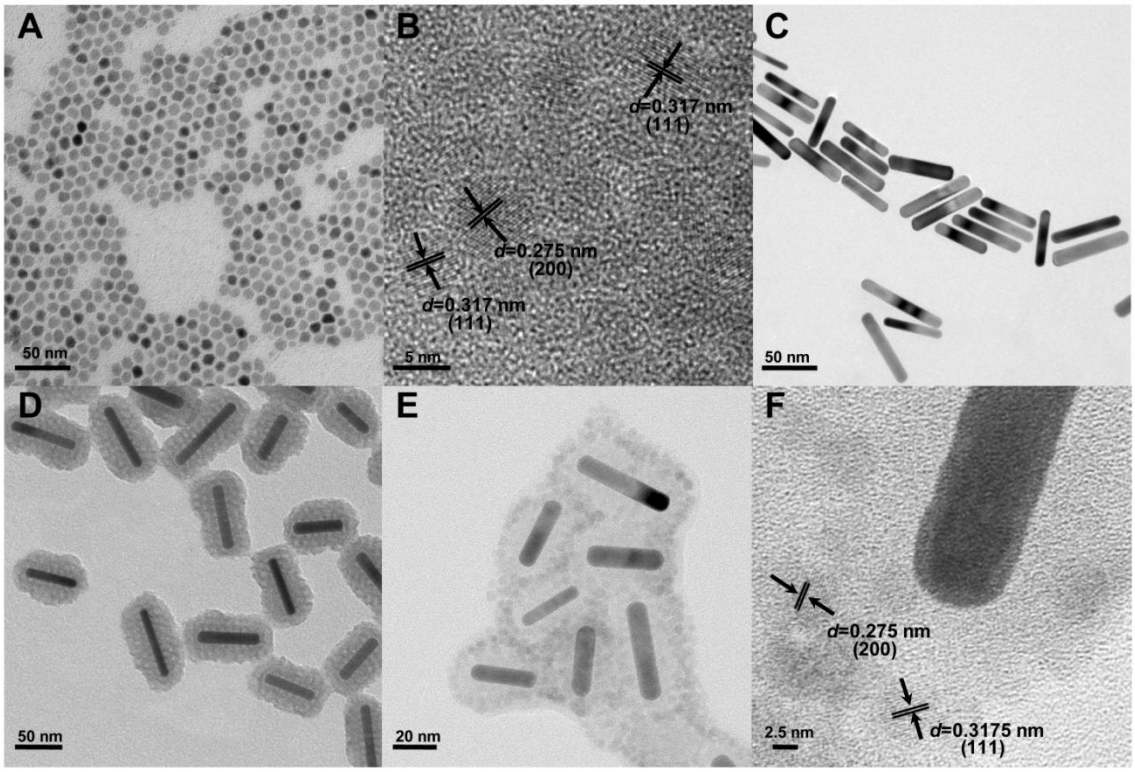

Fig. 1 (A) TEM and (B) HR-TEM images of the synthesized $NaGdF_4:Er^{3+}$, Yb^{3+} UCNPs. TEM images of the (C) synthesized GNRs, (D)the SiO_2 coated GNRs, and (E) the hybrid SiO_2 coated GNRs decorated with $NaGdF_4:Er^{3+}$, Yb^{3+} UCNPs (GNR@SiO_2@UCNPs).(F) HR-TEM image of the GNR@SiO_2@UCNPs interface.

After functionalization of the SiO_2-coated GNRs using amino-propyltriethoxylsilane (APTES), they were mixed with citrate-capped UCNPs. At pH 6 of the colloidal solution, the amino group of APTES was fully protonated (NH_4^+), whereas UCNPs possessed negative charges (cit^-). Hence, electrostatic forces between the UCNPs and APTES functionalized SiO_2-coated GNRs' surface allowed for their surface decoration. Fig. 1E shows the morphology of the SiO_2-coated GNRs following attachment of UCNPs and the interface between UCNPs and GNR@SiO_2 was further characterized by HR-TEM. As shown in Fig. 1F, two lattice fringes of the $NaGdF_4:Er^{3+}$, Yb^{3+} UCNPs were visible, with the spacing of ~0.275 nm corresponding to the {200} planes and the larger lattice spacing of 0.317 nm matching the {111} crystal planes of α-$NaGdF_4:Er^{3+}$, Yb^{3+} UCNPs. This

attachment and the assembly of the hybrid nanocomposite composed of $NaGdF_4$ UCNPs and GNRs could be further confirmed by XRD (Fig. 2B). The main diffraction peaks coincide well with the pure α-phase $NaGdF_4$ crystal (JCPDS No: 27-0697) and face-centered cubic (fcc) structure of metallic Au (JCPDS No: 04-0784). In addition, compositional analysis by energy-dispersive X-ray microanalysis (EDX) indicated that Na, Gd, F, Yb, Er, Au, Si elements are also detected in this nanocomposite (Fig. 2C), further confirming this hybrid nanocomposite consisting $GNR@SiO_2$ and UCNPs.

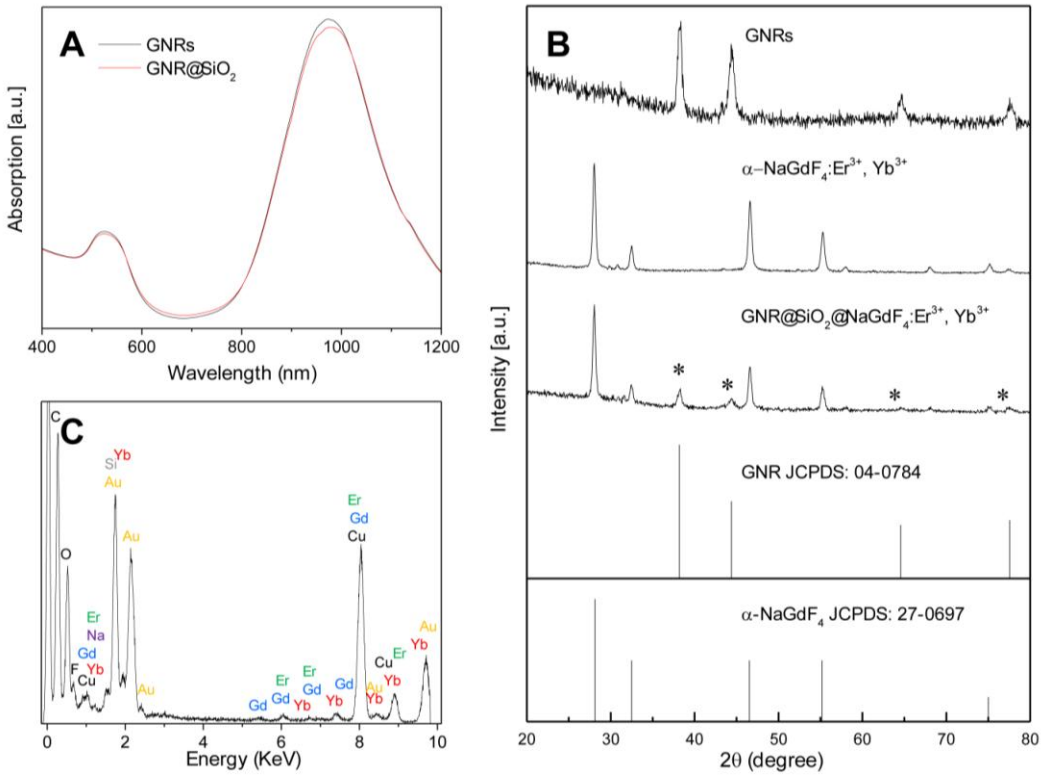

Fig.2 (A) Extinction spectra of GNRs and $GNR@SiO_2$. (B) XRD pattern of (i) GNRs, (ii) α-$NaGdF_4$:Er^{3+}, Yb^{3+}, (iii) hybrid nanocomposite of GNRs and $NaGdF_4$:Er^{3+}, Yb^{3+}. The standard pattern of pure GNRs (JCPDS file No: 04-0784), pure α-$NaGdF_4$ (JCPDS file No: 27-0697). The stars show the diffraction peaks of GNRs. (C) Elemental analysis of hybrid of GNRs and $NaGdF_4$:Er^{3+}, Yb^{3+} by EDX.

3.2 Photoluminescence properties of the GNR@SiO₂@UCNPs

This upconversion mechanism through the energy state diagrams of Yb^{3+} and Er^{3+} is illustrated schematically in Fig. S2 of the supporting information. It is well known that $NaGdF_4$:Er^{3+}, Yb^{3+} UCNPs possess a large absorption at 980 nm and can be efficiently excited *via* a continuous wave NIR laser. In this mechanism, the Yb^{3+} ions (the sensitizers) are excited from the ground state ($^2F_{7/2}$) to the excited state ($^2F_{5/2}$) and then undergo subsequent energy transfers to the Er^{3+} ions (the activators) in close proximity. This excites the Er^{3+} ions from the ground state ($^4I_{15/2}$) to the first intermediate excited state ($^4I_{11/2}$) and further to the $^4F_{7/2}$ excited state. Following multiphonon (non-radiative) decay, the lower energy $^2H_{11/2}$ and $^4S_{3/2}$ emitting states are populated, which produce the green emission at 525 and 545 nm through radiative decay from the $^2H_{11/2}$ and $^4S_{3/2}$ excited states to the $^4I_{15/2}$ ground state, respectively. The red emission at around 660 nm is produced from the radiative transition of the $^4F_{9/2}$ excited state to the ground state. As in the red emitting states, the $^4F_{9/2}$ excited state is populated *via* non-radiative decay from the upper states, in this case $^2H_{11/2}$/$^4S_{3/2}$. However, the $^4F_{9/2}$ state can also be populated by direct energy transfer. In this case, once the Er^{3+} ion is excited to the $^4I_{11/2}$ intermediate state, it can also undergo non-radiative decay to the $^4I_{13/2}$ excited state. A transfer of energy from an excited Yb^{3+} ion in the $^2F_{5/2}$ state can then directly populate the $^4F_{9/2}$ state.

Previous reports have demonstrated that the upconverted emission intensity could possibly be used to monitor changes in temperature of the environment [8, 9]. For Er^{3+} ions, given that the difference in energy between the $^2H_{11/2}$ and $^4S_{3/2}$ excited states is only several hundred wavenumbers (cm^{-1}), the lower energy $^4S_{3/2}$ state could easily thermally populate the upper $^2H_{11/2}$ state. This is generally referred to as the Luminescence Intensity Ratio (LIR) technique. Therefore, the relative intensity ratio between the $^2H_{11/2} \rightarrow {}^4I_{15/2}$

and $^4S_{3/2} \rightarrow {}^4I_{15/2}$ emission bands could be calculated based on the Boltzmann distribution for thermometry applications

$$R = C \times \exp\left(\frac{-\Delta E}{kT}\right) \qquad (1)$$

where R represents the LIR of the $^2H_{11/2} \rightarrow {}^4I_{15/2}$ and the $^4S_{3/2} \rightarrow {}^4I_{15/2}$, C is a constant, ΔE is the energy gap between the two excited states, k is the Boltzmann constant, and T is the absolute temperature. Fig. 3A presents two upconversion emission spectra (excited at 980 nm) of the UCNPs at two different temperatures, 20 and 60 ℃. Comparing both distinct bands between 515-535 nm, and 535-570 nm, the ratio increases with temperature, and this ratio increment also follows a linear relation with temperature, as can be observed in the graph in Fig. 3B. In this case, the experimental determination of this ratio yields a direct temperature measurement. Indeed, this increase in the ratio between the corresponding emitting peak intensities could therefore employed for thermal sensing [8, 33]. Afterwards, based on this ratio, the same procedure was followed to estimate the temperature of the GNR@SiO_2@UCNPs hybrid nanocomposite sample.

From the detailed analysis of data in Fig. 3C, the ratio of the upconversion intensity between the 515-535 nm and 535-570 nm emissions of the GNRs@SiO_2@UCNPs nanocomposites clearly increases when compared with that of the bare UCNPs at the same conditions. The thermal change of the GNRs@SiO_2@UCNPs nanocomposites under NIR excitation was determined by the previously obtained linear regression equation for the $NaGdF_4$:Er^{3+}, Yb^{3+} UCNPs. Thus, the calculated temperature increase reached 20.41K for the GNRs@SiO_2@UCNPs nanocomposites. This heat was generated by the absorption of the 980 nm excitation beam by the SPR of GNRs. This increase in

the *in situ* temperature results in a variation of the green upconverted emission of the UCNPs. In this nanocomposite, the GNRs could therefore easily be used as nanoheaters when excited at 980 nm, while the UCNPs decorated on the surface of the SiO_2 shell effectively behave as thermal sensors. Moreover, it is worth noting that the total emission from the Er^{3+} ions in the GNRs@SiO_2@UCNPs nanocomposite was enhanced when compared with bare UCNPs. This is due to the fact that when the SPR of the GNRs overlaps with the excitation of UCNPs ($^2F_{5/2}$ from Yb^{3+} and $^4I_{11/2}$ from Er^{3+} at 980 nm), as shown in Fig. 3D, the energy harnessed by the plasmonic nanostructures (GNRs) could be transferred to the electrons of the UCNPs, resulting in an increase in the their absorption cross-section [21, 34]. Further to this, the SPR can have either enhancement or quenching effects on the upconversion luminescence depending on the relative position of the SPR from the excitation or emission of UCNPs and the distance separating the UCNPs from the metal surface, that is to say, the thickness of the spacer layer between the UCNPs and the surface of the GNRs [35]. There are three competitive effects that contribute to this behavior: the plasmonic field causing luminescence enhancement, the radiative decay rate from coupling of the upconversion emission with the SPR of GNRs resulting in luminescence enhancement and the non-radiative energy transfer resulting in luminescence quenching. In this study, the SPR (980 nm) of GNRs was far away from the upconversion emission, therefore, the radiative decay rate played a negligible role. If the fluorescent species (UCNPs) are close the metal surface, the upconversion luminescence decreases as the non-radiative energy transfer is dominant. With the increase of the distance between the two species (*i.e.* the thickness of the spacer layer in

this SiO_2), the plasmonic field enhancement becomes dominant leading to the observed increase of the UCNP luminescence.

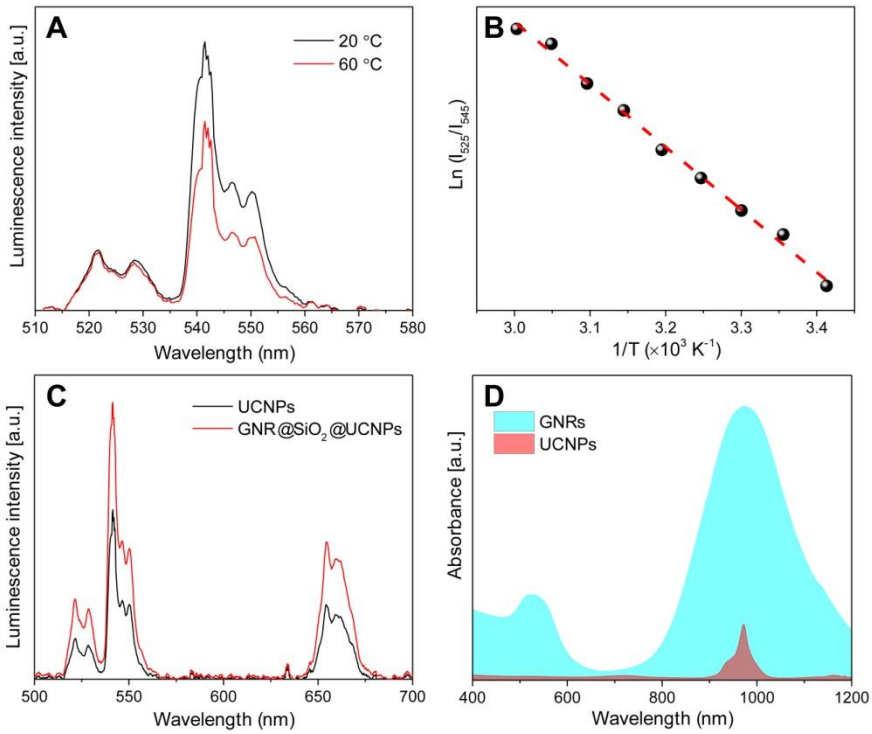

Fig.3 (A) Upconversion luminescence spectra of UCNPs at two different temperatures. (B) The temperature dependence of the ratio calculated from the luminescence spectra. Dots are experimental results and the red line is the best linear fit. (C) Upconversion luminescence spectra of UCNPs and GNRs@SiO_2@UCNPs. (D) Normalized absorption spectra of UCNPs and GNRs.

3.3 Characterization of ZnPc loaded GNR@SiO_2@UCNPs and photodynamic effect

A photosensitizer ZnPc was selected as candidate to be loaded into the mesoporous silica and to deliver the desired photodynamic effect. A concentrated solution of ZnPc was mixed with the GNR@SiO_2@UCNPs together until ZnPc absorbed into the porous silica. The ZnPc loading capacity was determined by the UV-VIS spectra and reached 1.8 % (w/w). Meanwhile, the luminescence intensity of ZnPc loaded GNR@SiO_2@UCNPs under NIR laser irradiation was also investigated and it was observed that a quenching of

the luminescence occurred after ZnPc was loaded into the GNRs@SiO_2@UCNPs nanocomposite (Fig. 4A). In fact, the red emission ($^4F_{9/2} \rightarrow {}^4I_{15/2}$) of the GNR@$SiO_2$@UCNPs from Er^{3+} decreased by 54%, which was significantly more than the decrease in green emission (29%). This quenching resulted from efficient energy transfer between the UCNPs (energy donors) and the ZnPc molecules (energy acceptors) due to the favorable spectral overlap between the red emission of the UCNPs at 660 nm and the absorption of ZnPc at 665 nm (Fig. 4B). Also, it is worth noting that the ratio of the green emission bands discussed above remains almost unchanged after ZnPc loading in the GNR@SiO_2@UCNPs nanocomposites indicating that the LIR technique can still be used for thermal sensing after loading.

The capacity of singlet oxygen ($^1O_2$) production was assessed using ABDA as a probe molecule to monitor the $^1O_2$ generation. As shown in Fig. 4C, there are three control groups, ABDA incubated with ZnPc loaded GNR@SiO_2@UCNPs without laser irradiation (blue triangles), ZnPc molecules with laser irradiation (black squares), and GNR@SiO_2@UCNPs alone with laser irradiation (red circles). It is clearly observed that there are no significant changes for these control groups over time, which indicates no $^1O_2$ generation occurred. However, for ABDA incubated with ZnPc loaded GNR@SiO_2@UCNPs following laser irradiation, the absorbance of ABDA decreased significantly indicating that both ZnPc molecules and GNR@SiO_2@UCNPs nanocomposites as well as 980 nm laser irradiation are necessary for the generation of $^1O_2$. To further confirm that $^1O_2$ production is triggered by laser irradiation, as shown in Fig. 4D, the suspension of ZnPc loaded GNR@SiO_2@UCNPs was exposed to laser irradiation cycles of 10 minutes and the results clearly demonstrated that the $^1O_2$

generation was reduced when the laser was switched off. Similar results were observed when the laser cycling was repeated. This enhanced $^1O_2$ production upon laser irradiation could be attributed to the photodynamic process: UCNPs were excited by laser irradiation, and the emitted luminescence was absorbed by ZnPc molecules, subsequently converting the absorbed energy to triplet oxygen, generating reactive and cytotoxic reactive oxygen species (ROS) for cancer treatment.

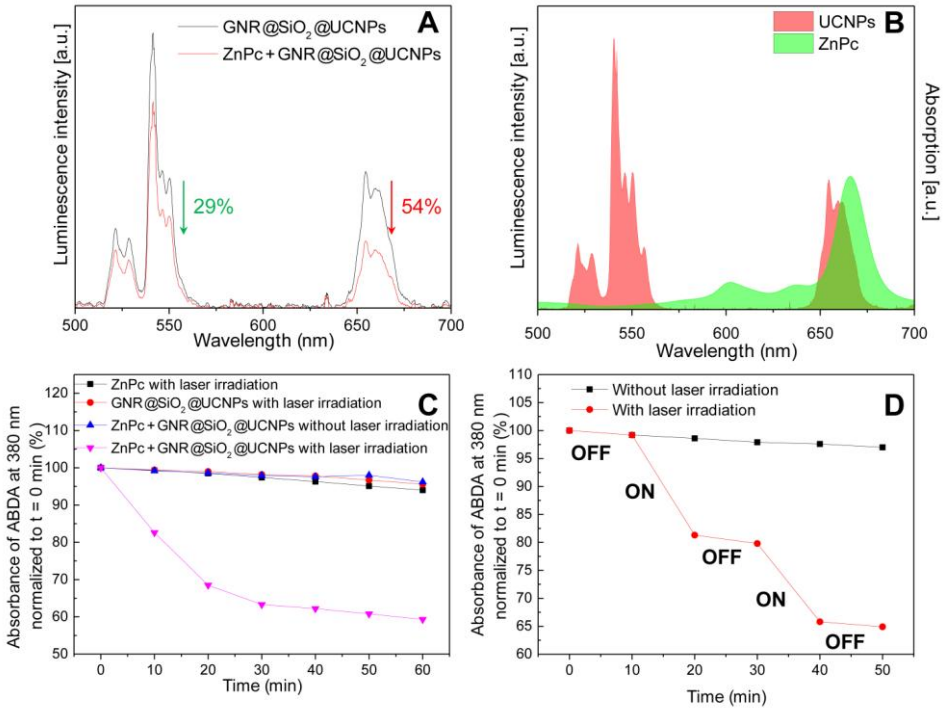

Fig. 4 (A) Upconversion luminescence spectrums of GNR@SiO_2@UCNPs and ZnPc loaded GNR@SiO_2@UCNPs under 980 nm laser irradiation. (B) Upconversion emission spectrum of UCNPs and UV-VIS absorption spectra of ZnPc, indicating the partial spectral overlap between the ZnPc absorption and the UCNPs emission. (C) Production of $^1O_2$ under consumption of ABDA for different samples over time. (D) Production of $^1O_2$ under consumption of ABDA in the absence and presence of laser irradiation.

3.4 Cytotoxicity study and cell uptake

The cytotoxicity of the UCNPs, GNR@SiO_2 and GNR@SiO_2@UCNPs was investigated by MTT assay on HeLa cervical cancer cells. The result in Fig. 5 demonstrates that there are no significant decrease in the cell viability of the UCNPs and GNR@SiO_2 samples at

a concentration of 50 μg/ml. Compared with UCNPs and GNR@SiO_2, a slightly higher cytotoxicity was observed after cell incubation with the GNR@SiO_2@UCNPs nanocomposites, a surviving fraction of *ca*. ~96.3% was observed after incubation for 24 h at a concentration of 50 μg/ml. This slightly lower viability may be attributed to the positively APTES capped GNR@SiO_2 nanostructures, which could lead to the cellular cytotoxicity in terms of causing mitochondrial and lysosomal damage [36, 37].

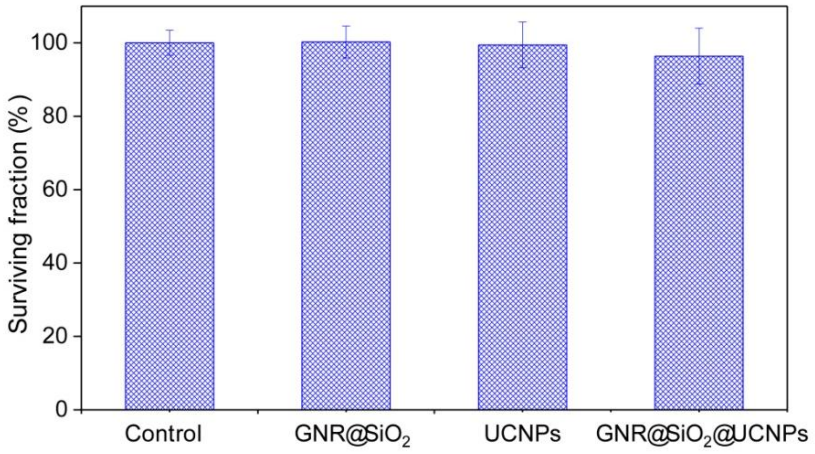

Fig. 5 Percent survival of HeLa cells incubated for a period of 24 h with GNR@SiO_2, UCNPs and GNR@SiO_2@UCNPs. Each point corresponds to the mean value ± SD from three different experiments.

To monitor the intracellular uptake of UCNPs and GNR@SiO_2@UCNPs, HeLa cells were incubated with different samples for 4 h. Fig. 6 shows the confocal microscopy images in bright field and luminescence field after incubation with UCNPs and GNR@SiO_2@UCNPs under laser irradiation and an obvious red upconversion emission was observed in the cells. The merged images demonstrate that the luminescence of the UCNPs appears in the cellular regions, indicating that the UCNPs and GNR@SiO_2@UCNPs nanocomposites have been successfully uptaken into the cells. In addition, for GNR@SiO_2@UCNPs, the image shows a more intense luminescence in the cells compared to that of the UCNPs group, which might be ascribed to the plasmonically enhanced luminescence of GNRs@SiO_2@UCNPs compared with the bare UCNPs under identical laser irradiation.

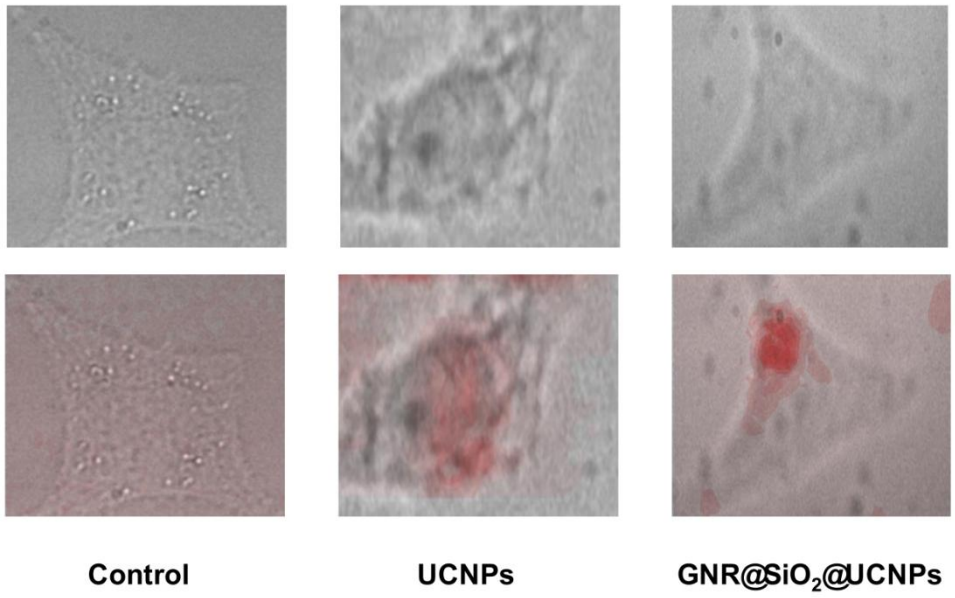

Fig. 6 Left row shows (from the top to bottom) the optical transition images and superimposed image of HeLa cells. Center row shows (from the top to bottom) the optical transition images and superimposed image of HeLa cells incubated with UCNPs. Right row shows (from the top to bottom) the optical transition images and superimposed image of Hela cells incubated with GNR@SiO_2@UCNPs.

4. Conclusion

In summary, a novel GNR@SiO_2@UCNPs nanocomposite was prepared and characterized. We studied the luminescence properties of GNR@SiO_2@UCNPs and observed that the ratio of the intensities of the green upconverted emission between the $^2H_{11/2} \rightarrow {}^4I_{15/2}$ and $^2S_{3/2} \rightarrow {}^4I_{15/2}$ transitions changed as a function of temperature and could be exploited for thermal sensing. Furthermore, the total luminescence intensity of UCNPs was increased in the presence of GNRs (compared to the UCNPs alone), and this enhancement could be attributed to the overlap of the excitation of the UCNPs and the SPR of the GNRs at 980 nm, as well as the spacer distance between the UCNPs and GNR. Thus, the luminescence of the UCNPs was influenced by the localized electromagnetic field created by the GNRs, which leads to the observed enhancement luminescence intensity. ZnPc was selected as a photosensitizer to load into the mesoporous silica layer and a quenching of the UCNPs was observed demonstrating that the emitted luminescence was effectively absorbed by the ZnPc molecules, subsequently transferring it to the triplet oxygen and ultimately generating the ROS. Finally, *in vitro* experiments were performed to assess their cytotoxicity and potential as a multimodal imaging probe. The results showed the absence of cytotoxicity and cellular imaging experiments on the incubated cells determined they were excellent biocompatible nanocomposites. Therefore, these interesting results confirm that they have the potential to be used as NIR-excited multifunctional nanoplatforms for theranostic applications, specifically due to their photothermal and photodynamic capabilities.

5. Acknowledgements

F.V. and F.R. acknowledge funding from the Natural Sciences and Engineering Research Council (NSERC Discovery Grants) of Canada and Fonds de Recherche du Québec-Nature et technologies (FRQNT) for supporting this research. F.V. also wholeheartedly thanks the Fondation Sibylla Hesse for funding. Y.H. acknowledges financial support from the Merit Scholarship Program for Foreign Students from the Ministère de l'Éducation, du Loisir et du Sport du Québec. F.R. is grateful to the Canada Research Chairs program for partial salary support and acknowledges NSERC for an EWR Steacie Memorial Fellowship. F.R. is also grateful to the AvH Foundation for a FW Bessel Award.

6. References

1. J. Zhou, Q. Liu, W. Feng, Y. Sun and F.Y. Li, Upconversion luminescent materials: advances and applications. *Chem. Rev*., 115 (2015): 395-465.
2. G.Y. Chen, H.L. Qju, P.N. Prasad and X.Y. Chen, Upconversion nanoparticles: design, nanochemistry, and applications in theranostics. *Chem. Rev*., 114 (2014): 5161-5214.
3. F. Wang, D. Banerjee, Y.S. Liu, X.Y. Chen and X.G. Liu, Upconversion nanoparticles in biological labeling, imaging, and therapy. *Analyst*, 135 (2010): 1839-1854.
4. X.G. Liu, C.H. Yan and J.A. Capobianco, Photon upconversion nanomaterials. *Chem. Soc. Rev*., 44 (2015): 1299-1301.
5. H. Dong, L.D. Sun and C.H. Yan, Basic understanding of the lanthanide related upconversion emissions. *Nanoscale*, 5 (2013): 5703-5714.
6. J. Zhou, Z. Liu and F.Y. Li, Upconversion nanophosphors for small-animal imaging. *Chem. Soc. Rev*., 41 (2012): 1323-1349.
7. M. Wang, G. Abbineni, A. Clevenger, C.B. Mao and S.K. Xu, Upconversion nanoparticles: synthesis, surface modification and biological applications. *Nanomed. Nanotechnol*. *Biol. Med*. 7 (2011): 710-729.
8. F. Vetrone, R. Naccache, A. Zamarron, A.J. de la Fuente, F. Sanz-Rodriguez, L.M. Maestro, E.M. Rodriguez, D. Jaque, J.G. Sole and J.A. Capobianco, Temperature sensing using fluorescent nanothermometers. *ACS Nano*, 4 (2010): 3254-3258.
9. D. Jaque and F. Vetrone, Luminescence nanothermometry. *Nanoscale*, 4 (2012): 4301-4326.
10. P.K. Jain, X.H. Huang, I.H. El-Sayed and M.A. El-Sayed, Noble Metals on the nanoscale: optical and photothermal properties and some applications in imaging, sensing, biology, and medicine. *Acc. Chem. Res*., 41 (2008): 1578-1586.
11. N.S. Abadeer and C.J. Murphy, Recent progress in cancer thermal therapy using gold nanoparticles. *J. Phys. Chem. C*, 120 (2016): 4691-4716.
12. A.M. Alkilany, L.B. Thompson, S.P. Boulos, P.N. Sisco and C.J. Murphy, Gold nanorods: their potential for photothermal therapeutics and drug delivery, tempered by the complexity of their biological interactions. *Adv. Drug Deliver Rev*., 64 (2012): 190-199.
13. X.H. Huang, S. Neretina and M.A. El-Sayed, Gold nanorods: from synthesis and properties to biological and biomedical applications. *Adv. Mater*., 21 (2009): 4880-4910.
14. Z.J. Zhang, J. Wang and C.Y. Chen, Gold nanorods based platforms for light-mediated theranostics. *Theranostics*, 3 (2013): 223-238.
15. G. Baffou, R. Quidant and C. Girard, Heat generation in plasmonic nanostructures: Influence of morphology. *Appl. Phys. Lett*., 94 (2009).
16. A.M. Alkilany, P.K. Nagaria, C.R. Hexel, T.J. Shaw, C.J. Murphy and M.D. Wyatt, Cellular uptake and cytotoxicity of gold nanorods: molecular origin of cytotoxicity and surface effects. *Small*, 5 (2009): 701-708.
17. E. Locatelli, I. Monaco and M.C. Franchini, Surface modifications of gold nanorods for applications in nanomedicine. *RSC Adv*., 5 (2015): 21681-21699.
18. Z.J. Zhang, L.M. Wang, J. Wang, X.M. Jiang, X.H. Li, Z.J. Hu, Y.H. Ji, X.C. Wu and C.Y. Chen, Mesoporous silica-coated gold nanorods as a light-mediated multifunctional theranostic platform for cancer treatment. *Adv. Mater*., 24 (2012): 1418-1423.
19. S. Shen, H.Y. Tang, X.T. Zhang, J.F. Ren, Z.Q. Pang, D.G. Wang, H.L. Gao, Y. Qian, X.G. Jiang and W.L. Yang, Targeting mesoporous silica-encapsulated gold nanorods for

chemo-photothermal therapy with near-infrared radiation. *Biomaterials*, 34 (2013): 3150-3158.

20. A.J. Gormley, N. Larson, S. Sadekar, R. Robinson, A. Ray and H. Ghandehari, Guided delivery of polymer therapeutics using plasmonic photothermal therapy. *Nano Today*, 7 (2012): 158-167.
21. A.L. Feng, M.L. You, L.M. Tian, S. Singamaneni, M. Liu, Z.F. Duan, T.J. Lu, F. Xu and M. Lin, Distance-dependent plasmon-enhanced fluorescence of upconversion nanoparticles using polyelectrolyte multilayers as tunable spacers. *Sci. Rep.,* 5 (2015): 7779.
22. F. Zhang, G.B. Braun, Y.F. Shi, Y.C. Zhang, X.H. Sun, N.O. Reich, D.Y. Zhao and G. Stucky, Fabrication of $Ag@SiO_2@Y_2O_3$:Er nanostructures for bioimaging: tuning of the upconversion fluorescence with silver nanoparticles. *J. Am. Chem. Soc.,* 132 (2010): 2850-2851.
23. W. Ge, X.R. Zhang, M. Liu, Z.W. Lei, R.J. Knize and Y.L. Lu, Distance dependence of gold-enhanced upconversion luminescence in $Au/SiO_2/Y_2O_3:Yb^{3+}$, Er^{3+} nanoparticles. *Theranostics*, 3 (2013): 282-288.
24. G. Valduga, E. Reddi, S. Garbisa and G. Jori, Photosensitization of cells with different metastatic potentials by liposome-delivered Zn(II)-phthalocyanine. *Int. J. Cancer*, 75 (1998): 412-417.
25. C.N. Zhou, S.J. Chi, J.S. Deng, J.L. Liang, G. Jori and C. Milanesi, Apoptosis of mouse MS-2 fibrosarcoma cells induced by photodynamic therapy with Zn(II)-phthalocyanine. *J. Photochem. Photobiol. B*, 33 (1996): 219-223.
26. R. Naccache, P. Chevallier, J. Lagueux, Y. Gossuin, S. Laurent, L. Vander Elst, C. Chilian, J.A. Capobianco and M.A. Fortin, High relaxivities and strong vascular signal enhancement for $NaGdF_4$ nanoparticles designed for dual MR/optical imaging. *Adv. Healthcare Mater*., 2 (2013): 1478-1488.
27. B. Nikoobakht and M.A. El-Sayed, Preparation and growth mechanism of gold nanorods (NRs) using seed-mediated growth method. *Chem. Mater*., 15 (2003): 1957-1962.
28. T. Zhao, H. Wu, S.Q. Yao, Q.H. Xu and G.Q. Xu, Nanocomposites containing gold nanorods and porphyrin-doped mesoporous silica with dual capability of two-photon imaging and photosensitization. *Langmuir,* 26 (2010): 14937-14942.
29. F. Denizot and R. Lang, Rapid Colorimetric Assay for Cell-Growth and Survival - Modifications to the tetrazolium dye procedure giving improved sensitivity and reliability. *J. Immunol. Methods*, 89 (1986): 271-277.
30. H.X. Mai, Y.W. Zhang, R. Si, Z.G. Yan, L.D. Sun, L.P. You and C.H. Yan, High-quality sodium rare-earth fluoride nanocrystals: controlled synthesis and optical properties. *J. Am. Chem. Soc.,* 128 (2006): 6426-6436.
31. X. Ye, L. Jin, H. Caglayan, J. Chen, G. Xing, C. Zheng, V. Doan-Nguyen, Y. Kang, N. Engheta, C.R. Kagan and C.B. Murray, Improved size-tunable synthesis of monodisperse gold nanorods through the use of aromatic additives. *ACS Nano*, 6 (2012): 2804-2817.
32. I. Gorelikov and N. Matsuura, Single-step coating of mesoporous silica on cetyltrimethyl ammonium bromide-capped nanoparticles. *Nano Lett*., 8 (2008): 369-373.
33. Y. Huang, F. Rosei and F. Vetrone, A single multifunctional nanoplatform based on upconversion luminescence and gold nanorods. *Nanoscale*, 7 (2015): 5178-5185.
34. M. Saboktakin, X.C. Ye, U.K. Chettiar, N. Engheta, C.B. Murray and C.R. Kagan, Plasmonic enhancement of nanophosphor upconversion luminescence in Au nanohole arrays. *ACS Nano*, 7 (2013): 7186-7192.

35. M. Saboktakin, X. Ye, S.J. Oh, S.H. Hong, A.T. Fafarman, U.K. Chettiar, N. Engheta, C.B. Murray and C.R. Kagan, Metal-enhanced upconversion luminescence tunable through metal nanoparticle-nanophosphor separation. *ACS Nano*, 6 (2012): 8758-8766.
36. E. Frohlich, The role of surface charge in cellular uptake and cytotoxicity of medical nanoparticles. *Int. J. Nanomed*., 7 (2012): 5577-5591.
37. S. Bhattacharjee, L.H.J. de Haan, N.M. Evers, X. Jiang, A.T.M. Marcelis, H. Zuilhof, I.M.C.M. Rietjens and G.M. Alink, Role of surface charge and oxidative stress in cytotoxicity of organic monolayer-coated silicon nanoparticles towards macrophage NR8383 cells. *Part. Fibre Toxicol*., 7 (2010): 25.

Supporting Information

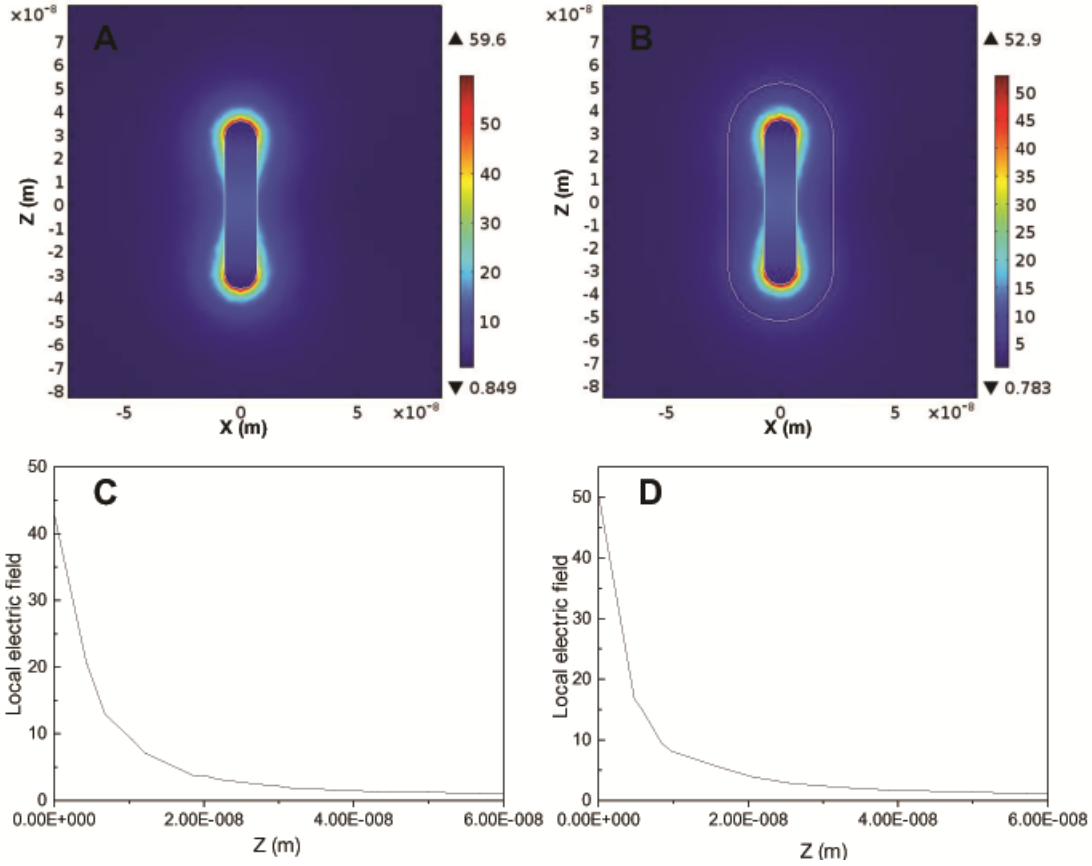

Fig. S1 Simulated results of electric fields surrounding the surface of individual (A) (C) GNR and (B) (D) GNR@SiO_2.

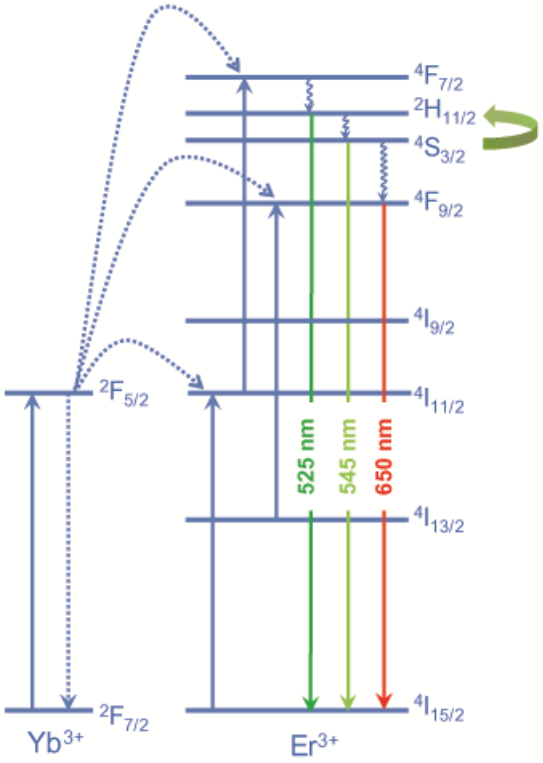

Fig. S2 Scheme showing the upconversion mechanism of the $NaGdF_4:Er^{3+}$, Yb^{3+} UCNPs. The temperature sensitivity of the $NaGdF_4:Er^{3+}$, Yb^{3+} UCNPs occurs as a result of the closely spaced $^2H_{11/2}$ and $^4S_{3/2}$ energy states.

DOI : 10.1021/acs.jpcb.6b02013

Chapter 6

Multifunctional liposome nanocarriers combining upconverting nanoparticles and anticancer drugs

Yue Huang, Eva Hemmer, Federico Rosei, Fiorenzo Vetrone

J. Phys. Chem. B, 2016, 120, 4992–5001

It is introduced in Chapter 1 that UCNPs can be considered as efficient and versatile optical probes for bioimaging and therapeutic tools. A major advantage of UCNPs is the use of NIR light as an excitation source in the biomedical community due to reduced absorption and scattering from biological structures when compared to UV-visible light. Aside, the broad and tunable emission wavelength range (by choice of the appropriate lanthanide ions) provides the potential for multifunctionality resulting in bioprobes suitable for applications beyond bioimaging, such as light mediated therapy or drug delivery and release. In the context of drug delivery and release, the development of innovative delivery systems is essential in order to guarantee the efficient impact of the drug where needed while reducing potentially severe side effects. A further important aspect is the monitoring of the drug administration and release. In this paper, we first prepare liposome nanocarriers, based on the co-encapsulation of Er^{3+} and Yb^{3+} co-doped $NaGdF_4$ UCNPs and the model anticancer drug doxorubicin (DOX). Liposomes, with similar structures as the cell membrane, are good candidates for drug administration owing to their excellent biocompatibility and high therapeutic efficacy. Under NIR (980 nm) laser irradiation, the UCNPs emit in the green wavelength region following an upconversion process. However, upon co-loading of DOX with the UCNPs into the

liposome nanocarriers, a significant decrease of the green upconversion emission is observed. This is because of the partial spectral overlap between the absorption of DOX and the green emission of the UCNPs: thus, energy transfer from the UCNPs to the DOX molecules occurs resulting in the quenching of the green emission. DOX release studies further demonstrated the recovery of the green emission from the UCNPs upon release of DOX from the liposome nanocarriers. This allows for the application of liposome encapsulated UCNPs as probes for drug release monitoring in addition to its use as a luninescence probe. In this way, co-encapsulated UCNPs and the anticancer drug DOX in liposomes would exploit the potential use for the simultaneous delivery of therapeutic and diagnostic agents.

Chapter 7 Conclusions and Perspectives

7.1 Conclusions

To date, the integration of nanoparticles and nanotechnology in industrial and scientific applications has yet to reach its peak and this is certainly true for biological applications where nanoparticles can address several challenges associated with conventional fluorophores and provide much needed solutions. UCNPs may fulfill the above needs particularly in biological applications due to their unique optical properties different from other conventional fluorophores. The results of this thesis project are divided into two parts based on the structure of nanocomposites and potential bioapplications combining with other therapeutic modalities.

Part I is mainly focused on the nanocomposites, coupling a nanothermometer with a nanoheater based on their distinct optical and thermal properties. In this part, UCNPs can be applied as nanothermometers based on the temperature dependent luminescence where their luminescence intensity ratios (LIR) vary as a function of temperature. Two types of GNRs were designed as nanoheaters, whose SPR overlaps with the emission/or excitation of UCNPs, so that the luminescence of UCNPs was influenced by the localized electromagnetic field created by GNRs. In addition, these novel nanocomposites could also be considered as excellent thermo-responsive control drug release nanoplatforms.

Part I is divided into two sections, each corresponding to one type of nanostructure. In section I, we developed a multifunctional nanoplatform composed of a GNR core and an outer shell of upconverting $NaYF_4:Er^{3+}$, Yb^{3+} UCNPs. The GNR core has a longitudinal SPR centered at 660 nm, overlapping perfectly with the red emission from the Er^{3+}

$^4F_{9/2} \rightarrow {}^4I_{15/2}$ transition. This nanocomposite was capable of inducing a localized heating *via* the GNR core while the outer shell could be used to simultaneously monitor the surrounding temperature increases. Heating is generated by absorption of the upconverted red light from the Er^{3+} $^4F_{9/2} \rightarrow {}^4I_{15/2}$ transition. The absorption from the GNR core was evidenced by the more drastic quenching of the upconverted red emission compared to the upconverted green emission. The relative intensities of the upconverted emissions from the $^2H_{11/2} \rightarrow {}^4I_{15/2}$ and $^4S_{3/2} \rightarrow {}^4I_{15/2}$ transitions were sensitive to temperature and allowed the outer $NaYF_4$:Er^{3+}, Yb^{3+} shell to act as a nanothermometer. Finally, when this nanocomposite was loaded with a model anticancer drug, we showed that this photothermal effect could trigger fast drug release, especially at low pH values. This drug release behavior, which depends on high temperature and low pH, is favorable in tumor extracellular environment, and hence has promising applications in cancer therapy.

In section II, we developed a novel nanocomposite GNR@SiO_2@UCNPs. The $NaGdF_4$:Er^{3+}, Yb^{3+} UCNPs were synthesized *via* thermal decomposition method, and these UCNPs were electronically coupled with GNRs whose SPR absorption at 980 nm, which overlapping perfectly with the excitation from the Yb^{3+} $^2F_{7/2} \rightarrow {}^2F_{5/2}$ transition. We investigated the luminescence properties of GNR@SiO_2@UCNPs, the ratio of the intensity of green emission of upconversion between the $^2H_{11/2} \rightarrow {}^4I_{15/2}$ and $^2S_{3/2} \rightarrow {}^4I_{15/2}$ were enhanced when compared with the bare UCNPs, which responds to temperature changes and could be exploited for thermal sensing. The total luminescence intensity of UCNPs was increased in the presence of GNRs when compared with bare UCNPs. This enhancement could be attributed to the overlap of the excitation of UCNPs and the SPR

of GNRs at 980 nm influencing the luminescence of the UCNPs by the localized electromagnetic field created by the GNRs. ZnPc was further selected as a photosensitizer to load into the mesoporous silica layer. The luminescence of UCNPs was quenched after ZnPc loading, since the luminescence emitted from the UCNPs was effectively absorbed by the ZnPc molecules, and transferred to the triplet oxygen, generating the ROS. Finally, cellular experiments were performed, the results of the absence of cytotoxicity and cellular imaging in the incubated cells make it an excellent biocompatible nanocomposite. Therefore, it could be considered as a potential multifunctional nanoplatform for cancer treatment based on the upconversion luminescence, photothermal and photodynamic system.

In part II, we selected liposomes as nanocarriers to encapsulate Er^{3+} and Yb^{3+} co-doped $NaGdF_4$ UCNPs and the model anticancer drug DOX. Under 980 nm laser excitation, the liposome encapsulated UCNPs showed strong green emission. Conversely, after loading DOX, quenching of the upconverted green emission was observed, due to partial spectral overlap between the absorption of DOX and the green emission of the UCNPs, and the resultant energy transfer between the UCNPs (donor) and DOX molecules (acceptor). This energy transfer from the UCNPs to the DOX molecules can only happen if both the donor and acceptor moieties are in sufficiently close proximity. In addition, DOX release was investigated and the data demonstrated a recovery of the green upconversion emission intensity of the UCNPs, which correlated well with the extent of DOX release. This luminescence enhancement as function of drug release could be developed for monitoring drug release through UCNPs luminescence. Thus, the nanocarrier presented here, a liposome co-encapsulated with UCNPs and the anticancer drug DOX, provided a

promising theranostics platform for simultaneous bioimaging and therapy. Future work will focus on the surface functionalization of these nanocarriers with targeting moieties to endow them with selectivity and specificity relevant for targeted diagnostics and therapeutics for diseases such as cancer.

7.2 Perspectives

We have developed several multifunctional nanostructures based on the UCNPs and other therapeutic modalities. However, research in the bioapplications of UCNPs is still at the infancy stage; more research is required to optimize the efficiency of these nanocomposites and overcome the challenges related to optical properties and future bioapplications. Therefore, there are several interesting directions for future work in the areas of research presented in this thesis.

7.2.1 Optimization of UCNPs properties and materials

In chapter 4, we select $NaYF_4$ as upconversion host, due to the intense luminescence achieved in that host. In order to develop materials to broaden their functionalities, $NaGdF_4$ can also be considered as a good host for upconversion and, due to the presence of Gd^{3+} ions which brings the possibility of using the nanostructure as a contrast agent for magnetic resonance imaging.

Leaving aside the challenges related to host materials for UCNPs, we selected Yb^{3+}/Er^{3+} ion pairs for luminescence investigation in this thesis, owing to Er^{3+} ions showing some of the highest upconversion efficiency. However, the visible emitted wavelength generated by Er^{3+} ions restricts their real bioapplication due to their short tissue penetration depths (caused by tissue scattering and specific absorptions of tissue

components such as melanin and hemoglobin) [138]. To overcome this problem, Yb^{3+}/Tm^{3+} ions might be considered as an alternative because of the excited luminescence bands lying within the so-called “biological window” (700 - 900 nm) in the near future.

In this thesis, all the nanomaterials are normally excited at 980 nm. This wavelength accounts for better penetration depth in biological tissues than visible or ultraviolet light, but it can still be absorbed by water molecules and thus can be hardly included in a biological transparency window. Consequently, to fully exploit the advantages of NIR excitation regarding penetration depth, it would be interesting to move towards different excitation wavelengths. Recently, we are starting to exploit the use of Nd^{3+} ions, since it can be excited at 800 nm that lies within the first biological window. In this case, the wavelength used for imaging is not obtained by upconversion, but by standard luminescence as Nd^{3+} emits also in the NIR at 1300 nm [139]. It has been demonstrated that this wavelength is advantageous in terms of transparency of the biological samples (it is in the second biological window), but also to avoid autofluorescence.

7.2.2 Investigation of distance dependence of upconversion luminescence

In chapter 4 and chapter 5, we introduce metal nanoparticles to incorporate with UCNPs to act as nanoheater and nanothermomemter, respectively. The presence of these metal nanoparticles (*e.g.* GNRs), is known for enhancing or quenching luminescence of UCNPs through influencing both the emission and absorption. Typically, the enhancement effect stems from two possible mechanisms including the local field effect upon optical excitation of its SPR; radiative decay arising from the resonance of the emission from

luminescent materials. While quenching effect could be caused due to non-radiative decay resulting in energy transfer from the UCNPs to metal surface. During the competition of these processes, the thickness of the spacer layer between a plasmonic metal nanostructure and fluorophore is a critical factor in determining which process plays dominant or whether the upconversion luminescence is plasmonically enhanced or quenched.

In chapter 4, the quenching of the nanocomposites is observed compared with the UCNP nanoshell, due to the fact that the spacer thickness is below the critical distance for enhancement. For the synthesis of GNR@UCNPs, $NaBF_4$ was introduced to release H^+ and F^- ions under high temperature and pressure causing the silica middle layer to simultaneously corrode. This small spacer has the effect of leading to a quenching of the upconversion luminescence by non-radiative energy transfer from UCNPs to the gold surface. In chapter 5, the total emission of GNR@SiO_2@UCNPs was enhanced when compared with the bare UCNPs. During the process of GNR@SiO_2@UCNPs nanocomposite preparation, silica layer was functionalized by APTES and combining with UCNPs through electrostatic interaction between the UCNPs with a negative surface charge and the positively charged APTES without corroding. This silica layer distance between UCNPs and GNRs make local plasmonic field become dominant leading to the enhancement of UCNPs luminescence. Although out of the scope of this thesis, the upconversion luminescence intensity for such structures as a function of silica spacer thickness will be investigated in the future.

7.2.3 Surface modification of UCNPs-based nanostructures

The physicochemical characteristics of the UCNPs' surface are important to determine their toxicity and effectivity when they are introduced into a biological environment. However, the design of all the nanostructures in this thesis is still at the stage of demonstrating their optical properties and other possibilities, but not totally designing for *in vivo* applications. It is important to consider that the surface of the UCNPs may non-specifically adsorb proteins (opsonization). This makes them eventually more visible for phagocytic cells belonging to the immune system, which would clear them from the blood stream.

To improve the circulation time of the nanostructures, it is also important to extend PEG modification, as it has been demonstrated that it helps escaping the reticulo-endothelial system scavenging and some nonspecific uptake levels. PEGylated nanostructures could particularly increase the targeting efficiency of the therapies *via* enhanced permeation retention (EPR) effect. Also, the additional use of targeting ligands is important. We will try to conjugate targeting ligand (*e.g.* folic acid) with PEG to direct the nanocomposites only to infected areas. In this case, the nanocomposites can not only improve therapeutic efficiency, but also minimize toxicity and therefore side-effects to the patient, by targeted release of the therapeutic drugs and maintaining the optimum concentration at precise sites in the organs.

7.2.4 Biological experiments with a collaborator

In this thesis, we mainly focus on the preparation and characterization of novel nanocomposites. However, the biological experiments (with a collaborator) including

cellular assays and *in vivo* assay are required and will be undertaken. Specifically, 1) further toxicity studies including cytotoxicity in normal cells, nanocomposite distribution, metabolism, pharmacokinetics and pharmacodynamics in animal models are required; 2) PDT, PTT and drug delivery based on the UCNPs mentioned in the thesis will be performed in the cellular and animal models, and the multifunctional bioimaging and therapeutic effects will be evaluated in the near future.

References

1. C.K. Jorgensen, Lanthanides since 1839 - from crowded elements to quantum-chemical rosetta stone. *Inorg. Chim. Acta,* 139 (1987): 1-5.
2. J.B. Hedrick, The Global Rare-Earth Cycle. *J. Alloys Compd*., 225 (1995): 609-618.
3. J.M. Klinger, A historical geography of rare earth elements: From discovery to the atomic age. *Extr. Ind. Soc.,* 2 (2015): 572-580.
4. S.V. Eliseeva and J.C.G. Bunzli, Rare earths: jewels for functional materials of the future. *New J. Chem*., 35 (2011): 1165-1176.
5. M. Bethencourt, F.J. Botana, J.J. Calvino, M. Marcos and M.A. Rodriguez-Chacon, Lanthanide compounds as environmentally-friendly corrosion inhibitors of aluminium alloys: A review. *Corros. Sci*., 40 (1998): 1803-1819.
6. V. Gonzalez, D.A.L. Vignati, C. Leyval and L. Giamberini, Environmental fate and ecotoxicity of lanthanides: are they a uniform group beyond chemistry? *Environ. Int*., 71 (2014): 148-157.
7. M. Lin, Y. Zhao, S.Q. Wang, M. Liu, Z.F. Duan, Y.M. Chen, F. Li, F. Xu and T.J. Lu, Recent advances in synthesis and surface modification of lanthanide-doped upconversion nanoparticles for biomedical applications. *Biotechnol. Adv*., 30 (2012): 1551-1561.
8. M.C. Heffern, L.M. Matosziuk and T.J. Meade, Lanthanide probes for bioresponsive Imaging. *Chem. Rev*., 114 (2014): 4496-4539.
9. G.H. Dieke, H.M. Crosswhite and H. Crosswhite, Spectra and energy levels of rare earth ions in crystals. (Interscience Publishers, New York, 1968)
10. S.A. Cotton, Lanthanide and actinide chemistry. Inorganic chemistry. (John Wiley & Sons, Ltd, Chichester, UK, 2006)
11. F. Auzel, Upconversion and anti-stokes processes with f and d ions in solids. *Chem. Rev*., 104 (2004): 139-173.
12. L.M. Maestro, E.M. Rodriguez, F. Vetrone, R. Naccache, H.L. Ramirez, D. Jaque, J.A. Capobianco and J.G. Sole, Nanoparticles for highly efficient multiphoton fluorescence bioimaging. *Opt. Express,* 18 (2010): 23544-23553.
13. J. Zhou, Q. Liu, W. Feng, Y. Sun and F.Y. Li, Upconversion luminescent materials: advances and applications. *Chem. Rev*., 115 (2015): 395-465.
14. G.Y. Chen, H.L. Qju, P.N. Prasad and X.Y. Chen, Upconversion nanoparticles: design, nanochemistry, and applications in theranostics. *Chem. Rev*., 114 (2014): 5161-5214.
15. C. Renero-Lecuna, R. Martin-Rodriguez, R. Valiente, J. Gonzalez, F. Rodriguez, K.W. Kramer and H.U. Gudel, Origin of the high upconversion green luminescence efficiency in beta-$NaYF_4$:2%Er^{3+}, 20%Yb^{3+}. *Chem. Mater*., 23 (2011): 3442-3448.
16. R. Kumar, M. Nyk, T.Y. Ohulchanskyy, C.A. Flask and P.N. Prasad, Combined optical and MR bioimaging using rare earth ion doped $NaYF_4$ Nanocrystals. *Adv. Funct. Mater*., 19 (2009): 853-859.
17. G.Y. Chen, T.Y. Ohulchanskyy, R. Kumar, H. Agren and P.N. Prasad, Ultrasmall monodisperse $NaYF_4$:Yb^{3+}/Tm^{3+} nanocrystals with enhanced near-infrared to near-infrared upconversion photoluminescence. *ACS Nano,* 4 (2010): 3163-3168.
18. G.S. Yi and G.M. Chow, Synthesis of hexagonal-phase $NaYF_4$:Yb,Er and $NaYF_4$:Yb,Tm nanocrystals with efficient up-conversion fluorescence. *Adv. Funct. Mater*., 16 (2006): 2324-2329.

19. J.C. Boyer, L.A. Cuccia and J.A. Capobianco, Synthesis of colloidal upconverting $NaYF_4$: Er^{3+}/Yb^3+ and Tm^{3+}/Yb^{3+} monodisperse nanocrystals. *Nano Lett*., 7 (2007): 847-852.
20. F. Vetrone, R. Naccache, V. Mahalingam, C.G. Morgan and J.A. Capobianco, The Active-core/active-shell approach: A strategy to enhance the upconversion luminescence in lanthanide-doped nanoparticles. *Adv. Funct. Mater*., 19 (2009): 2924-2929.
21. R. Naccache, F. Vetrone, V. Mahalingam, L.A. Cuccia and J.A. Capobianco, Controlled synthesis and water dispersibility of hexagonal phase $NaGdF_4$:Ho^{3+}/Yb^{3+} nanoparticles. *Chem. Mater*., 21 (2009): 717-723.
22. Q. Liu, Y. Sun, T.S. Yang, W. Feng, C.G. Li and F.Y. Li, Sub-10 nm hexagonal lanthanide-doped $NaLuF_4$ upconversion nanocrystals for sensitive bioimaging in vivo. *J. Am. Chem. Soc*., 133 (2011): 17122-17125.
23. J.F. Suyver, J. Grimm, K.W. Kramer and H.U. Gudel, Highly efficient near-infrared to visible up-conversion process in $NaYF_4$:Er^{3+}/Yb^{3+}. *J. Lumin*., 114 (2005): 53-59.
24. K.W. Kramer, D. Biner, G. Frei, H.U. Gudel, M.P. Hehlen and S.R. Luthi, Hexagonal sodium yttrium fluoride based green and blue emitting upconversion phosphors. *Chem. Mater*., 16 (2004): 1244-1251.
25. F. Wang and X.G. Liu, Recent advances in the chemistry of lanthanide-doped upconversion nanocrystals. *Chem. Soc. Rev*., 38 (2009): 976-989.
26. Q. Liu, W. Feng, T.S. Yang, T. Yi and F.Y. Li, Upconversion luminescence imaging of cells and small animals. *Nat. Protoc*., 8 (2013): 2033-2044.
27. J.C. Boyer, F. Vetrone, L.A. Cuccia and J.A. Capobianco, Synthesis of colloidal upconverting $NaYF_4$ nanocrystals doped with Er^{3+}, Yb^{3+} and Tm^{3+}, Yb^{3+} via thermal decomposition of lanthanide trifluoroacetate precursors. *J. Am. Chem. Soc*., 128 (2006): 7444-7445.
28. H.X. Mai, Y.W. Zhang, R. Si, Z.G. Yan, L.D. Sun, L.P. You and C.H. Yan, High-quality sodium rare-earth fluoride nanocrystals: controlled synthesis and optical properties. *J. Am. Chem. Soc*., 128 (2006): 6426-6436.
29. Y.H. Wang, R.X. Cai and Z.H. Liu, Controlled synthesis of $NaYF_4$: Yb, Er nanocrystals with upconversion fluorescence via a facile hydrothermal procedure in aqueous solution. *CrystEngComm*, 13 (2011): 1772-1774.
30. Q. Zhang and B. Yan, Phase control of upconversion nanocrystals and new rare earth fluorides though a diffusion-controlled strategy in a hydrothermal system. *Chem. Commun*., 47 (2011): 5867-5869.
31. M. Quintanilla, F.Q. Ren, D.L. Ma and F. Vetrone, Light management in upconverting nanoparticles: ultrasmall core/shell architectures to tune the emission color. *ACS Photonics,* 1 (2014): 662-669.
32. H.Q. Wang and T. Nann, Monodisperse upconversion GdF_3:Yb, Er rhombi by microwave-assisted synthesis. *Nanoscale Res. Lett*., 6 (2011): 267.
33. Y.W. Zhang, X. Sun, R. Si, L.P. You and C.H. Yan, Single-crystalline and monodisperse LaF_3 triangular nanoplates from a single-source precursor. *J. Am. Chem. Soc*., 127 (2005): 3260-3261.
34. E. Hemmer, M. Quintanilla, F. Legare and F. Vetrone, Temperature-induced energy transfer in dye-conjugated upconverting nanoparticles: A new candidate for nanothermometry. *Chem. Mater*., 27 (2015): 235-244.
35. X.J. Kang, C.X. Li, Z.Y. Cheng, P.A. Ma, Z.Y. Hou and J. Lin, Lanthanide-doped hollow nanomaterials as theranostic agents. *WIREs Nanomed. Nanobiotechnol*., 6 (2014): 80-101.

36. Z.H. Xu, Y. Cao, C.X. Li, P.A. Ma, X.F. Zhai, S.S. Huang, X.J. Kang, M.M. Shang, D.M. Yang, Y.L. Dai and J. Lin, Urchin-like $GdPO_4$ and $GdPO_4$:Eu^{3+} hollow spheres - hydrothermal synthesis, luminescence and drug-delivery properties. *J. Mater. Chem*., 21 (2011): 3686-3694.
37. Z.H. Xu, P.A. Ma, C.X. Li, Z.Y. Hou, X.F. Zhai, S.S. Huang and J. Lin, Monodisperse core-shell structured up-conversion Yb(OH)CO_3@$YbPO^4$:Er^{3+} hollow spheres as drug carriers. *Biomaterials,* 32 (2011): 4161-4173.
38. F. Zhang, Y.F. Shi, X.H. Sun, D.Y. Zhao and G.D. Stucky, Formation of hollow upconversion rare-earth fluoride nanospheres: nanoscale kirkendall effect during ion exchange. *Chem. Mater*., 21 (2009): 5237-5243.
39. D.M. Yang, X.J. Kang, P.A. Ma, Y.L. Dai, Z.Y. Hou, Z.Y. Cheng, C.X. Li and J. Lin, Hollow structured upconversion luminescent $NaYF_4$:Yb^{3+}, Er^{3+} nanospheres for cell imaging and targeted anti-cancer drug delivery. *Biomaterials,* 34 (2013): 1601-1612.
40. X. Michalet, F.F. Pinaud, L.A. Bentolila, J.M. Tsay, S. Doose, J.J. Li, G. Sundaresan, A.M. Wu, S.S. Gambhir and S. Weiss, Quantum dots for live cells, in vivo imaging, and diagnostics. *Science*, 307 (2005): 538-544.
41. U. Resch-Genger, M. Grabolle, S. Cavaliere-Jaricot, R. Nitschke and T. Nann, Quantum dots versus organic dyes as fluorescent labels. *Nat. Methods*., 5 (2008): 763-775.
42. J. Zhou, Z. Liu and F.Y. Li, Upconversion nanophosphors for small-animal imaging. *Chem. Soc. Rev*., 41 (2012): 1323-1349.
43. M. Wang, G. Abbineni, A. Clevenger, C.B. Mao and S.K. Xu, Upconversion nanoparticles: synthesis, surface modification and biological applications. *Nanomed. Nanotechnol*. *Biol. Med.,* 7 (2011): 710-729.
44. L.Y. Ang, M.E. Lim, L.C. Ong and Y. Zhang, Applications of upconversion nanoparticles in imaging, detection and therapy. *Nanomedicine-UK*, 6 (2011): 1273-1288.
45. J.C. Boyer, M.P. Manseau, J.I. Murray and F.C.J.M. van Veggel, Surface modification of upconverting $NaYF_4$ nanoparticles with PEG-phosphate ligands for NIR (800 nm) biolabeling within the biological window. *Langmuir,* 26 (2010): 1157-1164.
46. T.Y. Cao, Y. Yang, Y.A. Gao, J. Zhou, Z.Q. Li and F.Y. Li, High-quality water-soluble and surface-functionalized upconversion nanocrystals as luminescent probes for bioimaging. *Biomaterials,* 32 (2011): 2959-2968.
47. J. Chen, C.R. Guo, M. Wang, L. Huang, L.P. Wang, C.C. Mi, J. Li, X.X. Fang, C.B. Mao and S.K. Xu, Controllable synthesis of $NaYF_4$:Yb,Er upconversion nanophosphors and their application to in vivo imaging of Caenorhabditis elegans. *J. Mater. Chem*., 21 (2011): 2632-2638.
48. Y. Sun, M.X. Yu, S. Liang, Y.J. Zhang, C.G. Li, T.T. Mou, W.J. Yang, X.Z. Zhang, B.A. Li, C.H. Huang and F.Y. Li, Fluorine-18 labeled rare-earth nanoparticles for positron emission tomography (PET) imaging of sentinel lymph node. *Biomaterials,* 32 (2011): 2999-3007.
49. H.C. Liu, C.T. Xu and S. Andersson-Engels, Multibeam fluorescence diffuse optical tomography using upconverting nanoparticles. *Opt. Lett*., 35 (2010): 718-720.
50. H.S. Qian, H.C. Guo, P.C.L. Ho, R. Mahendran and Y. Zhang, Mesoporous-silica-coated up-conversion fluorescent nanoparticles for photodynamic therapy. *Small,* 5 (2009): 2285-2290.
51. N.M. Idris, M.K. Gnanasammandhan, J. Zhang, P.C. Ho, R. Mahendran and Y. Zhang, In vivo photodynamic therapy using upconversion nanoparticles as remote-controlled nanotransducers. *Nat. Med*., 18 (2012): 1580-1585.

52. L. Cheng, K. Yang, Y.G. Li, J.H. Chen, C. Wang, M.W. Shao, S.T. Lee and Z. Liu, Facile preparation of multifunctional upconversion nanoprobes for multimodal imaging and dual-targeted photothermal therapy. *Angew. Chem. Int. Ed*., 50 (2011): 7385-7390.
53. Y. Huang, F. Rosei and F. Vetrone, A single multifunctional nanoplatform based on upconversion luminescence and gold nanorods. *Nanoscale,* 7 (2015): 5178-5185.
54. C. Wang, L.A. Cheng and Z.A. Liu, Drug delivery with upconversion nanoparticles for multi-functional targeted cancer cell imaging and therapy. *Biomaterials,* 32 (2011): 1110-1120.
55. J.A. Liu, W.B. Bu, L.M. Pan and J.L. Shi, NIR-Triggered Anticancer Drug Delivery by Upconverting Nanoparticles with Integrated Azobenzene-Modified Mesoporous Silica. *Angew. Chem. Int. Ed*., 52 (2013): 4375-4379.
56. J.P. Lai, B.R. Shah, Y.X. Zhang, L.T. Yang and K.B. Lee, Real-time monitoring of ATP-responsive drug release using mesoporous-silica-coated multicolor upconversion nanoparticles. *ACS Nano*, 9 (2015): 5234-5245.
57. J.A. Capobianco, F. Vetrone, T. D'Alesio, G. Tessari, A. Speghini and M. Bettinelli, Optical spectroscopy of nanocrystalline cubic Y_2O_3:Er^{3+} obtained by combustion synthesis. *Phys. Chem. Chem. Phys*., 2 (2000): 3203-3207.
58. J.N. Shan, J.B. Chen, J. Meng, J. Collins, W. Soboyejo, J.S. Friedberg and Y.G. Ju, Biofunctionalization, cytotoxicity, and cell uptake of lanthanide doped hydrophobically ligated $NaYF(_4)$ upconversion nanophosphors. *J. Appl. Phys*., 104 (2008).
59. F. Vetrone, R. Naccache, A.J. de la Fuente, F. Sanz-Rodriguez, A. Blazquez-Castro, E.M. Rodriguez, D. Jaque, J.G. Sole and J.A. Capobianco, Intracellular imaging of HeLa cells by non-functionalized $NaYF_4$:Er^{3+}, Yb^{3+} upconverting nanoparticles. *Nanoscale*, 2 (2010): 495-498.
60. S.F. Lim, R. Riehn, W.S. Ryu, N. Khanarian, C.K. Tung, D. Tank and R.H. Austin, In vivo and scanning electron microscopy imaging of upconverting nanophosphors in Caenorhabditis elegans. *Nano Lett*., 6 (2006): 169-174.
61. D.K. Chatteriee, A.J. Rufalhah and Y. Zhang, Upconversion fluorescence imaging of cells and small animals using lanthanide doped nanocrystals. *Biomaterials*, 29 (2008): 937-943.
62. H.Y. Xing, W.B. Bu, S.J. Zhang, X.P. Zheng, M. Li, F. Chen, Q.J. He, L.P. Zhou, W.J. Peng, Y.Q. Hua and J.L. Shi, Multifunctional nanoprobes for upconversion fluorescence, MR and CT trimodal imaging. *Biomaterials*, 33 (2012): 1079-1089.
63. H.Y. Xing, X.P. Zheng, Q.G. Ren, W.B. Bu, W.Q. Ge, Q.F. Xiao, S.J. Zhang, C.Y. Wei, H.Y. Qu, Z. Wang, Y.Q. Hua, L.P. Zhou, W.J. Peng, K.L. Zhao and J.L. Shi, Computed tomography imaging-guided radiotherapy by targeting upconversion nanocubes with significant imaging and radiosensitization enhancements. *Sci. Rep*., 3 (2013): 1751.
64. Q. Liu, Y. Sun, C. Li, J. Zhou, C. Li, T. Yang, X. Zhang, T. Yi, D. Wu and F. Li, 18F-labeled magnetic-upconversion nanophosphors via rare-Earth cation-assisted ligand assembly. *ACS Nano*., 5 (2011): 3146-3157.
65. P. Zhang, W. Steelant, M. Kumar and M. Scholfield, Versatile photosensitizers for photodynamic therapy at infrared excitation. *J. Am. Chem. Soc*., 129 (2007): 4526-4527.
66. S. Hackbarth, J. Schlothauer, A. Preuss and B. Roder, New insights to primary photodynamic effects - Singlet oxygen kinetics in living cells. *J. Photochem. Photobiol. B*, 98 (2010): 173-179.
67. J.N. Shan, S.J. Budijono, G.H. Hu, N. Yao, Y.B. Kang, Y.G. Ju and R.K. Prud'homme, Pegylated composite nanoparticles containing upconverting phosphors and meso-

tetraphenyl porphine (TPP) for photodynamic therapy. *Adv. Funct. Mater*., 21 (2011): 2488-2495.

68. J.P. Celli, B.Q. Spring, I. Rizvi, C.L. Evans, K.S. Samkoe, S. Verma, B.W. Pogue and T. Hasan, Imaging and photodynamic therapy: mechanisms, monitoring, and optimization. *Chem. Rev*., 110 (2010): 2795-2838.
69. K. Liu, X.M. Liu, Q.H. Zeng, Y.L. Zhang, L.P. Tu, T. Liu, X.G. Kong, Y.H. Wang, F. Cao, S.A.G. Lambrechts, M.C.G. Aalders and H. Zhang, Covalently assembled NIR nanoplatform for simultaneous fluorescence imaging and photodynamic therapy of cancer cells. *ACS Nano*., 6 (2012): 4054-4062.
70. X.M. Liu, M. Zheng, X.G. Kong, Y.L. Zhang, Q.H. Zeng, Z.C. Sun, W.J. Buma and H. Zhang, Separately doped upconversion-C-60 nanoplatform for NIR imaging-guided photodynamic therapy of cancer cells. *Chem. Commun*., 49 (2013): 3224-3226.
71. L.C. Kennedy, L.R. Bickford, N.A. Lewinski, A.J. Coughlin, Y. Hu, E.S. Day, J.L. West and R.A. Drezek, A new era for cancer treatment: gold-nanoparticle-mediated thermal therapies. *Small*., 7 (2011): 169-183.
72. E.C. Dreaden, M.A. Mackey, X.H. Huang, B. Kang and M.A. El-Sayed, Beating cancer in multiple ways using nanogold. *Chem. Soc. Rev*., 40 (2011): 3391-3404.
73. D. Jaque, L.M. Maestro, B. del Rosal, P. Haro-Gonzalez, A. Benayas, J.L. Plaza, E.M. Rodriguez and J.G. Sole, Nanoparticles for photothermal therapies. *Nanoscale*., 6 (2014): 9494-9530.
74. Y. Song, G.X. Liu, X.T. Dong, J.X. Wang, W.S. Yu and J.M. Li, Construction of Au@$NaYF_4$:Yb^{3+}, Er^{3+}/Ho^{3+} bifunctional hybrid nanocomposites with upconversion luminescence and photothermal properties. *RSC Adv*., 4 (2014): 62802-62808.
75. L.P. Qian, L.H. Zhou, H.P. Too and G.M. Chow, Gold decorated $NaYF_4$:Yb,Er/$NaYF_4$/silica (core/shell/shell) upconversion nanoparticles for photothermal destruction of BE(2)-C neuroblastoma cells. *J. Nanopart. Res*., 13 (2011): 499-510.
76. S. Rohani, M. Quintanilla, S. Tuccio, F. De Angelis, E. Cantelar, A.O. Govorov, L. Razzari and F. Vetrone, Enhanced luminescence, collective heating, and nanothermometry in an ensemble system composed of lanthanide-doped upconverting nanoparticles and gold nanorods. *Adv. Opt. Mater*., 3 (2015): 1606-1613.
77. N. Niu, F. He, P.A. Ma, S.L. Gai, G.X. Yang, F.Y. Qu, Y. Wang, J. Xu and P.P. Yang, Up-conversion nanoparticle assembled mesoporous silica composites: synthesis, plasmon-enhanced luminescence, and near-infrared light triggered drug eelease. *ACS Appl. Mater. Interfaces*, 6 (2014): 3250-3262.
78. J.A. Barreto, W. O'Malley, M. Kubeil, B. Graham, H. Stephan and L. Spiccia, Nanomaterials: Applications in cancer imaging and therapy. *Adv. Mater*., 23 (2011): 18-40.
79. T. Neuberger, B. Schopf, H. Hofmann, M. Hofmann and B. von Rechenberg, Superparamagnetic nanoparticles for biomedical applications: possibilities and limitations of a new drug delivery system. *J. Magn. Magn. Mater*., 293 (2005): 483-496.
80. Y.F. Yang, Y.Q. Qu, J.W. Zhao, Q.H. Zeng, Y.Y. Ran, Q.B. Zhang, X.G. Kong and H. Zhang, Fabrication of and drug delivery by an upconversion emission nanocomposite with monodisperse LaF_3:Yb,Er core/mesoporous silica shell structure. *Eur. J. Inorg. Chem.,* (2010): 5195-5199.
81. Z.H. Xu, C.X. Li, P.A. Ma, Z.Y. Hou, D.M. Yang, X.J. Kang and J. Lin, Facile synthesis of an up-conversion luminescent and mesoporous Gd_2O_3:Er^{3+}@n$SiO_{(2)}$@m$SiO_{(2)}$ nanocomposite as a drug carrier. *Nanoscale*., 3 (2011): 661-667.

82. Z.Y. Hou, C.X. Li, P.A. Ma, G.G. Li, Z.Y. Cheng, C. Peng, D.M. Yang, P.P. Yang and J. Lin, Electrospinning preparation and drug-delivery properties of an up-conversion luminescent porous $NaYF_4$:Yb^{3+}, Er^{3+}@silica fiber nanocomposite. *Adv. Funct. Mater*., 21 (2011): 2356-2365.
83. B. Liu, C.X. Li, D.M. Yang, Z.Y. Hou, P.A. Ma, Z.Y. Cheng, H.Z. Lian, S.S. Huang and J. Lin, Upconversion-luminescent core/mesoporous-silica-shell structured beta-$NaYF_4$:Yb^{3+},Er^{3+}@SiO_2@mSiO(2) composite nanospheres: fabrication and drug-storage/release properties. *Eur. J. Inorg. Chem*., 2014 (2014): 1906-1913.
84. S.Q. He, K. Krippes, S. Ritz, Z.J. Chen, A. Best, H.J. Butt, V. Mailander and S. Wu, Ultralow-intensity near-infrared light induces drug delivery by upconverting nanoparticles. *Chem. Commun*., 51 (2015): 431-434.
85. D.M. Yang, Y.L. Dai, P.A. Ma, X.J. Kang, Z.Y. Cheng, C.X. Li and J. Lin, One-step synthesis of small-sized and water-soluble $NaREF_4$ upconversion nanoparticles for In vitro cell imaging and drug delivery. *Chem. Eur. J*., 19 (2013): 2685-2694.
86. W.L. Ren, G. Tian, S. Jian, Z.J. Gu, L.J. Zhou, L. Yan, S. Jin, W.Y. Yin and Y.L. Zhao, TWEEN coated $NaYF_4$:Yb,Er/$NaYF_4$ core/shell upconversion nanoparticles for bioimaging and drug delivery. *RSC Adv*., 2 (2012): 7037-7041.
87. J.N. Liu, W.B. Bu, L.M. Pan, S. Zhang, F. Chen, L.P. Zhou, K.L. Zhao, W.J. Peng and J.L. Shi, Simultaneous nuclear imaging and intranuclear drug delivery by nuclear-targeted multifunctional upconversion nanoprobes. *Biomaterials*, 33 (2012): 7282-7290.
88. X.K. Jia, J.J. Yin, D.G. He, X.X. He, K.M. Wang, M. Chen and Y.H. Li, Polyacrylic acid modified upconversion nanoparticles for simultaneous pH-triggered drug delivery and release imaging. *J. Biomed. Nanotechnol*., 9 (2013): 2063-2072.
89. W.T. Al-Jamal, K.T. Al-Jamal, A. Cakebread, J.M. Halket and K. Kostarelos, Blood circulation and tissue biodistribution of lipid-quantum dot (L-QD) hybrid vesicles intravenously administered in mice. *Bioconjugate Chem*., 20 (2009): 1696-1702.
90. W.T. All-Jamal, K.T. Al-Jamal, B. Tian, A. Cakebread, J.M. Halket and K. Kostarelos, Tumor targeting of functionalized quantum dot-liposome hybrids by intravenous administration. *Mol. Pharm.,* 6 (2009): 520-530.
91. D.B. Chithrani, M. Dunne, J. Stewart, C. Allen and D.A. Jaffray, Cellular uptake and transport of gold nanoparticles incorporated in a liposomal carrier. *Nanomed. Nanotechnol*. *Biol. Med.,* 6 (2010): 161-169.
92. Y.N. He, L.H. Zhang, D.W. Zhu and C.X. Song, Design of multifunctional magnetic iron oxide nanoparticles/mitoxantrone-loaded liposomes for both magnetic resonance imaging and targeted cancer therapy. *Int. J. Nanomed*., 9 (2014): 4055-4066.
93. Y. Huang, E. Hemmer, F. Rosei and F. Vetrone, Multifunctional liposome nanocarriers combining upconverting nanoparticles and anticancer drugs. *J. Phys. Chem. B*, 120 (2016): 4992-5001.
94. X.D. Wang, X.H. Song, C.Y. He, C.J. Yang, G.N. Chen and X. Chen, Preparation of reversible colorimetric temperature nanosensors and their application in quantitative two-dimensional thermo-imaging. *Anal. Chem*., 83 (2011): 2434-2437.
95. F.M. Ye, C.F. Wu, Y.H. Jin, Y.H. Chan, X.J. Zhang and D.T. Chiu, Ratiometric temperature sensing with semiconducting polymer dots. *J. Am. Chem. Soc*., 133 (2011): 8146-8149.
96. J.M. Yang, H. Yang and L.W. Lin, Quantum dot nano thermometers reveal heterogeneous local thermogenesis in living cells. *ACS Nano*, 5 (2011): 5067-5071.
97. E.J. McLaurin, V.A. Vlaskin and D.R. Gamelin, Water-soluble dual-emitting nanocrystals for ratiometric optical thermometry. *J. Am. Chem. Soc*., 133 (2011): 14978-14980.

98. C.H. Hsia, A. Wuttig and H. Yang, An accessible approach to preparing water-soluble Mn^{2+}-Doped (CdSSe) ZnS (Core) shell nanocrystals for ratiometric temperature sensing. *ACS Nano*, 5 (2011): 9511-9522.
99. G.W. Walker, V.C. Sundar, C.M. Rudzinski, A.W. Wun, M.G. Bawendi and D.G. Nocera, Quantum-dot optical temperature probes. *Appl. Phys. Lett*., 83 (2003): 3555-3557.
100. S. Li, K. Zhang, J.M. Yang, L.W. Lin and H. Yang, Single quantum dots as local temperature markers. *Nano Lett*., 7 (2007): 3102-3105.
101. L.M. Maestro, E.M. Rodriguez, F.S. Rodriguez, M.C.I. la Cruz, A. Juarranz, R. Naccache, F. Vetrone, D. Jaque, J.A. Capobianco and J.G. Sole, CdSe quantum dots for two-photon fluorescence thermal imaging. *Nano Lett*., 10 (2010): 5109-5115.
102. S.M. Borisov and O.S. Wolfbeis, Temperature-sensitive europium (III) probes and their use for simultaneous luminescent sensing of temperature and oxygen. *Anal. Chem*., 78 (2006): 5094-5101.
103. H.S. Peng, M.I.J. Stich, J.B. Yu, L.N. Sun, L.H. Fischer and O.S. Wolfbeis, Luminescent europium (III) nanoparticles for sensing and imaging of temperature in the physiological range. *Adv. Mater*., 22 (2010): 716-719.
104. C.D.S. Brites, P.P. Lima, N.J.O. Silva, A. Millan, V.S. Amaral, F. Palacio and L.D. Carlos, A luminescent molecular thermometer for long-term absolute temperature measurements at the nanoscale. *Adv. Mater*., 22 (2010): 4499-4504.
105. H.S. Peng, S.H. Huang and O.S. Wolfbeis, Ratiometric fluorescent nanoparticles for sensing temperature. *J. Nanopart. Res*., 12 (2010): 2729-2733.
106. F. Vetrone, R. Naccache, A. Zamarron, A.J. de la Fuente, F. Sanz-Rodriguez, L.M. Maestro, E.M. Rodriguez, D. Jaque, J.G. Sole and J.A. Capobianco, Temperature sensing using fluorescent nanothermometers. *ACS Nano*, 4 (2010): 3254-3258.
107. L.H. Fischer, G.S. Harms and O.S. Wolfbeis, Upconverting nanoparticles for nanoscale thermometry. *Angew. Chem. Int. Ed*., 50 (2011): 4546-4551.
108. L. Aigouy, E. Saidi, L. Lalouat, J. Labeguerie-Egea, M. Mortier, P. Low and C. Bergaud, AC thermal imaging of a microwire with a fluorescent nanocrystal: Influence of the near field on the thermal contrast. *J. Appl. Phys*., 106 (2009).
109. E. Saidi, B. Samson, L. Aigouy, S. Volz, P. Low, C. Bergaud and M. Mortier, Scanning thermal imaging by near-field fluorescence spectroscopy. *Nanotechnology*, 20 (2009).
110. X. Wang, X.G. Kong, Y. Yu, Y.J. Sun and H. Zhang, Effect of annealing on upconversion luminescence of ZnO: Er^{3+} nanocrystals and high thermal sensitivity. *J. Phys. Chem. C*, 111 (2007): 15119-15124.
111. V.K. Tikhomirov, K. Driesen, V.D. Rodriguez, P. Gredin, M. Mortier and V.V. Moshchalkov, Optical nanoheater based on the Yb^{3+}-Er^{3+} co-doped nanoparticles. *Opt. Express*, 17 (2009): 11794-11798.
112. S.K. Singh, K. Kumar and S.B. Rai, Multifunctional Er^{3+}-Yb^{3+} codoped Gd_2O_3 nanocrystalline phosphor synthesized through optimized combustion route. *Appl. Phys. B: Lasers Opt*., 94 (2009): 165-173.
113. N. Chandrasekharan and L.A. Kelly, A dual fluorescence temperature sensor based on perylene/exciplex interconversion. *J. Am. Chem. Soc*., 123 (2001): 9898-9899.
114. W.G.J.H.M. van Sark, J. de Wild, J.K. Rath, A. Meijerink and R.E.I. Schropp, Upconversion in solar cells. *Nanoscale Res. Lett*., 8 (2013): 81.
115. J.C. Goldschmidt and S. Fischer, Upconversion for photovoltaics - a review of materials, devices and concepts for performance enhancement. *Adv. Opt. Mater*., 3 (2015): 510-535.

116. J. Mendez-Ramos, P. Acosta-Mora, J.C. Ruiz-Morales, T. Hernandez, M.E. Borges and P. Esparza, Turning into the blue: materials for enhancing TiO_2 photocatalysis by up-conversion photonics. *RSC Adv*., 3 (2013): 23028-23034.
117. V. Vaiano, O. Sacco, G. Iervolino, D. Sannino, P. Ciambelli, R. Liguori, E. Bezzeccheri and A. Rubino, Enhanced visible light photocatalytic activity by up-conversion phosphors modified N-doped TiO_2. *Appl. Catal. B,* 176 (2015): 594-600.
118. F. Zhang, C.L. Zhang, H.Y. Peng, H.P. Cong and H.S. Qian, Near-infrared photocatalytic upconversion nanoparticles/TiO_2 nanofibers assembled in large scale by electrospinning. *Part. Part. Syst. Char*., 33 (2016): 248-253.
119. W.F. Yang, X.Y. Li, D.Z. Chi, H.J. Zhang and X.G. Liu, Lanthanide-doped upconversion materials: emerging applications for photovoltaics and photocatalysis. *Nanotechnology*, 25 (2014).
120. J. Wang, F.Y. Wen, Z.H. Zhang, X.D. Zhang, Z.J. Pan, L. Zhang, L. Wang, L. Xu, P.L. Kang and P. Zhang, Degradation of dyestuff wastewater using visible light in the presence of a novel nano TiO_2 catalyst doped with upconversion luminescence agent. *J. Environ. Sci. (China*), 17 (2005): 727-730.
121. Y.N. Tang, W.H. Di, X.S. Zhai, R.Y. Yang and W.P. Qin, NIR-responsive photocatalytic activity and mechanism of $NaYF_4$:Yb,Tm@TiO_2 core-shell Nanoparticles. *ACS Catal*., 3 (2013): 405-412.
122. Z.H. Xu, M. Quintanilla, F. Vetrone, A.O. Govorov, M. Chaker and D.L. Ma, Harvesting lost photons: plasmon and upconversion enhanced broadband photocatalytic activity in core@shell microspheres based on lanthanide-doped $NaYF_4$, TiO_2, and Au. *Adv. Funct. Mater*., 25 (2015): 2950-2960.
123. F. Zhang, C.L. Zhang, W.N. Wang, H.P. Cong and H.S. Qian, Titanium dioxide/upconversion nanoparticles/cadmium sulfide nanofibers enable enhanced full-spectrum absorption for superior solar light driven photocatalysis. *ChemSusChem*. 9 (2016): 1449-1454.
124. A. Gajovic, S. Sturm, B. Jancar, A. Santic, K. Zagar and M. Ceh, The synthesis of pure-phase bismuth ferrite in the Bi-Fe-O system under hydrothermal conditions without a mineralizer. *J. Am. Ceram. Soc*., 93 (2010): 3173-3179.
125. D.W. Cao, Z.J. Wang, Nasori, L.Y. Wen, Y. Mi and Y. Lei, Switchable charge-transfer in the photoelectrochemical energy-conversion process of ferroelectric $BiFeO_3$ Photoelectrodes. *Angew. Chem. Int. Ed*., 53 (2014): 11027-11031.
126. S. Li, Y.H. Lin, B.P. Zhang, J.F. Li and C.W. Nan, $BiFeO_3$/TiO_2 core-shell structured nanocomposites as visible-active photocatalysts and their optical response mechanism. *J. Appl. Phys*., 105 (2009).
127. T. Liu, Y.B. Xu and J.Y. Zhao, Low-temperature synthesis of $BiFeO_{(3)}$ via PVA sol-gel route. *J. Am. Ceram. Soc*., 93 (2010): 3637-3641.
128. X. Zhang, L. Bourgeois, J. Yao, H. Wang and P.A. Webley, Tuning the morphology of bismuth ferrite nano- and microcrystals: from sheets to fibers. *Small*, 3 (2007): 1523-1528.
129. S. Li, J.M. Zhang, M.G. Kibria, Z.T. Mi, M. Chaker, D.L. Ma, R. Nechache and F. Rosei, Remarkably enhanced photocatalytic activity of laser ablated Au nanoparticle decorated $BiFeO_3$ nanowires under visible-light. *Chem. Commun*., 49 (2013): 5856-5858.
130. S.M. Sun, W.Z. Wang, L. Zhang and M. Shang, Visible light-induced photocatalytic oxidation of phenol and aqueous ammonia in flowerlike $Bi_2Fe_4O_9$ suspensions. *J. Phys. Chem. C*, 113 (2009): 12826-12831.

131. J.M. Zhang, Y. Huang, L. Jin, F. Rosei, F. Vetrone F, J.P. Claverie, Efficient upconverting multiferroic core@shell photocatalysts: visible-to-near-infrared photon harvesting. *ACS Appl. Mater. Interfaces*, 9 (2017): 8142-8150.
132. Z.Y. Hou, Y.X. Zhang, K.R. Deng, Y.Y. Chen, X.J. Li, X.R. Deng, Z.Y. Cheng, H.Z. Lian, C.X. Li and J. Lin, UV-emitting upconversion-based TiO_2 photosensitizing nanoplatform: near-infrared light mediated in vivo photodynamic therapy via mitochondria-involved apoptosis pathway. *ACS Nano*, 9 (2015): 2584-2599.
133. S.S. Lucky, N.M. Idris, Z.Q. Li, K. Huang, K.C. Soo and Y. Zhang, Titania coated upconversion nanoparticles for near-infrared light triggered photodynamic therapy. *ACS Nano*, 9 (2015): 191-205.
134. B. Nikoobakht and M.A. El-Sayed, Preparation and growth mechanism of gold nanorods (NRs) using seed-mediated growth method. *Chem. Mater*., 15 (2003): 1957-1962.
135. R. Naccache, P. Chevallier, J. Lagueux, Y. Gossuin, S. Laurent, L. Vander Elst, C. Chilian, J.A. Capobianco and M.A. Fortin, High relaxivities and strong vascular signal enhancement for $NaGdF_4$ nanoparticles designed for dual MR/optical imaging. *Adv. Healthcare Mater*., 2 (2013): 1478-1488.
136. W.T. Al-Jamal, K.T. Al-Jamal, P.H. Bomans, P.M. Frederik and K. Kostarelos, Functionalized-quantum-dot-liposome hybrids as multimodal nanoparticles for cancer. *Small*, 4 (2008): 1406-1415.
137. G. Haran, R. Cohen, L.K. Bar and Y. Barenholz, Transmembrane ammonium-sulfate gradients in liposomes produce efficient and stable entrapment of amphipathic weak bases. *Biochim. Biophys. Acta*, 1151 (1993): 201-215.
138. G. Zonios, J. Bykowski and N. Kollias, Skin melanin, hemoglobin, and light scattering properties can be quantitatively assessed in vivo using diffuse reflectance spectroscopy. *J. Invest. Dermatol*., 117 (2001): 1452-1457.
139. I. Villa, A. Vedda, I.X. Cantarelli, M. Pedroni, F. Piccinelli, M. Bettinelli, A. Speghini, M. Quintanilla, F. Vetrone, U. Rocha, C. Jacinto, E. Carrasco, F.S. Rodriguez, A. Juarranz, B. del Rosal, D.H. Ortgies, P.H. Gonzalez, J.G. Sole and D.J. Garcia, 1.3 μm emitting $SrF_2:Nd^{3+}$ nanoparticles for high contrast in vivo imaging in the second biological window. *Nano Res*., 8 (2015): 649-665.
140. S.W. Wu, G. Han, D.J. Milliron, S. Aloni, V. Altoe, D.V. Talapin, B.E. Cohen and P.J. Schuck, Non-blinking and photostable upconverted luminescence from single lanthanide-doped nanocrystals. *Proc. Natl. Acad. Sci. U.S.A*., 106 (2009): 10917-10921.

Appendice B

Résumé

L'introduction

Au cours des dernières années, des nanoparticules de la conversion ascendante dopées aux lanthanides (Ln^{3+}) - (en anglais: Upconverting nanoparticles; UCNPs) sont émergentes pour une bioimagerie efficace et polyvalente ainsi que des méthodes thérapeutiques. Généralement, ces nanoparticules peuvent être excitées avec la lumière proche infrarouge (en anglais: near-infrared; NIR) et peuvent s'émettre des photons de haute énergie qui comprennent l'ultraviolet (UV), visible et NIR par un processus multiphotonique, dit dont la conversion ascendante (upconversion). Pendant ce processus, la conversion ascendante est réalisée par l'absorption d'énergie par deux ou plus de photons d'excitation pour la génération d'une émission de photons, et elle est caractérisée par l'émission de lumière à des longueurs d'onde plus courtes que la longueur d'onde d'excitation [11]. Particulièrement, contrairement à la luminescence à deux photons, (en anglais: two-photon luminescence; TPL), l'absorption des photons est séquentielle et non simultanée [12]. Dans ce dernier cas, elle est nécessaire d'une excitation par des lasers avec des impulsions ultra-rapides (femtosecondes). Le processus de la conversion ascendante se bénéficie d'états excités intermédiaires réels possédant de longues durées de vie en général dans les échelles de µs à ms [13]. Celui-ci permet de l'absorption séquentielle et de l'étape progressive de photons NIR pour réaliser l'excitation de l'état d'énergie final, suivi par la génération d'un photon d'énergie plus élevée.

Il y plusieurs types de processus de la conversion ascendante. Généralement, le processus de la conversion ascendante des UCNPs dopées aux lanthanides pourrait comprendre des trois stages: l'absorption de l'état excité (en anglais: excited state absorption; ESA), la conversion ascendante de relaxation croisée (en anglais: cross-relaxation; CR), et la conversion ascendante du transfert d'énergie (en anglais: energy transfer upconversion; ETU). Il est à noter que le processus d'ETU est celle le plus efficace de la conversion ascendante et la plupart des UCNPs utilisées aujourd'hui se profitent de ce mécanisme. Dans le processus d'ETU, le transfert d'énergie a lieu d'entre deux ions lanthanides voisins. Le processus d'ETU commence par une absorption de photons par un ion, puis un transfert d'énergie non radiatif subséquente d'ions voisins conduit la population d'un état très excité de l'ion émettant. Donc, la concentration de dopant qui détermine la distance moyenne entre les ions dopants voisins a une forte influence sur l'efficacité de la conversion ascendante d'un processus d'ETU. Bien que l'émission de la conversion ascendante puisse être théoriquement réalisée sur la plupart des ions des lanthanides, les exigences des niveaux d'énergie ont limité les ions émettant à plusieurs ions lanthanides. Typiquement, Yb^{3+} est utilisé comme sensibilisateur pour transférer l'énergie des ions émettant voisins dans le processus de l'ETU, tandis que les ions d'émission les plus utilisés sont Er^{3+}, Tm^{3+}, *etc* [25]. L'ion du sensibilisateur (par exemple, Yb^{3+}) est excité par une source de lumière NIR qui se transfères non radiatifs ensuite cette énergie à l'ion d'émetteur (par exemple, Er^{3+} ou Tm^{3+}) qui émet un photon de détection. La figure 1 montre l'illustration schématique du processus de la conversion ascendante de NIR à visible et UV.

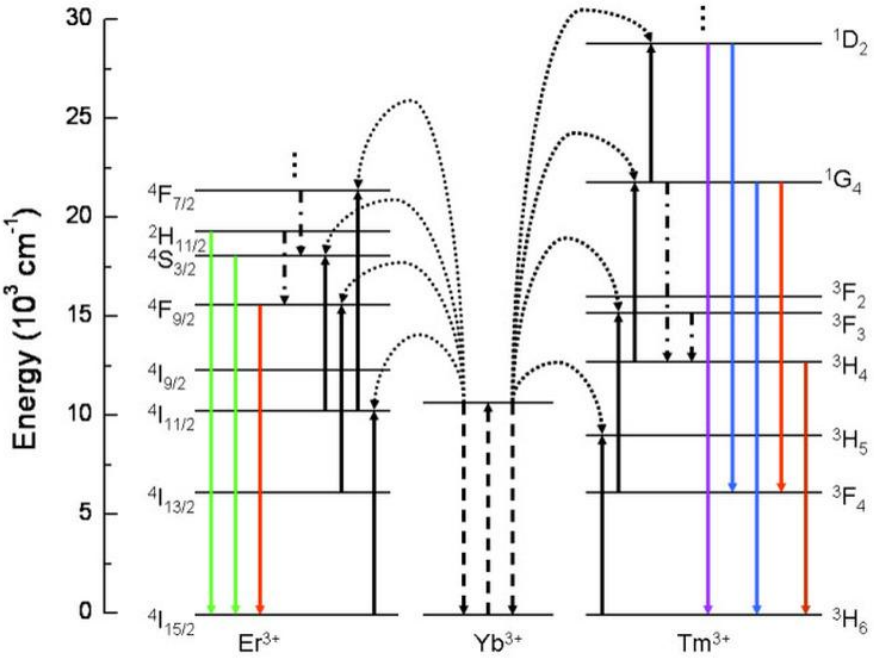

Figure 1 Diagramme des niveaux d' énergie pour UCNPs en Yb^{3+}/Er^{3+} et Yb^{3+}/Tm^{3+} [26]

Bénéficiant de mécanisme de la conversion ascendante d'émission des ions de dopant lanthanides, ces UCNPs se présentent des propriétés optiques spécifiques, tels que les petites tailles de bandes des émissions, un grand décalage anti-Stokes, la photostabilité élevée, le faible contexte d'autofluorescence, la grande profondeur de pénétration et la résolution temporelle [42]. Par exemple, il a été démontré que l'UCNP individuel représente de la photostabilité et un comportement non-clignotant et montrent aucune perte d'intensité après une heure d'excitation continue [140]. En outre, autre que les propriétés optiques, la détection thermique est également la propriété importante pour les UCNPs. À ce jour, il y a des plusieurs exemples démontrant que l'intensité des transitions intra-4*f* et de la durée de vie d'un état excité 4*f* particulier sont fonction de la température. Associé aux UCNPs, quelques émissions des ions lanthanides ont un équilibre thermique

déterminé par le facteur de Boltzmann. Par conséquent, les UCNPs pourraient être utilisés comme nanothermomètres lors de la combinaison de l'utilisation des propriétés thermiques et optiques.

UCNPs ont démontré un potentiel important dans les applications de bio-imagerie et la thérapie du cancer. Dans bio-imagerie, UCNPs ont été utilisés pour l'imagerie *in vitro*, l'imagerie *in vivo* et, plus récemment, d'autres techniques de bio-imagerie telles que la tomographie par émission de positons (PET) [48] et la tomographie optique diffusé (DOT) [49]. Par exemple, Vetrone *et al*. a étudié l'imagerie intracellulaire de cellules HeLa en utilisant $NaYF_4:Er^{3+}$, Yb^{3+} UCNPs fonctionnalisé avec polyéthylènimine (PEI). Les résultats ont montré une redistribution des UCNPs à l'intérieur de la cellule comme la durée d'incubation augmentée, ce qui promet de l'application d'UCNPs pour l'imagerie en temps réel de dynamiques cellulaires [59]. En outre, pour l'imagerie *in vivo*, en 2006, Lim et ses collègues ont montré un exemple précédent d'imagerie Caenorhabditis elegans en utilisant nanoparticules $Y_2O_3:Yb^{3+}$, Er^{3+}. La taille des nanoparticules est d'environ de 50 à 150 nm et la distribution des UCNPs chez Caenorhabditis elegans peut être clairement visualisé à l'excitation de longueur d'onde de 980 nm. Cette étude se démontre qu'UCNPs pourrait être un outil fort pour la bioimagerie [60]. En outre, en base de la relation entre les propriétés optiques et thermiques, d'un type particulier de capteur de température a également été développée. Par exemple, Vetrone *et al*. ont démontré la détection de la température intracellulaire en utilisant le $NaYF_4:Er^{3+}$, Yb^{3+} UCNPs. Ce travail s'ouvre une nouvelle direction pour les bio-applications d'UCNPs. Le capteur de température sur la base d'UCNP pourrait fonctionner de 300 à 2000 K [106].

UCNPs sont également étudiées pour la thérapie du cancer où leur luminescence a été exploitée pour des applications telles que la thérapie photodynamique (en anglais: photodynamic therapy; PDT), la thérapie photothermique (en anglais: photothermal therapy; PTT) et la livraison de médicaments. La thérapie photodynamique est un type de traitement médical activé par la lumière, ce qui provoque la mort contrôlée des cellules malades comme des cellules tumorales. Il est en base sur un processus dans lequel un médicament sensible à la lumière appelé un photosensibilisateur est introduit dans les cellules, et est ensuite excité par la lumière à une longueur d'onde appropriée. L'énergie absorbée est transférée à l'oxygène moléculaire présentent dans l'environnement, en produisant des échantillons réactives de l'oxygène et cytotoxiques (en anglais: reactive oxygen species; ROS), dont la présence pourras déclencher la mort des cellules [65, 66]. De nos jours, la combinaison de médicaments PDT avec UCNPs a concentré sur l'attention. UCNPs NIR-excités peuvent émettre UV/photons visibles qui peuvent être utilisés pour activer les photosensibilisateurs à la proximité proche, puis générer des ROS pour tuer les cellules cancéreuses dans l'environnement. Ce serait, par exemple, permettre le traitement du carcinome plus profond et d'étendre la polyvalence de cette modalité thérapeutique [67, 68]. En outre, la possibilité de cellules de cancer du ciblage spécifique des composés PDT peut être contrôlée par UCNPs localisant les maladies bien que l'imagerie par fluorescence. Par exemple, le premier travail de combinaison d'UCNPs et PDT a été publiée par Zhang *et al* [65]. Dans leur étude, UCNPs ont été revêtues par une couche de silice, où les molécules PDT ont été incorporées et leurs résultats ont démontré qu'une amélioration du transfert d'énergie entre l'UCNP et le

composé PDT peut être obtenue en utilisant des dopants supplémentaires comme ions lanthanides.

La thérapie photothermique (PTT) est une stratégie de traitement basée sur les dommages que les températures élevées peuvent se produire dans les cellules, *i.e.* il utilise la chaleur pour tuer les cellules cancéreuses [71]. Afin de générer une augmentation de la température dans les cellules, un mécanisme très efficace consiste à transférer à partir d'une source lumineuse, plus pratiquement un laser, par l'absorption optique. Par conséquent, les nanoparticules avec un coefficient d'absorption optique élevée et le taux de dissipation thermique peuvent s'augmenter l'efficacité de PTT. Les métaux nobles comme l'or ou l'argent, sont considérés comme d'excellents candidats pour PTT en raison de leur forte absorption de résonance plasmonique de surface (en anglais: surface plasmon resonance; SPR) qui peut être suivie par l'émission de lumière et, plus important ici, la libération de chaleur. La résonance plasmonique de surface (SPR) est l'oscillation de résonance des électrons de conduction à l'interface métal stimulée par la lumière incidente. Ces nanoparticules ont souvent le SPR dans le visible, bien que pour certaines morphologies il peut descendre au NIR. Particulièrement, les nanosphères d'or, qui sont particulièrement pratique en raison de la facilité de synthèse, ont la bande d'absorption SPR au range de la spectrale verte/jaune, bien que la longueur d'onde précise peut être réglée en changeant la taille des particules. Un exemple particulièrement a été donné par Qian *et al.* que UCNPs préparées décorée par l'or appliquant une méthode de microémulsion inverse [75]. Ils ont observé que UCNPs dopées Er^{3+} qui émettent une lumière verte après l'excitation de NIR, peuvent être utilisées pour exciter les nanoparticules d'or, puis a déclenché l'augmentation de la température. Les données *in*

vitro ont démontré que les cellules cancéreuses ont été tuées efficacement après l'irradiation avec un laser à 980 nm, ce qui prouve qu'UCNPs peut être utilisé comme l'antenne pour le rayonnement.

Une autre application récente de la conversion ascendante dans la thérapie est la livraison de médicaments ciblés. Les systèmes de livraison de médicaments actuels sont basés sur des nanostructures (nanoparticules, des liposomes, des micelles, des dendrimères, des nanoémulsions, *etc.*) [78] avec une distribution de taille entre 10 et 100 nm pour empêcher la clairance par le système réticulo-endothélial [79], et par conséquent, de les maintenir en le courant sanguin pendant une durée plus longue [80]. Les propriétés de ces nanostructures peuvent être améliorées, bien que, par l'étiquette optique, pour visualiser leur distribution *in vivo* et, par conséquent, de contrôler l'efficacité du traitement. Pour cette raison, UCNPs sont émergentes comme un élément intéressant dans nanosystèmes de livraison de médicaments, en participant à la surveillance de location des médicaments et l'étude de l'interaction avec d'autres composants cellulaires. Par exemple, *Liu* et ses collaborateurs ont utilisé le polymère amphiphilede polyéthylène glycol greffé (en anglais: polyethylene glycol grafted amphiphilic polymer) à fonctionnaliser les UCNPs. Les nanoparticules obtenues ont été utilisées comme porteurs pour la livraison de doxorubicin (DOX) [54].

Les objectifs

Cette thèse se compose de deux parties: la première partie est principalement sur le développement de nanocomposites multifonctionnels combinées UCNPs et nanobâtons d'or (en anglais: gold nanorods; GNRs).

Jusqu'à présent, UCNPs ont montré d'être des outils efficaces et versatiles pour bioapplications. Une des applications les plus intéressantes est l'utilisation d'UCNPs comme nanothermomètres optiques. La majorité des nanothermomètres d'UCNP sont basées sur la luminescence dépendante de la température à laquelle les rapports d'intensité de luminescence varient en fonction de la température. Ces types de nanothermomètres s'ouvrent la porte à des possibilités thérapeutiques pour de nombreuses maladies, où une température locale augmente à la mort induite par la chaleur. En basé sur ça, ces nanothermomètres sont envisagées pour combiner avec nanoréchauffeur locales dont le rôle principe est de provoquer la température augmente contenait afin d'induire la mort cellulaire. Pendant ce processus, GNRs sont considérés comme d'excellents candidats pour nanoréchauffeur, en raison de leur forte absorption SPR accordable entre 650 et 1200 nm, en particulier lorsque le plasmon est situé dans le NIR, avec des applications *in vivo* compatible. Les GNRs absorbent la lumière provoquant des électrons pour subir des transitions de l'état du sol à l'état excité. L'énergie d'excitation électronique se conduit par une augmentation de l'énergie cinétique, ce qui conduit à la surchauffe de l'environnement local autour de l'espèce absorbant la lumière. Par conséquent, les cellules ou les tissus locaux pourraient être détruits par la chaleur produite. Récemment, PTT utilisant les bandes SPR localisées de nanoparticules d'or et les UCNPs a été rapporté. Cependant, il y a encore des défis et des questions qui doivent être abordées considérables. Par exemple, les cellules saines avoisinantes peuvent être endommagées en raison de l'augmentation de la température en même temps que les cellules malades. Par conséquent, il faut prendre soin d'obtenir un contrôle précis sur l'incrément de température locale afin de ne pas exposer les cellules saines entourantes à

ce chauffage localisé. Pour finir ce travail, les nanoréchauffeurs peuvent être couplés à un nanothermomètre mais doivent être situés dans le même espace cellulaire. Par conséquent, ils doivent être transportés dans le même véhicule. Ainsi, la détection thermique avec UCNPs pourrait être utilisée pour commander le traitement des PTT, ce qui minimise les dommages collatéraux dans les tissus sains entourant de la cible de l'hyperthermie. Par conséquent, le nanocomposite n'est pas seulement adapté sur la bioimagerie, mais aussi peut potentiellement être utilisé pour des applications où un gradient thermique doit être généré et surveillé par un thermomètre. En particulier, un médicament moléculaire pourrait être également chargé dans ces nanocomposites, et le comportement de la libération de médicament pourrait être renforcé par la chaleur générée par les GNRs. Cela se conduirait par un nanocomposite à volets multiples ou multi-modale apte à délivrer deux modalités thérapeutiques. Les objectifs de cette partie sont: (1) la préparation et la caractérisation de nouveaux nanocomposites multifonctionnels combinant UCNPs et GNRs. (2) recherche sur le rapport d'intensité de luminescence UCNPs en fonction de la température et de l'utilisation pour détecter les changements de température de nanocomposites sous irradiation laser. (3) comparé la luminescence UCNPs avant et après la combinaison GNRs et analyser l'influence des GNRs sur le changement de luminescence. (4) des médicaments du modèle ont été sélectionnés et chargés dans les nanocomposites, des profils de libération de médicament ont été évalués.

Les liposomes sont artificiellement nanoporteurs préparés composant une phase lamellaire bicouche lipidique. Ils sont considérés comme de bons candidats pour l'administration de médicaments en raison du fait que leur structure est semblable à celle des membranes cellulaires. Grand potentiel pour biocompatibilité améliorée, une toxicité

réduite et une meilleure efficacité thérapeutique a été rapportée pour la livraison de médicaments à base de liposomes. Récemment, dans le cadre de nanoporteurs à base de liposomes, des rapports de recherche ont montré que l'encapsulation de nanostructures, comme des boîtes quantiques (QDs), métallique, ou des nanoparticules d'oxyde de fer au sein de liposomes fournit une multitude d'approches novatrices pour des applications biomédicales et pharmaceutiques. Cependant, leur utilisation comme systèmes de livraison pour les différents types de nanoparticules est encore en train de la recherche. En particulier pour les liposomes encapsulé UCNPs, les données sont encore rares, et d'autres études sur la conception, la caractérisation et l'application des liposomes encapsulé UCNPs sont nécessaires pour développer leur application dans le domaine biomédical. Par conséquent, nous construisons un liposome co-encapsulé UCNPs et DOX, qui combine l'imagerie optique et les modalités thérapeutiques. Les deux UCNPs et DOX sont répartis dans la phase aqueuse interne des liposomes en raison de leur caractère hydrophile. Pendant ce temps, parce qu'il y a une superposition des spectres partiels entre le spectre d'absorption de la DOX et de l'émission verte de la conversion ascendante des UCNPs dans la longueur d'onde entre 510 et 570 nm, les UCNPs et les molécules DOX sont les donneurs d'énergie et accepteurs d'énergie, respectivement. Le transfert d'énergie de résonance de luminescence (en anglais: luminescence resonance energy transfer; LRET) aurait lieu sur la base de la distance étroite entre UCNPs et DOX, ce qui pourrait en outre utilisé pour le système de surveillance de libération du médicament en temps réel très sensible. Par conséquent, ce nanoporteur de liposome encapsulé avec UCNPs et DOX pourrait être utilisé pour biomédecine multimodale, impliquant la détection et le traitement d'une maladie simultanée. Les objectifs de cette partie sont: (1) Préparation et

caractérisation des liposomes encapsulants UCNPs et DOX. (2) Étude de la luminescence UCNPs et d'analyser l'influence de UCNPs luminescence par chargement DOX. (3) Utilisation de l'intensité de la luminescence du UCNPs pour surveiller la libération du médicament en investiguant quantitativement le transfert d'énergie de résonance de luminescence (LRET) de UCNPs à DOX.

Partie I: nanocomposites multifonctionnels combinant UCNPs et GNRs

La partie I est principalement concentrée sur les nanocomposites, le couplage d'un nanothermomètre avec un nanoréchauffeur en fonction de leurs propriétés optiques et thermiques distinctes. Dans cette partie, UCNPs peuvent être appliqués comme nanothermomètres basées sur la luminescence dépendante de la température à laquelle les rapports d'intensité de luminescence (LIR) varient en fonction de la température. Deux types de GNRs ont été effectués comme nanoréchauffeurs, dont superposition de SPR avec l'émission / ou l'excitation de UCNPs, de sorte que la luminescence de UCNPs a été influencée par le champ électromagnétique localisé créé par les GNRs. En outre, ces nouveaux nanocomposites pourraient également être considérés comme excellents nanoplatforms pour la libération de médicaments contrôlée par le capteur à la chaleur.

Chapitre 4: Nanoplateforme multifonctionnel unique basé sur la conversion ascendante luminescence et des GNRs

Dans le chapitre 4, nous avons développé une nanoplateforme multifonctionnel composé d'un noyau GNR et une enveloppe extérieure de la conversion ascendante $NaYF_4$:Er^{3+}, Yb^{3+} UCNPs. Le noyau GNR a une SPR longitudinale centrée à 660 nm, qui se superpose parfaitement avec l'émission rouge de la transition Er^{3+} $^4F_{9/2} \rightarrow {}^4I_{15/2}$. Ce

nanocomposite est capable d'induire un échauffement localisé par l'intermédiaire du noyau GNR tandis que l'enveloppe extérieure peut être utilisée pour contrôler simultanément la température augmente entourant. Le chauffage est généré par l'absorption de la lumière rouge de la conversion ascendante de transition Er^{3+} $^4F_{9/2} \rightarrow {}^4I_{15/2}$. L'absorption du noyau GNR a été mise en évidence par la trempe plus drastique du rouge par rapport aux transitions vertes. Les intensités relatives des émissions de la conversion ascendante de transitions $^2S_{11/2} \rightarrow {}^4I_{15/2}$ et $^4S_{3/2} \rightarrow {}^4I_{15/2}$ étaient sensibles à la température et ont permis à l'enveloppe $NaYF_4$ extérieure: Er^{3+}, Yb^{3+} pour s'agir comme nanothermomètre. Enfin, lorsque ce nanocomposite a été chargé avec un médicament du modèle anticancer, nous avons montré que cet effet photothermique pourrait déclencher la libération du médicament rapide, en particulier aux faibles valeurs de pH. Ce comportement de libération du médicament, qui dépend de la température élevée et la valeur de pH faible, est favorable dans la tumeur milieu extracellulaire, et a donc des applications prometteuses dans la thérapie du cancer.

Figure 2 Illustration schématique de la procédure synthétique pour les nanocomposites GNR@$NaYF_4$:Er^{3+},Yb^{3+}.

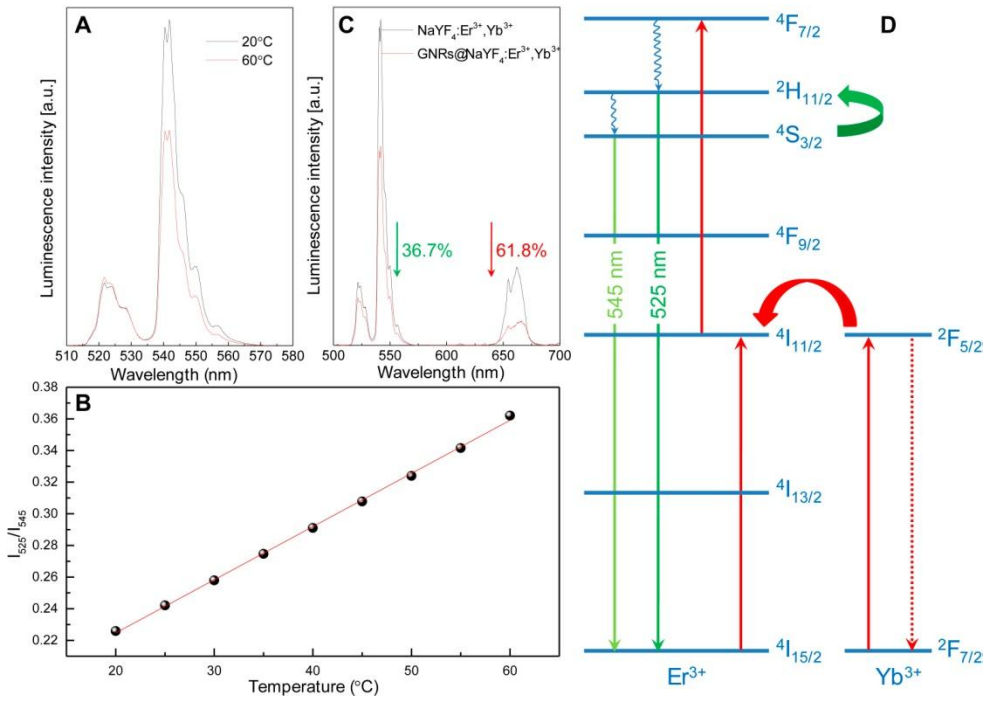

Figure 3 (A) Spectres de luminescencede la conversion ascendante de $NaYF_4$: Er^{3+}, Yb^{3+} à deux températures différentes. (B) La dépendance en température du rapport calculé à partir des spectres de luminescence. Sphères sont des résultats expérimentaux, et la ligne rouge est le meilleur ajustement linéaire. (C) Spectres de la conversion ascendante luminescence de $NaYF_4$: Er^{3+}, Yb^{3+} et GNR @ $NaYF_4$: Er^{3+}, Yb^{3+}. (D) Un schéma montrant le niveau de l'Yb^{3+} et des ions Er^{3+} dopantes et le mécanisme de conversion ascendante énergie. La sensibilité à la température de l'$NaYF_4$: Er^{3+}, Yb^{3+} se produit en raison de l'étroite espacées $^2H_{11/2}$ et $^4S_{3/2}$ états d'énergie.

L'article sur les résultats décrits dans le présent chapitre est le suivant:

Y. Huang, F. Rosei, F. Vetrone. A single multifunctional nanoplatform based onupconversion luminescence and gold nanorods. Nanoscale, 2015; 7(12):5178-5185[53]

Chapitre 5: Nanocomposites multifonctionnels à base de nanoparticules de la conversion ascendante combinées l'effet photothermique et l'effet photodynamique.

Dans le chapitre 5, un nouvel nanocomposite GNR@SiO_2@UCNPs a été préparé et caractérisé. Nous avons étudié les propriétés de luminescence de GNR@SiO_2@UCNPs et constaté que le rapport des intensités de l'émission de la conversion ascendante verte entre transitions de $^2H_{11/2}\rightarrow{}^4I_{15/2}$ et $^4S_{3/2}\rightarrow{}^4I_{15/2}$ a changé en fonction de la température et pourrait être exploitée pour la détection thermique. En outre, l'intensité de luminescence totale d'UCNPs a été augmentée en présence d'GNRs (par rapport aux seuls UCNPs), et cette amélioration peut être attribuée à la superposition de l'excitation des UCNPs et la SPR de GNRs à 980 nm, ainsi que la distance d'espace entre UCNPs et GNR. Ainsi, la luminescence des UCNPs a été influencée par le champ électromagnétique localisé créé par les GNRs, ce qui se conduit à l'enfoncementde l'intensité de luminescence observée. Zinc phthalocyanin (ZnPc) a été choisi comme l'agent de photosenibilisateur pour charger dans la couche de silice mésoporeuse et une trempe des UCNPs a été observée ce qui démontre que la luminescence émise a été effectivement absorbée par les molécules ZnPc, à transférer ensuite à l'oxygène triplet et, finalement, générer l'ROS. Enfin, des expériences *in vitro* ont été réalisées pour évaluer leur cytotoxicité et leur potentiel en tant que sonde d'imagerie multimodale. Les résultats ont montré l'absence de cytotoxicité et des expériences d'imagerie cellulaire sur les cellules incubées déterminées, ils étaient excellents nanocomposites biocompatibles. Par conséquent, ces résultats intéressants confirment qu'ils ont le potentiel d'être utilisé comme nanoplatforms multifonctionnels excités NIR pour des applications de combinaison de diagnostics et de thérapies (théranostiques), en particulier en raison de leur capacités photothermiques et photodynamiques.

Figure 4 Illustration schématique de la procédure de synthèse pour le nanocomposite GNR@SiO_2@UCNPs.

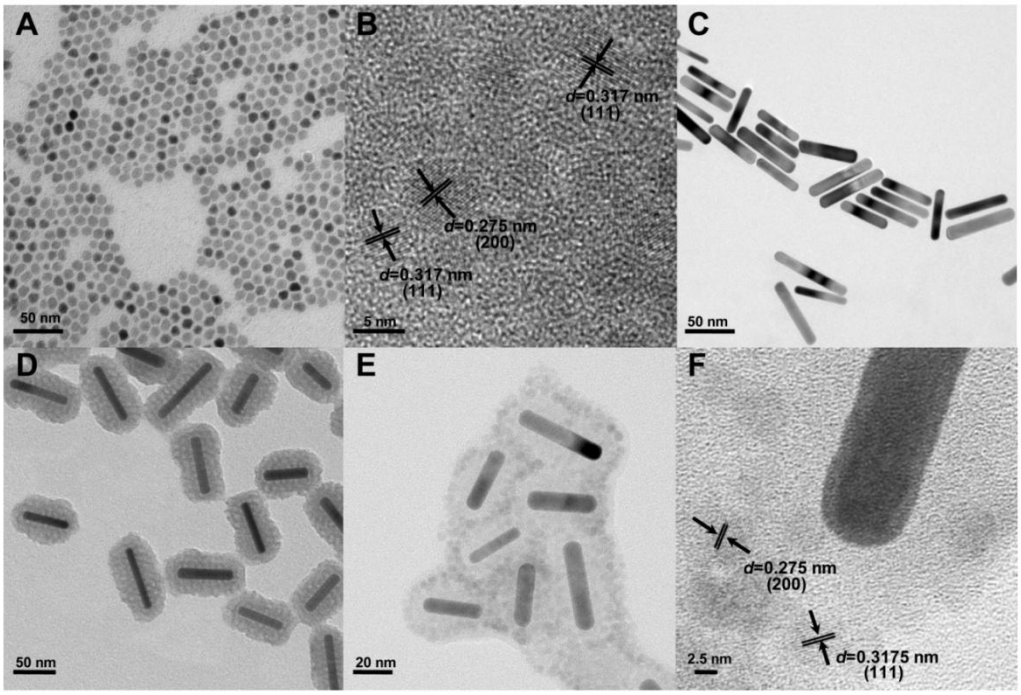

Figure 5 (A) Images de microscopie électronique en transmission (en anglais: transmission electron microscopy; TEM) et (B) TEM à haute résolution de $NaGdF_4$: Er^{3+}, Yb^{3+} UCNPs synthétisé. (C) TEM de GNRs synthétisées, (D) les GNRs enduits SiO_2, et (E) hybride de GNRs revêtus SiO_2 décorées avec $NaGdF_4$:Er^{3+}, Yb^{3+} UCNPs (GNR@SiO_2@UCNPs). (F) image de TEM à haute résolution de la interface de GNR@SiO_2@UCNPs.

L'article sur les résultats décrits dans le présent chapitre est le suivant:

Y. Huang, L. L. Páez, P. H. González, D. Jaque, F. Rosei, F. Vetrone. Multifunctional nanocomposites based on upconverting nanoparticles with combined photothermal and photodynamic effects. En préparation.

Partie II: Nanoporteurs de liposomes multifonctionnels combinant UCNPs et les médicaments anticancéreux

Dans la deuxième partie, nous avons sélectionné des liposomes comme nanoporteurs pour encapsuler UCNPs $NaGdF_4$ co-dopées par Er^{3+} et Yb^{3+} et le modèle de DOX de médicament anticancéreux. Sous l'excitation du laser avec longueur d'onde de 980 nm, les liposomes encapsulé UCNPs ont montré une forte émission verte. Contrairement, après le chargement de la DOX, la trempe de l'émission verte de la conversion ascendante a été observée en raison de la superposition de spectral partiel entre l'absorption de la DOX et l'émission verte des UCNPs, et le transfert d'énergie qui en résulte entre les UCNPs (donneur) et des molécules DOX (accepteur). Ce transfert d'énergie à partir des UCNPs aux molécules DOX ne peut se produire si les deux fractions donneur et accepteur sont suffisamment proches. En outre, la libération DOX a été étudiée et les données ont démontré une récupération de l'intensité d'émission verte de la conversion ascendante des UCNPs, qui est bien corrélée avec l'ampleur de la libération DOX. Cet enfoncement de la luminescence en fonction de libération du médicament pourrait être développé pour la surveillance de la libération du médicament à travers de luminescence UCNPs. Ainsi, le nanoporteur présenté ici, un liposome co-encapsulé avec UCNPs et le médicament anticancéreux DOX, a fourni un plateau théranostique prometteur pour la bioimagerie et la thérapie simultanée. Les travaux futurs se concentreront sur la

fonctionnalisation de surface de ces nanoporteurs avec des fractions ciblées pour les doter de la sélectivité et la spécificité pertinente pour le diagnosticcibléet la thérapeutique pour les maladies comme le cancer.

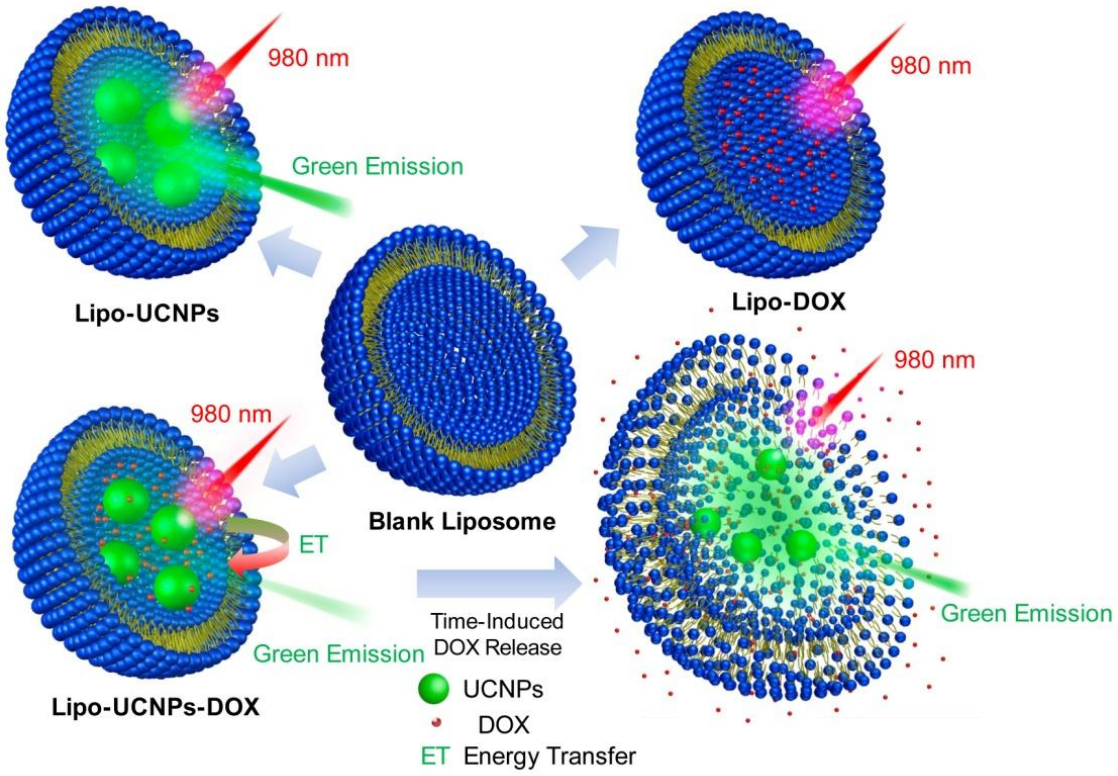

Figure 6 Représentation schématique des structures de liposomes à blanc, UCNPs encapsulées dans des liposomes (Lipo-UCNPs) DOX encapsulée dans des liposomes (Lipo-DOX) et UCNPs, DOX co-encapsulés dans des liposomes (Lipo-UCNPs-DOX).

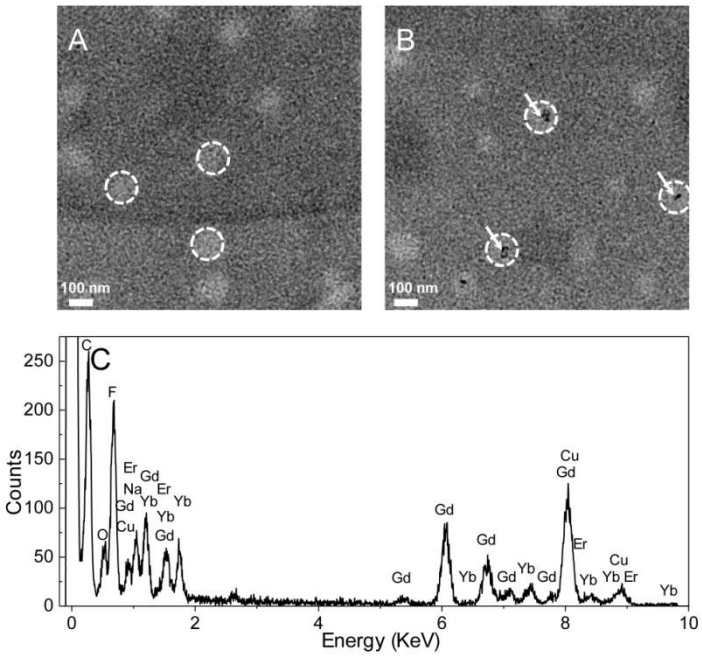

Figure 7 Image de TEM de (A) liposomes à blanc et (B) Lipo-UCNPs. Les flèches blanches indiquent la présence de l'UCNP. (C) Analyse élémentaire de lipo-UCNPs par spectroscopie à rayons X à dispersion d'énergie (en anglais : Energy-dispersive X-ray spectroscopy; EDX).

L'article sur les résultats décrits dans le présent chapitre est le suivant:

Y. Huang, E. Hemmer, F. Rosei, F. Vetrone. Multifunctional liposome nanocarriers combining upconverting nanoparticles and anticancer drugs. *J. Phys. Chem. B.* 2016;120(22):4992-5001[93]